Pile Groups Subjected to Cyclic Torsional Loads

A Thesis

SUBMITTED IN FULFILMENT OF THE REQUIREMENTS FOR THE

AWARD OF DEGREE OF

DOCTOR OF PHILOSOPHY

IN

CIVIL ENGINEERING

BY

SAGAR MEHRA

(2K17/PHDCE/22)

Under the supervision of

Prof. A. Trivedi

Professor, Department of Civil Engineering

Delhi Technological University, Delhi-110042

Department of Civil Engineering

Delhi Technological University

Delhi-110042, India

Sadhan Pad

प्रकाशक्रियास्थितिशीलं भूतेन्द्रियात्मकं भोगापवर्गार्थं दृश्यम्

सूत्रार्थ: प्रकाश क्रिया और स्थिति जिसका स्वभाव है, भूत और इन्द्रियाँ जिसका स्वरूप हैं, पुरुष के लिए भोग और मुक्ति ही जिसका प्रयोजन है, वह दृश्य है ।

Meaning: The experienced is composed of elements and sense organs, is of the nature of illumination, action and inertia,whose purpose is to provide both experiences and emancipation to the Purusha.

Reference: Patanjali Yog Sutra, Sadhan Pad, ||2.18||

TABLE OF CONTENTS

Delhi Technological University

Shahbad Daulatpur, Bawana Road, Delhi-110042

DECLARATION

I, Sagar Mehra, hereby declare that this thesis entitled " **Pile Groups Subjected to Cyclic Torsional Loads** " is entirely my research work except where otherwise acknowledged. The research work has been accomplished under the guidance of Prof. Ashutosh Trivedi. The data, figures, and results presented in this thesis are authentic and accurately represent the findings of my research. The present research work has not been submitted, either in whole or in part, for any other degree or qualification at this or any other institution.

New Delhi **Sagar Mehra**

Roll No. 2k17/PhD/CE/22

Delhi Technological University

Shahbad Daulatpur, Bawana Road, Delhi-110042

CERTIFICATE

This is to certify that the thesis titled **"Pile Groups Subjected to Cyclic Torsional Loads"** which is being submitted by **Mr Sagar Mehra** for the fulfilment of the requirements for the award of the degree of **Doctor of Philosophy,** is a record of the student's work carried out at Delhi Technological University, Delhi, India under my supervision and guidance. The matter embodied in this has not been submitted elsewhere for the award of any other degree or diploma.

New Delhi

Prof. A. Trivedi

Professor, Department of Civil Engineering

Delhi Technological University, Delhi, India

ACKNOWLEDGEMENT

I would like to express my deepest gratitude to my supervisor, **Prof. Ashutosh Trivedi**, for their invaluable guidance, encouragement, and unwavering support throughout the entirety of this research journey. Their expertise, patience, and constructive feedback have been instrumental in shaping the direction and quality of this thesis.

I am immensely thankful to Prof. K.C Tiwari, Head of the Civil Engineering Department, Prof. V.K Minocha, DRC Chairman and DRC committee members for their insightful comments, constructive criticism, and dedication to ensuring the rigour and coherence of this work.

I am indebted to Delhi Technological University for its infrastructure support, which made this research possible. I would like to acknowledge the staff and resources of Delhi Technological University, whose facilities and services have facilitated the smooth progress of this research project.

Heartfelt thanks are extended to my friends and family for their unwavering love, encouragement, and understanding throughout this challenging endeavour. Their support has been a constant source of motivation and strength.

Finally, I wish to express my profound gratitude to all the students of ITS and SD Lab who generously contributed their time.

Sagar Mehra

ABSTRACT

The pile groups support large structures namely offshore platforms, wind turbines, high-rise buildings, bridges, railway embankments, and traffic and signal pole foundations which often experience axial, lateral and torsional loads. As a result, they undergo vertical, lateral, and eccentric movements. Therefore, the numerical scheme supported by a set of experimental observations has been considered to capture pile-soil interaction for the pile groups subjected to axial, lateral and torsional loads. The coupling effect of axial load on torsional pile response conversely has been studied with a nonlinear three-dimensional finite-element analysis, while the conventional subgrade reaction method of pile analysis cannot consider this interaction. In addition, the geomaterials experience controlled and uncontrolled displacement at varying amplitudes of loading due to earthquakes, wind loads, machine foundations, vibratory compactors and pile driving. The heave due to cyclic loads is often observed in areas such as coastal regions where there are wave actions or in areas with high seismic activity. Appropriate foundation designs considering this phenomenon are to be implemented to interpret heave displacement due to cyclic torsional loads.

In the present research, the progressive twist and displacement in the sand are investigated for a set of pile groups (1,2; 1,3; 2,2) corresponding to the application of the torsional loads. The torque mobilisation, progressive twist, and displacement have been computed for a range of the initial shear modulus ratio for the entire set of pile groups. As a result of twisting, the torsional energy zones are set into the soil and there is the formation of a heave and cavity around the pile group. The torsional energy and twist rigidity parameters were evaluated for a range of shear modulus ratios of the soil. It has been observed that the torsional energy of the pile group (1,2) is significantly higher than pile groups (1,3; 2,2). A classification for torsional energy zones associated with twist rigidity and displacement

rigidity factor has been suggested to set the limits for twist and displacement of the pile groups relative to a single pile. A relationship of the torsional energy with progressive twist and displacement is obtained. The components of torsional energy associated with progressive twist and displacement were obtained in the range of 0.43-0.50 and 0.50-0.57 respectively.

An attempt has been made to find out the solutions for pile groups subjected to combined axial and torsional loads. Therefore, a novel numerical scheme has been presented to capture the nonlinear pile-soil interaction in flow-controlled geomaterial to make allowance for the yield effects. Based upon the numerical scheme, a three-dimensional finite element analysis has been performed on pile groups subjected to combined axial and torsional loads in flow-controlled geomaterial using a computational program. The flow potential for the yield surface of flow-controlled geomaterial is a hyperbolic function of stresses in the meridional stress plane and the smooth elliptic function in the deviatoric stress plane, respectively. The load-displacement relationship of a large diameter pile (LDP) and pile groups (1,2 and 2,2) have been compared with the experimental pile load test and the numerical results reported in the literature. It has been observed that the resultant displacement increases significantly with the torsional load for the LDP and pile groups. Similarly, the twist increases significantly with an increase in axial load. The displacement and twist parameters have been classified which in turn depend on the plastic strain and dilation angle of the geomaterial.

In addition, this work also presents the study of the response of cyclic torsional loads on pile foundation groups. A numerical scheme is proposed to capture the behaviour of the symmetrical pile group in the flow-controlled geomaterial under cyclic torsional loading. Based on the numerical scheme, three-dimensional finite element analysis was performed

to capture the nonlinear response of the pile group using a computational program. The results from the numerical analysis have been compared with the experimental observations. The peak twist and peak shear stress logarithmically decrease and then become asymptotic after a number of cycles of loading for a pile group (2,2) in a flow-controlled geomaterial. A set of cyclic degradation parameters of flow-controlled geomaterial is identified for the pile group and presented as a function of dilation.

A numerical campaign is proposed to capture the surface displacement of the geomaterial. The constitutive relations from the numerical campaign are placed into the computational program to apprehend the nonlinear response of the geomaterial using a three-dimensional finite element analysis (3D-FE). The outcome of the research has been validated with the experimental results. The surface displacement of the geomaterial tends to increase with a number of cycles of loading and the peak angle of friction. After a number of torsional loading cycles, the surface heave consisting of uplift and lateral flow ranges between 10-25 mm and 5-10 mm, respectively for varied peak angles of friction. Conversely, the measure of surface heave and lateral flow shall allow the designers to predict the permissible number of cycles at the outset of torsional loading. A set of surface displacement parameters for the geomaterial are identified and presented.

Having an understanding of the coupling effect of torsional loads inclusive of the cyclic effects and torsional energy around the pile groups in the flow-controlled geomaterial, an appropriate pile foundation design procedure is placed for the use of practitioners and experts in the industry.

Keywords: Torsional loads; cyclic loads; flow-controlled geomaterial; torsional energy; surface displacement; coupling effect

LIST OF FIGURES

LIST OF TABLES

LIST OF NOTATIONS

Progressive Twist, Displacement and Torsional Energy Around Pile Groups

T/T_{max}	normalized applied torque, the ratio of the instantaneous torque, T and the maximum torque, T_{max}, where T_{max} is 100 N-m
T	instantaneous torque on pile group (N-m)
$\left[\Lambda_P^{(i,j,k)}\right]$	stiffness matrix of the pile element (kN/m)
$[\Lambda_P]$	global stiffness matrix of all the elements of pile group
$[s\Lambda]$	global stiffness matrix of all the elements of soil
$\left[s\Lambda_{Te}\right]$	initial stiffness of torsional spring (kN-m/m)
$\left[s\Lambda_{\mathrm{He}}\right]$	initial stiffness of lateral spring (kN-m/m)
$[\Lambda_{PP}]$	pile element in bending
$[\Lambda_{PT}]$	pile element in torsion
$\frac{U_z{}^c}{D_P}$	displacement ratio in cavity zone (ratio of displacement in z-direction and diameter of the pile)
$\frac{U_z{}^h}{D_P}$	displacement ratio in heave zone (ratio of displacement in z-direction and diameter of the pile)
$\xi(i,j)$	twist rigidity factor
$\zeta(i,j)$	displacement rigidity factor
θ	twist angle (radians)
δ	lateral displacement (m)
ψ	rotation of pile group (radians)
E_s	initial elastic modulus of soil deposit (MPa)
E_p	young modulus of pile material (MPa)
E_T	Torsional energy (J)
J_p	centroidal polar moment of inertia of the individual pile cross-section (m^4)
G_s	initial shear modulus of soil deposit (MPa)
G_p	modulus of rigidity of the pile material (GPa)
μ_p	poisson ratio of pile material
μ_s	initial poisson ratio of soil deposit
G_s/G_{max}	initial shear modulus ratio, the ratio of the instantaneous shear modulus, G_s to the maximum shear modulus considered, G_{max}=19.23 (MPa)
γ_s	effective unit weight of soil deposit (kN/m3)
γ_p	young modulus of pile material (GPa)
ϕ_d	dilation angle of soil (degrees)
ϕ_c	constant volume friction angle (degrees)
ϕ_p	peak value of angle of internal friction of soil (degrees)

D_p	diameter of the pile in pile group (m)
L_p	length of the pile in pile group (m)
t_s	layer thickness of soil deposit (m)
S_p	pile-pile spacing in pile group (m)
τ	torsional shear stress
P	lateral soil reaction per unit length of the pile (kN/m)
k_θ	modulus of subgrade reaction for torsional loading (kN/m^3)
k_h	modulus of subgrade reaction for horizontal loading (kN/m^3)
k_{TH}	stiffness at node $(i = 1; j = 2; k = 1)$ due to the torsional constituent of soil deformation due to unit lateral load at node $(i = 1; j = 1; k = 1)$ on another pile
k_{HT}	stiffness at node $(i = 1; j = 2; k = 1)$ due to the lateral constituent of soil deformation due to unit torsional load at node $(i = 1; j = 1; k = 1)$ on another pile
g	plastic potential
f	yield criterion or surface
ξ_p	progressive twist
ζ_p	progressive displacement
ξ_n	instantaneous progressive twist
ζ_n	instantaneous progressive displacement
ξ_{min}	minimum progressive twist
ζ_{min}	minimum progressive displacement
ξ_{max}	maximum progressive twist
ζ_{max}	maximum progressive displacement
$[E_T^\theta]$	torsional energy due to progressive twist
$[E_T^d]$	torsional energy due to progressive displacement
η_θ	component of energy associated with the twist
1-η_θ	component of energy associated with the displacement

Pile Groups Subjected to Axial and Torsional Loads in Flow Controlled Geomaterial

$A/A_{(max)}$	normalized axial load, the ratio of the instantaneous axial load, A to the maximum axial load considered, $A_{(max)}$ ~ 12000 (kN)
$T/T_{(max)}$	normalized applied torque at pile head, the ratio of the instantaneous torque, T to the maximum torque considered, $T_{(max)}$ ~ 10000 (kN-m)
$\delta/\delta_{(max)}$	normalized pile head displacement, the ratio of the instantaneous resultant displacement, δ to the maximum resultant displacement obtained, $\delta_{(max)}$ ~ 48 (mm)
θ/θ_{max}	normalized pile head twist, torque ratio, the ratio of the instantaneous

	twist, θ to the maximum twist obtained, $\theta_{(\max)}$ ~ 1(degree)
$\left[\Lambda_P^{(i,j,k)}\right]$	stiffness of the pile element (kN/m)
$[\Lambda_P]$	global stiffness matrix of all the elements of pile gro
$[s\Lambda]$	global stiffness matrix of all the elements of geomaterial
$\left[s\Lambda_{Q_e}\right]$	initial stiffness of axial spring (kN/m)
$\left[s\Lambda_{T_e}\right]$	initial stiffness of torsional spring (kN-m/m)
$\left[s\Lambda_{H_e}\right]$	initial stiffness of lateral spring (kN/m)
$\left[s\Lambda_{H_f}\right]$	resulting stiffness of lateral spring (kN/m)
$\left[s\Lambda_{Q_f}\right]$	resulting stiffness of axial spring (kN/m)
$\left[s\Lambda_{T_f}\right]$	resulting stiffness of torsional spring (kN-m/m)
γ_s	effective unit weight of geomaterial (kN/m^3)
γ_p	young modulus of pile material (GPa)
ϕ_d	dilation angle of geomaterial (degrees)
ϕ_s	effective friction angle of geomaterial (degrees)
L_p	length of the pile (m)
S_p	pile-pile spacing in pile group (m)
t_s	layer thickness of geomaterial (m)
D_p	diameter of the pile (m)
t_p	thickness of pipe pile (mm)
ψ	rotation of pile group (radians)
θ	twist angle (radians)
k_θ	modulus of subgrade reaction for torsional loading (kN/m^3)
k_q	subgrade modulus for bearing (kN/m^3)
k_h	modulus of subgrade reaction for horizontal loading (kN/m^3)
G_p	modulus of rigidity of the pile material (GPa)
G_s	shear modulus of geomaterial (MPa)
E_s	initial elastic modulus of geomaterial (MPa)
E_p	young modulus of pile material (MPa)
J_p	centroidal polar moment of inertia of the individual pile cross-section (m^4)
q	bearing pressure (kN/m^2)
P	lateral soil reaction per unit length of the pile (kN/m)
y	lateral displacement (m)
I_1	first stress invariant indicates the effect of mean stress
J_2, J_3	stress invariant of deviatoric stress, J_2 represents the magnitude of shear stress, J_3 determine the direction of shear stress
z	depth coordinate (m)

μ_s	poisson ratio of geomaterial
μ_p	poisson ratio of pile material
ε_{ij}^{p}	plastic strain tensor
σ_{ij}	stress tensor
$\sigma_{1,}\sigma_{2,}\sigma_3$	principal stresses
f	yield criterion or surface
$\{F\}$	external loads applied on the pile groups
R	resultant force (kN)
$\{\mathrm{d_s}\}$	vector deformation at soil nodes
$\{d_p\}$	vector deformation at pile nodes
M	moment induced due to the applied torque at pile head (kN-m)
P	lateral force induced due to applied torque at pile head (kN)
M_b	moment resistance at pile base (kN-m)
F_p	lateral force resistance at pile node (kN)
T_b	torsional resistance at pile base (kN-m)
F_b	resistance force at pile base (kN)
F_v	vertical force resistance at pile node (kN)
F_h	lateral force resistance at pile node (kN)
λ	positive scalar
g	plastic potential

Cyclic Degradation Parameters of Flow Controlled Geomaterial

T_0	instantaneous cyclic torsional load on pile group (N-m)
$\left[\Lambda_{P(i,j,k)}\right]$	stiffness matrix of the pile element
$[\Lambda_P]$	global stiffness matrix of all the elements of pile group
$[\Lambda_{PP}]$	pile element matrix in bending
$[\Lambda_{PT}]$	pile element matrix in torsion
$[s\Lambda]$	global stiffness matrix of all the elements of geomaterial
$[s\Lambda_T]$	initial stiffness matrix of torsional spring
$[s\Lambda_{\mathrm{H}}]$	initial stiffness matrix of lateral spring
f_s	curve fitting parameter
g_s	curve fitting parameter
ω	circular frequency (rad/sec)
α	degradation parameter for geomaterial lateral modulus
β	degradation parameter for geomaterial torsional modulus
k_h	lateral loading subgrade modulus (N/m^2/m)
k_θ	torsional loading subgrade modulus (N-m/m^2/m)

c_h	coefficient of damping for lateral cyclic loading (N-s/m)
c_θ	coefficient of damping for torsional cyclic loading (Nm-s/m)
θ	angle of twist of pile element (radians)
δ	lateral deformation of pile element (m)
ψ	rotation of pile element (radians)
D_p	diameter of the pile in pile group (m)
g	plastic potential
f	yield criterion or surface
N	number of load cycles
E_s	initial modulus of elasticity of geomaterial (MPa)
E_p	young modulus of pile material (MPa)
J_p	centroidal polar moment of inertia of the individual pile cross section (m^4)
G_p	modulus of rigidity of pile material (GPa)
$G_P J_P$	torsional rigidity of pile
G_s	initial shear modulus of geomaterial (MPa)
G_{max}	maximum shear modulus of geomaterial (MPa)
G_{se}	equivalent shear modulus of geomaterial (MPa)
ρ_s	density of the geomaterial (kg/m^3)
μ_p	poisson ratio of pile material
μ_s	initial Poisson ratio of geomaterial
τ_u	limiting shaft friction (N/m^2)
τ_i	pile–geomaterial interfacial shear stress (N/m^2)
γ_s	effective unit weight of geomaterial (kN/m^3)
γ_p	unit weight of pile material (kN/m^3)
ϕ_d	dilation angle of geomaterial (degrees)
ϕ_c	constant volume friction angle (degrees)
ϕ_p	peak friction angle of geomaterial (degrees)
ε_p	plastic strain (%)
S_p	pile–pile spacing in pile group (m)
L_p	length of the pile in pile group (m)
a_t, b_t	logarithmic degradation parameters for the twist
a_s, b_s	logarithmic degradation parameters for the shear stress
$D_f^{"}, D_f', D_f$	flow-controlled cyclic degradation parameters

Surface Displacement of the Geomaterial due to Cyclic Torsional Loading on Pile Groups

T_c	instantaneous cyclic torsional load on pile group (N-m)
$\left[\Lambda_{P(i,j,k)}\right]$	stiffness matrix of the pile element
$[\Lambda_P]$	global stiffness matrix of all the elements of pile group
$[\Lambda_{PP}]$	pile element matrix in bending
$[\Lambda_{PT}]$	pile element matrix in torsion
$[s\Lambda]$	global stiffness matrix of all the elements of geomaterial
$[s\Lambda_T]$	initial stiffness matrix of torsional spring
$[s\Lambda_{\mathrm{H}}]$	initial stiffness matrix of lateral spring
ρ	density of the pile material (kg/m^3)
ρ_s	density of the geomaterial (kg/m^3)
ω	circular frequency (rad/sec)
N	number of load cycles
$\theta(z,t)$	angle of twist of pile element (radians)
$\delta(z,t)$	lateral deformation of pile element (m)
$\psi(z,t)$	rotation of pile elements (radians)
D_p	diameter of the pile in pile group (m)
E_s	initial modulus of elasticity of geomaterial (MPa)
E_p	young modulus of pile material (MPa)
J_p	centroidal polar moment of inertia of the individual pile cross-section (m^4)
G_p	modulus of rigidity of pile material (GPa)
$G_P J_P$	torsional rigidity of pile
G_s	initial shear modulus of geomaterial deposit (MPa)
G_{se}	equivalent share modulus of geomaterial deposit (MPa)
μ_p	poisson ratio of pile material
μ_s	initial Poisson ratio of geomaterial deposit
τ_u	limiting shaft friction (N/m^2)
τ_i	pile-geomaterial interfacial shear stress (N/m^2)
V_h	lateral geomaterial reaction (N)
g	plastic potential
f	yield criterion or surface
m	mass of the geomaterial
$\alpha_{L(r)}$	poulos interaction factor
$S_{h1}; S_{h2}$	functions of the dimensionless frequency depend upon the poison's ratio
$H_n^{(2)}$	hankel functions of the second kind of order *n*
k_h	lateral loading subgrade modulus (N/m^2/m)

k_θ	torsional loading subgrade modulus (N-m/m^2/m)
c_θ	coefficient of damping for torsional cyclic loading (Nm-s/m)
c_h	coefficient of damping for lateral cyclic loading (N-s/m)
γ_s	effective unit weight of geomaterial deposit (kN/m^3)
z	depth coordinate (m)
γ_p	unit weight of pile material (kN/m^3)
$J_0(a_0), J_1(a_0)$	bessel functions of the first kind and order 0 and 1, respectively
θ_h	torsional geomaterial reaction (N-m/m)
ϕ_d	dilation angle of geomaterial (degrees)
t_s	layer thickness of geomaterial deposit (m)
L_p	length of the pile in pile group (m)
S_p	pile-pile spacing in pile group (m)
$f_{x1};\ f_{x2}$	stiffness and damping parameters for sliding vibration
$Y_0(a_0), Y_1(a_0)$	bessel functions of the second kind and order 0 and 1, respectively
ϕ_c	constant volume friction angle (degrees)
ϕ_p	peak friction angle of geomaterial (degrees)
$S_{\theta 1}(a_0)$	stiffness parameter
$S_{\theta 2}(a_0)$	damping parameter
a_0	dimensionless frequency
$\emptyset_h^{R_c}$	angle of the heave; the ratio of the surface displacement in uplift and lateral flow due to heave at surface heave contour, $R_{c\to(1-10)}$ for the number of cycles, *N*.
$R_{c\to(1-10)}$	surface heave contours described in Fig.6.3
$u_h^{"}, u_h', u_h$	surface parameters for uplift due to heave
$l_h^{"}, l_h', l_h$	surface parameters for lateral flow due to heave

1 INTRODUCTION

This chapter contains the relevant literature review on "Pile Groups Subjected to Cyclic Torsional Loads". It consists of an introduction, scope, objectives of the research work, publications, structure, organisation of the thesis, and benefits to practitioners, researchers and society.

1.1 General Introduction

The design and analysis of pile foundations indeed involve a myriad of complex factors namely, mode of loading, soil properties, initial conditions, pile geometry, method of construction and load transfer mechanisms. Certain structures, like offshore platforms, tall buildings, and electric transmission towers are subjected to lateral loads of considerable magnitude from wind and wave actions, ship impacts, high-speed vehicles, and other sources of loading, significant torsional forces and moments can be transferred to the foundation piles by the virtue of eccentric lateral loading.

Torsional wind loading on tall buildings has been noted by many researchers (Isyumov 1983; Cheung 1992; Boggs et. al. 2000; Liang et. al. 2004). Wind tunnel tests play a crucial role in understanding and predicting the behaviour of structures, especially in regions prone to strong winds like those caused by typhoons or hurricanes. Torsional loads, resulting from wind-induced forces acting on a building or structure, are an important aspect of these tests. Boggs et. al. (2000) identified several common sources of torsional loading in terms of building shape, interfering effects of nearby buildings, and dynamic characteristics of the structural frame. The foundation piles under a tall building may undergo large torsional loads as well as horizontal loads. Insufficient design of the foundation against these loads may affect the serviceability and survivability of the building. A tornado hit North Delhi, Delhi University in March 1978. The rotating wind, which lasted a mere five minutes, flung scooters yards away, reduced shops to rubble and uprooted trees. Thirty-two people died

and eight hundred were injured (Gupta and Ghosh 1980). The damage was estimated at rupees one crore, excluding that caused to two transmission towers of All India Radio (Figure 1.1).

Figure 1.1 The image showing the uprooting of trees due to the torsional forces caused by a tornado that hit North Delhi, Delhi University on March 1978

The cases of the Mayer-Kaiser building in Miami and the Great Plains Life building in Lubbock, Texas, experiencing permanent damage and marked deformations from wind-induced torsion highlight the importance of considering and mitigating torsional effects in tall building design (Vikery 1979). Piers are an essential part of bridge construction and are responsible for supporting the bridge deck and transferring loads to the foundation. They are subjected to eccentrically horizontal loads from high-speed vehicles, wind, hydrodynamic forces from waves and current and even ship impacts. Therefore, torsional resistance in the design of foundations for bridges is indeed of paramount importance. Torsional forces, which cause twisting or rotation around a vertical axis, can have severe consequences if not adequately considered and addressed in foundation design. The 6.82 km Sunshine Skyway Bridge collapse in 1980 was a tragic event in the history of civil engineering. The collapse occurred on May 9, 1980, when the freighter MV Summit

Venture collided with a support pier of the southbound span of the bridge during a severe thunderstorm. (Barker and Puckett 1997). About 395 m of the bridge fell into the sea, resulting in thirty-five deaths. One significant aspect of Hong Kong's climate and geographical location is its susceptibility to typhoons. The 50-year return peak gust wind velocity in Hong Kong is about 250 km/hr, which may generate large lateral and torsional on tall buildings and bridge piers. These loads are finally resisted by their foundation piles. In conclusion, the proper consideration of both strength and serviceability limit states in the design of foundation piles is fundamental to ensuring public safety and cost-effectiveness.

1.2 Flow Controlled Geomaterial

Frictional geomaterials are normally treated corresponding to the Mohr-Coulomb failure criterion. However, the Mohr-Coulomb plasticity has certain discontinuities on the yield surface with edges at which the yield function is not with the flow, which needs special treatment for the pile group subjected to cyclic torsional loads. Assumptions for flow controlled geomaterial are expressed as follows:

- The behaviour of geomaterial is elastic inside the yield surface. Isotropic hardening is assumed for the initial behaviour of the Mohr-Coulomb yield surface to quantify cohesion as a special case. It conforms to a mixed hardening model in the reverse loading cycle following the hardening rule of the yield surface expansion and translation.
- The flow controlled geomaterial follows a law for stress-strain relation as a function of I_1, J_2, J_3 and has an onset of nonlinearity at $\varepsilon_{ij}^{p} > 0$.
- The shear criterion has an onset of controlled granular flow, which intersects Mohr-Coulomb as a special case, having a smooth yield surface such that, $f = 0$.

- The flow controlled geomaterial follows a plastic stress-strain relation defined by a chain rule such that, $\frac{\partial f}{\partial \sigma_{ij}} \partial \sigma_{ij} > 0$.
- The smooth flow potential for geomaterial has a hyperbolic shape with a constant eccentricity in the meridional stress plane and a piecewise elliptic shape in the deviatoric stress plane.

1.3 Progressive Twist, Displacement and Torsional Energy

Torsional moments are transferred to the foundation due to the actions of wind and waves, ship impacts, moving trains, and electric transmission towers having lateral loads in high-tension wires. The practice in design offices is usually based on ignoring the stiffness of the geomaterial and only the stiffness of the pile is taken into account (Das and Luo 2016) without the consideration of progressive failure. The numerical concept of progressive failure was initially applied to the shallow foundations by a couple of investigators (Parkins and Madson, 2000; Trivedi and Sud, 2007). The physical observation that progressive twist and displacement, being defined in terms of the non-uniformity of shear zones and mobilised torsional energy in the geomaterial at the peak load, decreases, as the number of piles in the pile group increases. The potential for progressive twist and displacement, defined by the difference between the peak and effective torsional energy of the pile group, decreases as the shear modulus of the geomaterial surrounding the pile group increases. The torsional energy of the pile group is equal to the work done by the external torsional load inclusive of the plastic energy. It is the area covered by the plot of normalized applied torque and twist rigidity factor for the pile groups. The twist rigidity factor is defined as the twist of the pile group relative to the single pile (Mehra and Trivedi 2023a).

1.4 Combined Axial and Torsional Loads

The pile groups have been used as a foundation substructure for large structures such as

offshore platforms, wind turbines, high-rise buildings, bridges, railway embankments, traffic, and signal pole structures for several causes, such as wind, earthquake, water current, earth pressure, the effect of moving vehicles or ships, plants, and equipment, etc. These complex structures experience large axial, lateral, and torsional loads. Conventionally, the piles have been analysed for displacement due to axial loads and then for eccentric lateral loading to compute deflections and twists. Therefore, in the present work, the authors investigated the effects of torsional loading on axial pile displacements along with the influence of axial loads on the torsional pile response (Mehra and Trivedi 2021).

1.5 Cyclic Torsional Loads

The dynamics of pile groups are important due to their applications in machine foundations and structures exposed to cyclic loads such as wind or earthquakes. The response of structures supported by pile groups depends upon the cyclic stiffness and damping generated by geomaterial-pile interaction. Due to complex geomaterial-pile interaction, the dynamics of pile groups are not well understood. There are no readily available methods that could evaluate the response of geomaterial-pile interaction hence the geomaterial stiffness is ignored and only the pile stiffness is considered. The omission of geomaterial-pile interaction makes the analysis of pile groups quite unrealistic (Novak and Sharnouby, 1984). The design of offshore pile groups requires consideration of the effects of cyclic torsional loading. Therefore, the present work considers a novel numerical scheme that provides a framework for the estimation of the behaviour of a pile group in the flow controlled geomaterial under cyclic torsional loading (Mehra and Trivedi 2023b).

1.6 Cyclic Torsional Loading Effect on the Surface Displacement of the Geomaterial

When torsional cyclic loads are applied to a pile group surrounding geomaterial, it leads to

a phenomenon called surface displacement namely heave. The term heave typically refers to the uplift and lateral flow of the geomaterial. The heave occurring in sands due to the application of the cyclic torsional loading causes the sand particles to rearrange leading to a reduction in the shear strength and change in volume. The volume change experienced by sand depends on several factors, including the initial density of the sand, the stress level, and the confining pressure. Therefore, the study considers a numerical scheme to provide a framework for the estimation of the surface displacement of the geomaterial surrounding a pile group under cyclic torsional loading.

1.7 Scope and Objectives of the Research

The major objective of this research is to analyse the behaviour of the pile group subjected to cyclic torsional loads in the flow controlled geomaterials. The scope of the study encompasses numerical model studies and laboratory experiments for evaluating the behaviour of the pile group subjected to cyclic torsional loads. The specific objectives listed below have been selected for additional research:

- The numerical formulation for the pile groups shall be performed to analyse the effect of torsional loads on pile groups in sand.
- To provide a solution and response for the pile groups to combine axial and torsional loading.
- Simulation of pile groups subjected to torsional loads using computational software.
- The experimental studies on the pile groups shall be done to analyse the effect of torsional loads on the behaviour of pile groups.
- To analyse the basis of geomaterial-pile interaction in the pile groups subjected to torsional loading with depth.
- Design recommendations for the pile groups subjected to cyclic torsional loads.

1.8 Publications from the thesis

Throughout the research process, efforts were made to format the thesis as research papers that have been submitted as conference proceedings and articles to peer-reviewed journals for possible publication. The following is a summary of the prepared or published papers:

1. Mehra, S., & Trivedi, A. (2018). Experimental studies on model single pile and pile groups subjected to torque. *In Proceedings of China-Europe Conference on Geotechnical Engineering*: Volume 2 (pp. 997-1000). Springer International Publishing.
2. Mehra, S. & Trivedi, A. (2018). "Analysis and simulation of cyclic torque application on pile groups." *Proceeding of 12th International Super Pile World*, Nanjing, Jiangsu, China, pp. 277-282.
3. Trivedi, A. and Mehra, S. (2018). "Development and application of deep foundations in India." *Proceeding of 12th International Super Pile World*, Nanjing, Jiangsu, China, pp. 71-86.
4. Mehra, S. & Trivedi, A. (2019). "Deep foundations subjected to combined axial and torsional loads." *International Symposium on Testing and Technology for Bearing Capacity of Deep Foundation*, Delhi, ISBN:978-93-5391-519-3, 19-20.
5. Mehra, S., & Trivedi, A. (2021). "Pile groups subjected to axial and torsional loads in flow-controlled geomaterial." *International Journal of Geomechanics*, 21(3), 04021002.
6. Mehra, S., & Trivedi, A. (2023). "Progressive twist, displacement and torsional energy around pile groups." *International Journal of Geotechnical Engineering*, 17(3), 246-259.

7. Mehra, S., & Trivedi, A. (2023). “Cyclic Degradation Parameters of Flow-Controlled Geomaterial for Pile Group Subjected to Torsional Loads.” *Applied Sciences*, 13(19), 10895.
8. Mehra, S., and Trivedi, A. (2023). "Cyclic Torsional Loads on Pile Groups" Indian Geotechnical Conference, IIT Roorkee, India, 14-16 December 2023.
9. Mehra, S., and Trivedi, A. (2024). “Surface Displacement of the Geomaterial Due to Cyclic Torsional Loading on Pile Groups.” Under Review.
10. Mehra, S., and Trivedi, A. (2024). “Effect of Torsional Loads on the Axial Response of the Offshore Pile Foundations.” Under Review.

1.9 Structure and Organisation of the Thesis

The thesis is divided into eight chapters, which include an introduction, a survey of the literature, four research papers, and a summary of conclusions, design recommendations and scope for future research.

Chapter 1 presents a brief introduction to the pile groups subjected to cyclic torsional loads.

Chapter 2 provides a thorough overview of the previous research investigations that are relevant to the current research. The numerical, experimental and field studies on single pile and pile groups subjected to torsional loads are also presented to recognise the gaps in the studies to identify the need for this research to achieve the objective of the present study.

Chapter 3 consists of an effect, the progressive twist, displacement and torsional energy around pile groups due to the application of the torsional loads on the pile groups. A numerical model has been proposed which is supported by a set of experimental observations considered to capture pile-soil interaction for the pile groups subjected to torsional loads.

Chapter 4 considers the combined effect of axial and torsional loads on the pile group embedded in the flow controlled geomaterial. The numerical scheme has been presented to capture the nonlinear pile-soil interaction in flow controlled geomaterial to make allowance for the yield effects. Based upon the numerical scheme, a three-dimensional finite element analysis has been performed on pile groups subjected to combined axial and torsional loads in flow controlled geomaterial using a computational program.

Chapter 5 provides the cyclic degradation parameters of flow-controlled geomaterial for pile groups subjected to torsional loads. A numerical scheme is proposed to capture the behaviour of the symmetrical pile group in the flow-controlled geomaterial under cyclic torsional loading. Based on the numerical scheme, three-dimensional finite element analysis was performed to capture the nonlinear response of the pile group using a computational program. The results from the numerical analysis have been compared with the experimental observations.

Chapter 6 discusses the surface displacement of the flow controlled geomaterial due to cyclic torsional loading on pile groups. A numerical campaign is proposed to capture the surface displacement of the geomaterial. The constitutive relations from the numerical campaign are placed into the computational program to apprehend the nonlinear response of the geomaterial using a three-dimensional finite element analysis (3D-FE). The outcome of the research has been validated with the experimental results.

Chapter 7 This chapter provides the design recommendation for the pile groups subjected to cyclic torsional loads.

Chapter 8 This chapter provides the summary of conclusions for the pile groups subjected

to cyclic torsional loads. The important contributions to knowledge made by this research are presented and highlighted in the conclusions, along with possible directions for future investigation.

1.10 Benefits to Practitioners, Researchers and Society

The significance of designing pile groups to withstand cyclic torsional loads cannot be overstated for practitioners. Excessive torsional deformation can result in the misalignment of structural elements and cracking of walls or slabs. Therefore, the cyclic degradation parameters for plastic strain and logarithmic degradation parameters for twist and shear have been classified and recommended for designing pile groups for practitioners, industries, and society as a whole to ensure the safety, reliability, and sustainability of structures and infrastructure systems. The practitioners should also take into account the coupling effect of axial load on torsional pile response conversely which has been studied with a nonlinear three-dimensional finite-element analysis, while the conventional subgrade reaction method of pile analysis cannot consider this interaction.

In addition, the measure of surface heave and lateral flow shall allow the practitioners and designers to predict the permissible number of cycles at the outset of torsional loading. A set of surface displacement parameters for the geomaterial are identified and presented for the use of practitioners. Speculatively, the torsional resistance is elusively approximated among 20% or more while 80% or less of torsional energy depends upon the mobilisation of lateral resistance related to pile locations within the group and pile-soil interactions. The component of energy resulting from torsional force and moments for progressive twist and progressive displacement respectively have to be taken into account while designing pile groups subjected to torsional loads.

References

Boggs, D. W., Hosoya, N., & Cochran, L. (2000). “Sources of torsional wind loading on tall buildings: Lessons from the wind tunnel.” Advanced Technology in Structural Engineering, 1-8.

Gupta, H. N., & Ghosh, S. K. (1980). “North Delhi tornado of 17 March 1978.” Mausam, 31(1), 93-100.

Puckett, J. A., & Barker, R. M. (1997). “Design of Highway Bridges: Based on AASHTO LRFD, Bridge Design Specifications.” Wiley-Interscience.

Cheung, J. C. K., & Melbourne, W. H. (1992). “Torsional moments of tall buildings.” Journal of Wind Engineering and Industrial Aerodynamics, 42(1-3), 1125-1126.

Isyumov, N., & Poole, M. (1983). “Wind-induced torque on square and rectangular building shapes.” Journal of Wind Engineering and Industrial Aerodynamics, 13(1-3), 183-196.

Liang, S., Li, Q. S., Liu, S., Zhang, L., & Gu, M. (2004). “Torsional dynamic wind loads on rectangular tall buildings.” Engineering Structures, 26(1), 129-137.

Vickery, B.J. (1979). “Wind effects on buildings and structures-critical unsolved problems.” In IAHR/IUTAM Practical Experiences with Flow-induced Vibrations symposium, Karlsruhe, Germany, 823-828.

2 LITERATURE REVIEW

The chapter contains the relevant literature review on "Pile Groups Subjected to Cyclic Torsional Loads". This chapter presents the research gap as well as an overview of earlier studies conducted in this area on a national and worldwide scale.

2.1 Introduction

An individual pile in a pile group subjected to torsion can undergo lateral, torsional, or even axial loading at its pile head. Therefore, in this chapter, one of the major contents is to review previous studies on laterally loaded single piles and torsionally loaded single piles, respectively, which is shown in Section 2.2. The review generally contains previous experimental studies, such as test techniques major conclusions obtained, and numerical modelling. The previous studies on the interactions between the different loading modes (i.e. axial, lateral and torsional loading modes in single piles) which are called load-deformation coupling effects in this study, are reviewed. The review focuses on the modelling of pile-soil-pile interactions using different methods.

2.2 Literature Review

2.2.1 Pile Subjected to Torsional Loads

A solution was established for the pile head torque twist relationship and a discrete element mechanical model was introduced (O'Neill 1964). The mechanical model is composed of rigid elements connected by torsional springs shown in Figure 2.1. These springs can simulate nonlinear twist behaviour and the spring constants can be varied to account for variable pile cross-section and shear modulus. Soil displacements were obtained by using Mindlin's equations (1936) for a horizontal subsurface point load. The solid aluminium model piles, ranging from 152 mm to 508 mm in length and 13 mm to 38 mm in diameter (Poulos 1975) and model tests of single piles in clay (Georgiadis and Saflekou 1990) were

performed to examine the relationship between the axial and torsional behaviour. According to the test results, torsional shear test data might be used to forecast the behaviour of axially loaded piles in clay. An elastic method was presented for the analysis of the response of a single cylindrical pile subjected to torsion (Poulos 1975). The rotation at any point was obtained by the integral equation technique. The state of stresses was presented on an element of soil around a torsionally loaded pile (Randolph 1981) as shown in Figure 2.2. In the soil distant from the pile, the variation in shear stress is represented by the following equation:

$$\tau_{r\theta} = \frac{(\tau_{r\theta})_0 r_0^2}{r^2} \tag{2.1}$$

where r_0 is the radius of the pile; $(\tau_{r\theta})_0$ is the shear stress at the pile shaft. The tests on large model piles were performed, including a circular pile of 48.3 mm outside diameter and a square pile of 50.8 mm outside diameter, in air-dried loose and dense sands under static loading (Dutt and O'Neill 1983). The investigation examines the influence of both the relative density of sand and the pile shape on the load transfer mechanism. The conclusion was drawn that the shape and the size of the pile and the relative density dictate the shear transfer distribution with depth. Based, on the test results, a normalised shear stress-strain curve for sand was proposed for use in numerical analysis. The discrete element model is presented for the analysis of the torsional response of piles in non-homogenous soil (Chow 1985). The governing equilibrium equation for the pile embedded in a soil modelled using the modulus of subgrade reaction is expressed as follows:

$$-(GJ)_p \frac{\partial^2 \theta}{\partial z^2} + k_\theta \theta = 0 \tag{2.2}$$

where G_p is the shear modulus of the pile shaft; J_p is the polar second moment of the area of the pile section; $G_P J_P$ is the torsional rigidity of the pile; z is the depth; k_θ are the modulus of subgrade reaction for torsional loading. An analysis was described for determining the coupling between axial and torsional pile responses (Georgiadis 1987) as shown in Figure 2.3. The pile was considered as an elastic beam while the soil was modelled with axial and torsional elastoplastic springs. The solutions for a single pile subjected to torsional loads were presented by Hache and Valsangkar (1988) based on the simplified electric stress field model by Randolph (1981).

The solutions were extended (Guo and Randolph 1996) as presented by Randolph (1981) to a more general non-homogeneity of the soil to include nonlinear soil response using a hyperbolic stress-strain law. The numerical model was modified (Georgiadis and Saflekou 1990) by Georgiadis (1987) to account for the non-linearity of the soil and to improve the interaction between the axial and torsional springs. The conventional model pile tests used 500 mm aluminium closed-ended piles of 19 mm outside diameter and 1.5 mm wall thickness (Georgiadis and Saflekou 1990). All piles were installed in a soft medium plasticity clay of size 700 mm wide, 1000 mm long and 800 mm deep. The torque was continuously applied to the pile head during the axial load for each test. As a result, the ultimate axial pile capacity was significantly reduced and increased axial displacement due to the application of torsional load at the pile head.

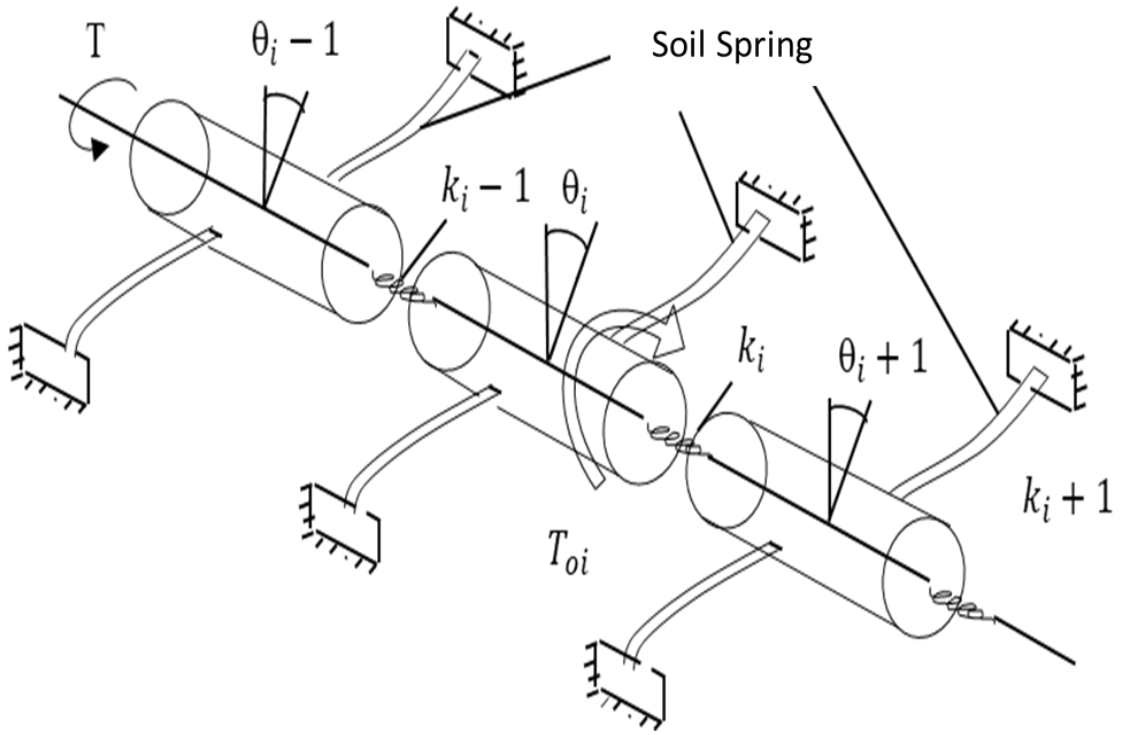

Figure 2.1 Discrete element mechanical model (after O'Neill 1964)

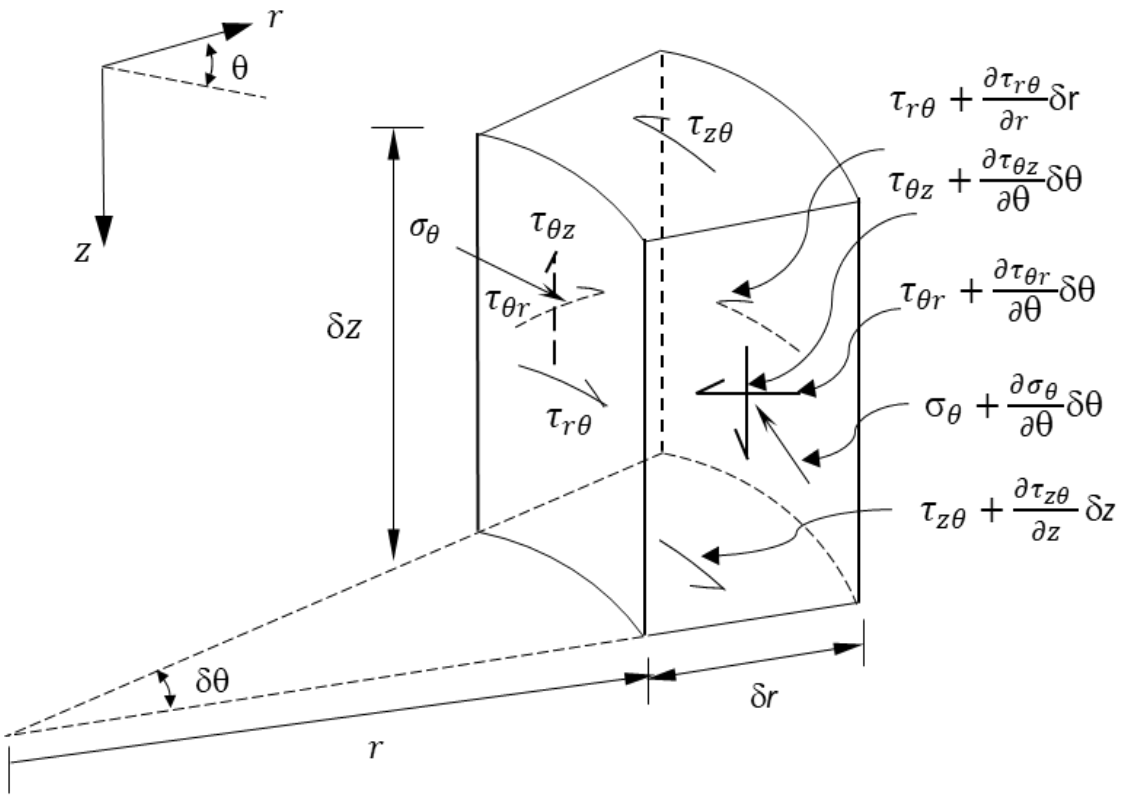

Figure 2.2 State of stresses around a torsionally loaded soil element (after Randolph 1981b)

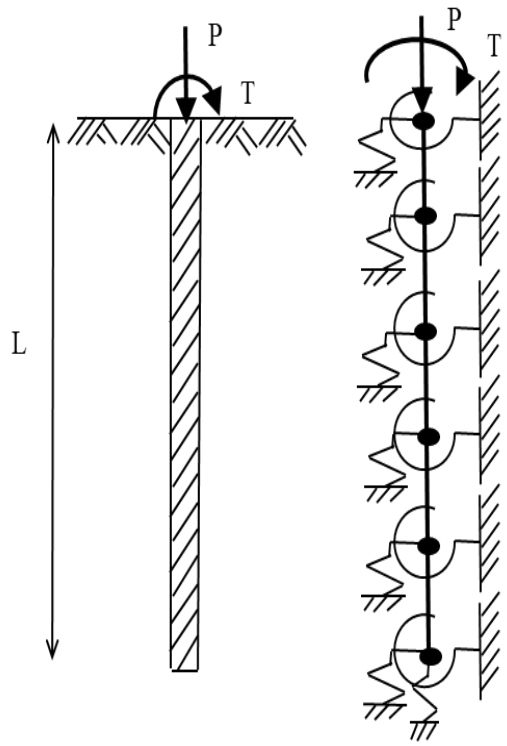

Figure 2.3 Numerical Pile Modal (after Georgiadis 1987)

2.2.2 Pile Subjected to Cyclic Lateral and Torsional Loads

The analysis for the behaviour of a single pile or symmetrical pile group in sand was studied under cyclic axial loading (Poulos 1989). The analysis was presented for the response of the pile subjected to cyclic lateral load (Poulos 1982). The effect of cyclic lateral loads on piles in the sand was investigated (Long and Vanneste 1994). The characteristics of the cyclic load, method of installation and soil density were the important parameters found to govern the behaviour of piles during cyclic loading. The experimental and numerical investigation was presented to find the settlement of the sand due to the cyclic twisting of a tube (Cudmani and Gudehas 2001). An analytical solution was developed to investigate the dynamic torsional response of the end-bearing pile in a saturated poroelastic medium (Wang et al. 2008). A numerical model was based on the boundary element approach for predicting the pile-soil interactive performance under torsional cyclic load (Basack and Nimbalkar 2017).

2.2.3 Pile Groups Subjected to Torsional Loads

Three diameter-spaced fixed-head pile groups subjected to torsion were examined in a series of model tests (Kong 2006, Kong and Zhang 2008). He observed that the pile group subjected to torsion simultaneously mobilises lateral and torsional resistances of individual piles. The torsional resistance is elusively approximated among 20% or more while 80% or less of torsional energy depends upon the mobilisation of lateral resistance related to pile locations within the group and pile-soil interactions. The program was introduced for the determination of the nonlinear response of the pile groups to torsional loading (Basile 2010). An analytical solution is presented to analyse the torsional response of pile groups and validated with the results of the centrifuge model tests (Chen et al. 2016). It was based upon the complete BEM solution of the soil continuum which uses the simple hyperbolic soil model offering the prospect of more realistic predictions and more effective design techniques. The test setup was proposed to impart torsional loads on pile groups (Mehra and Trivedi 2018). A series of experiments were reported on a single pile and pile groups subjected to static torsional loads. An empirical approach was introduced to analyse the nonlinear response of the pile group with arbitrarily distributed piles subjected to combined lateral and torsional loading (Kong et al. 2020).

2.2.4 Pile Groups Subjected to Cyclic Torsional Loads

The analysis of single piles and pile groups and laboratory experiments were performed subjected to dynamic horizontal loads (Novak 1911). The investigations were performed to find the resistance of the soil to the horizontal vibrating pile. An analytical solution was presented for a coupled response involving horizontal translation, rocking and torsion. For footings partially embedded into a semi-infinite medium or a stratum (Novak and Sachs 1973). An analytical solution is presented to obtain the formulas for dynamic damping and

stiffness of piles (Novak 1974). The soil was modelled as a linear viscoelastic layer with hysteretic material damping (Nogami and Novak 1977). The dynamic experiments were performed on a large group of small closely spaced piles in the field. The results from the experimental observations were compared with the theoretical predictions for vertical and horizontal responses (Novak and Sharnouby 1984). The literature reported is mainly focused on the generic behaviour of pile groups subjected to torsion while the cyclic torsion effect has not been considered. The centrifuge modelling of single piles and pile groups was conducted to investigate the influence of cyclic axial loads on the performance of piled foundations (Li et. al. 2012).

2.3 Gaps in Studies and Conclusions

The summary of the estimation of the torsional pile capacity and gaps in the literature were identified based on the search criteria as used in Section 2.2 and presented in Table 2.1. The following areas of research remain elusive and need to be investigated further:

- The previous studies were performed on the geomaterial without considering the flow potential of the flow controlled geomaterial.
- The progressive twist, displacement and torsional energy around the pile groups.
- The coupling effect of the axial and the torsional loading on the pile groups.
- The cyclic degradation parameters of the flow controlled geomaterial for the pile groups subjected to torsional loads.
- The surface displacement of the geomaterial due to cyclic torsional loading on the pile groups.

Table 2.1 Summary of Estimation of Torsional Pile Capacity and Gaps in Literature

Description	Gaps
Method to analyse torsionally loaded piles in elastic media[a]	Limited to the single pile and static torsional load
Torsional moments are generated due to the eccentricity of loads in laterally loaded piles[b]	Without the application of cyclic torsional load
Developed discrete element models to analyze torsionally loaded piles[c]	Limited to the single pile and static torsional load
Developed discrete element models to analyze torsionally loaded piles[d]	Limited to the single pile and static torsional load
Analyzed piles subjected to the combined action of axial force and torsion[e]	Limited to a single pile
Obtained analytical and numerical solutions for the torsional response of piles[f]	Limited to static torsional load and single pile
Developed a numerical method combining the subgrade-reaction and continuum approaches to analyse torsionally loaded pile groups[g]	Without the application of cyclic torsional load
An analytical solution was developed for torsionally loaded piles[h]	Limited to static torsional load
Numerical solution of single pile subjected to cyclic torsional load[i]	Without consideration of group action
An approach to analyse the nonlinear behaviour of pile groups[j]	No experimental work

[a] Poulos (1975), [b]Randolph (1981b), [c]Dutt and O'Neill (1983), [d]Chow (1985), [e]Georgiadis (1987) and Georgiadis and Saflekou (1990), [f]Guo and Randolph (1996), [g]Kong (2006) and Kong and Zhang (2008), [h]Zhang (2010), [i]Basack and Nimbalkar (2017), [j]Kong et. al. (2020)

References

Basile, F. (2010). “Nonlinear Analysis of Torsionally Loaded Pile Groups.” Soils and Foundations, 50(2), 337-340.

Basack, S., & Nimbalkar, S. (2017). “Numerical solution of single pile subjected to torsional cyclic load.” Int. J. Geomech., 17(8), 04017016.

Chow, Y. K. (1985). “Torsional response of piles in nonhomogeneous soil.” Journal of Geotechnical Engineering, 111(7), 942-947.

Chen, S. L., Kong, L. G., & Zhang, L. M. (2016). “Analysis of pile groups subjected to torsional loading.” Computers and Geotechnics, 71, 115-123.

Cudmani, R., & Gudehus, G. (2001). “Settlements of sand due to cyclic twisting of a tube.” In IUTAM Symposium on Theoretical and Numerical Methods in Continuum Mechanics of Porous Materials: Proceedings of the IUTAM Symposium held at the University of Stuttgart, Germany, September 5–10, 1999 (pp. 387-396). Dordrecht: Springer Netherlands.

Dutt, R. N., & O'Neill, M. W. (1983). “Torsional behaviour of model piles in sand.” In Geotechnical practice in offshore engineering (pp. 315-334). ASCE.

Georgiadis, M. (1987). “Interaction between torsional and axial pile responses.” International Journal numerical and analytical methods in geomechanics, 11(6), 645-650.

Georgiadis, M., & Saflekou, S. (1990). “Piles under axial and torsional loads.” Comput. Geotech., 9(4), 291-305.

Guo, W. D., & Randolph, M. F. (1996). “Torsional piles in non-homogeneous media.” Comput.Geotech., 19(4), 265-287.

Hache, R. A. G., & Valsangkar, A. J. (1988). “Torsional resistance of single pile in layered soil.” J. Geotech. Eng., 114(2), 216-220.

Kong, L.G. (2006). “Behavior of pile groups subjected to torsion.” PhD Thesis, Hong Kong University of Science and Technology, Hong Kong, 339p.

Kong, L.G. and Zhang, L.M. (2008). “Experimental study of interaction and coupling effects in pile groups subjected to torsion.” Canadian Geotech. J., 45, 1001-1017.

Kong, L. G., Zhang, Z. C., and Chen, Y. M. (2020). “Nonlinear analysis of pile groups subjected to combined lateral and torsional loading.” Journal of Zhejiang University-SCIENCE A, 21(3), 179-192.

Long, J. H., & Vanneste, G. (1994). “Effects of cyclic lateral loads on piles in sand.” Journal of Geotechnical Engineering, 120(1), 225-244.

Li, Z., Bolton, M. D., & Haigh, S. K. (2012). “Cyclic axial behaviour of piles and pile groups in sand.” Canadian Geotechnical Journal, 49(9), 1074-1087.

Menetrey, P., & Willam, K. J. (1995). “Triaxial failure criterion for concrete and its

generalization." Structural Journal, 92(3), 311-318.

Novak, M., & Sachs, K. (1973). "Torsional and coupled vibrations of embedded footings." Earthquake Engineering & Structural Dynamics, 2(1), 11-33.

Novak, M. (1974). "Dynamic stiffness and damping of piles." Canadian Geotechnical Journal, 11(4), 574-598.

Nogami, T., & Novak, M. J. E. E. (1977). Resistance of soil to a horizontally vibrating pile. Earthquake Engineering & Structural Dynamics, 5(3), 249-261.

Novak, M.; Sharnouby, B.E. (1984). "Evaluation of dynamic experiments on pile group." Journal of Geotechnical Engineering 1984, 110, 738–756.
Novak, M. (1991) Proceedings of Second International Conference on Recent Advances in Geotechnical Earthquake Engineering and Soil Dynamics, March 11-15, St. Louis, Missouri, Paper No. SOA14.

Mehra, S. & Trivedi, A. (2018). "Experimental studies on model single pile and pile groups subjected to torque." Proceedings of China-Europe Conference, Geotech. Engg., 10.1007/978-3-319-97115-5_24, 997-1000.

O'Neill (1964). "Determination of the pile-head torque-twist relationship for a circular pile embedded in clay soil." M.S. Thesis, University of Texas, Austin, Texas.

Poulos, H. G. (1975). "Torsional response of piles." Journal of Geotechnical Geoenvironmental Engineering, 101(10), 019-1035.

Poulos, H. G. (1982). "Single pile response to cyclic lateral load." Journal of the Geotechnical Engineering Division, 108(3), 355-375.

Poulos, H. G. (1989). "Cyclic axial loading analysis of piles in sand." Journal of Geotechnical Engineering, 115(6), 836-852.

Randolph, M. F. (1981). "Piles subjected to torsion." J. Geotech. Eng., 107(8), 1095-1111.

Wang, K., Zhang, Z., Leo, C. J., & Xie, K. (2008). "Dynamic torsional response of an end bearing pile in saturated poroelastic medium." Computers and Geotechnics, 35(3), 450-458.

3.0 PROGRESSIVE TWIST, DISPLACEMENT AND TORSIONAL ENERGY AROUND PILE GROUPS

This chapter is based on the work that has been listed in Section 1.8 and published in the International Journal of Geotechnical Engineering. To keep the presentation of the details consistent throughout the thesis, the details are offered here with some layout modifications.

3.1 Introduction

Torsional moments are transferred to the foundation due to the actions of wind and waves, ship impacts, moving trains, and electric transmission towers having lateral loads in high-tension wires. The torsional effects due to a single pile have been studied (Poulos 1975, Randolph 1981, Hache and Valsangkar 1988, Rajapakse 1988). The analytical solutions for the laterally loaded piles (Reese and Van Impe 2001) and the piles subjected to torsional loads (O'Neill 1964; Dutt and O'Neill 1983; Militano and Rajapakse 2008; Wang et. al.; Zheng et. al. 2014 and Wu et. al. 2016) have been studied. The solutions were obtained for the torsional response of piles in two-layered soil (Guo and Randolph 1996; Guo et al. 2007); interaction between torsional and axial pile responses (Georgiadis 1987) and the discrete element approach was presented for the analysis of the torsional response of pile in nonhomogeneous soils (Chow 1987). The boundary element method was considered to analyse pile groups subjected to torsion (Basile 2010). The numerical method was developed to analyse torsionally loaded pile groups (Kong 2006; Kong and Zhang 2008, 2009; Kong et.al. 2020). According to Kong and Zhang (2009), a pile group subjected to torsion simultaneously mobilises the torsional and lateral resistance of individual piles. Speculatively, the torsional resistance is elusively approximated among 20% or more while 80% or less of torsional energy depends upon the mobilisation of lateral resistance related to pile locations within the group and pile-soil interactions. Currently, there is no numerical

scheme available so far to precisely evaluate the magnitude of torsional and lateral resistance. The present numerical scheme estimates the components of torsional energy associated with progressive twist and displacement in the range of 0.43-0.50 and 0.50-0.57 respectively. The practice in design offices is usually based on ignoring the stiffness of the soil and only the stiffness of the pile is taken into account (Das and Luo 2016) without the consideration of progressive failure. The numerical concept of progressive failure was initially applied to the shallow foundations by a couple of investigators (Parkins and Madson, 2000; Trivedi and Sud, 2007).

In view of the arguments, a series of experiments were reported on a single pile and pile groups subjected to torsional loads. Mehra and Trivedi (2018) proposed a test set-up to impart torsional loads on pile groups (i, j) as shown in Figure 3.1. The combination of axial, torsional and associated lateral loads was considered in a resultant form. Further to it, the numerical model was developed for the pile groups subjected to combined axial and torsional loads in flow-controlled geomaterials (Mehra and Trivedi, 2021). It considered the pile groups for the combined effect of axial and torsional loads on twist and displacement using a stiffness matrix of 12 x 12. The actual loading conditions of pile groups are complex. The pure torsional loads as considered in this study are a special condition which needs to be examined over and above the earlier studies. Even though some analytical methods are available for vertically and torsionally loaded piles, the solutions for pile groups characterized by torsional energy zones are elusive. The experiments are performed on symmetrical (1,1; 2,2) and asymmetrical pile groups (1,2; 1,3) in loose and relatively homogeneous sand. A novel numerical formulation is proposed to incorporate pile-soil interactions for pile groups subjected to torsional loads. Based on the numerical formulation, the three-dimensional finite element models of pile groups are developed to analyse the torque-twist relationship and compare it with the experimental

observations. The soil undergoes the formation of heave and cavity as a result of the torsional energy zones set into the soil. The displacement in the direction and opposite to the twist along with heave and cavity formation has been captured to quantify the behaviour of pile groups. The results of the analysis of pile-soil interaction for pile groups subjected to torsional loads have been compared with displacement and twist of the single pile for design consideration.

Thus, it appears that a combination of the following activities takes place; (a) The physical observation that progressive twist and displacement, being defined in terms of the non-uniformity of shear zones and mobilised torsional energy in the soil at the peak load, decreases, as the number of piles in the pile group increases; and (b) the potential for progressive twist and displacement, defined by the difference between the peak and effective torsional energy of the pile group, decreases as the shear modulus of soil surrounding pile group increases. The torsional energy of the pile group is equal to the work done by the external torsional load inclusive of the plastic energy. It is the area covered by the plot of normalized applied torque and twist rigidity factor for the pile groups. The twist rigidity factor is defined as the twist of the pile group relative to the single pile. It is difficult to predict the point at which one effect offsets the other. The novelty in this paper is that the combination of these two effects can be described in terms of progressive twist and displacement, which are dictated by the shear modulus, confinement around the pile group and pile group geometry (number of piles in a group) characterised collectively by the torsional energy, twist and displacement rigidity factors.

3.2 Experimental Investigation

A test set-up has been fabricated to impart torque on pile groups (i, j) as shown in Figure 3.1. The essential components of the test setup include a pulley for hanging weights,

vertical suspension, connecting shaft and ancillary devices. The pile groups (1,2; 1,3; 2,2) with individual steel piles were fabricated. The diameter and length of the individual steel piles were 40 mm and 600 mm respectively. The distance between the individual piles was kept at $3D_p$, where D_p is the diameter of the individual pile. The pile group was installed in the soil chamber. The loose sand was deposited into the chamber under controlled conditions. Afterwards, the torsional load was applied to the pile group while monitoring the twist at the pile cap.

The torsional loading is applied through the pulley (Figure 3.1) for hanging weights (I) by the way of using components, high tensile wire (II) and gears (IX). The loading machine consists of vertical suspension (IV) and supporting frame (V) supported on the girder (III) and fixed using high tensile bolts. The holes were drilled on the girder (III) at equivalent spacing for moving the girder to any convenient location. The connecting shaft (VI) has been fixed on the pile cap (VII) and the torsional moment has been transferred assuming no force dissipation due to friction between the components of the loading machine. The torsional moment with different configurations of pile groups (VIII) may be varied using a connecting shaft. The pile groups, and disc for the angle of twist (XII) and shaft (VI) have been connected by couplers and bolts. The torque from the model tests has been placed into the numerical model to execute a computational program to capture the numerical results. The experimental results of the torque-twist relationship for the single pile and the pile groups (1,2; 1,3; 2,2) have been obtained for the geomaterial.

3.3 Interaction of Pile Group and Soil

3.3.1 Pile Zone

The pile groups have been connected by a rigid pile cap to have a fixed head connection.

The free-standing pile group in which the pile cap is not in contact with the underlying soil has been selected to examine the behaviour of pile groups (Poulos and Davis 1980).

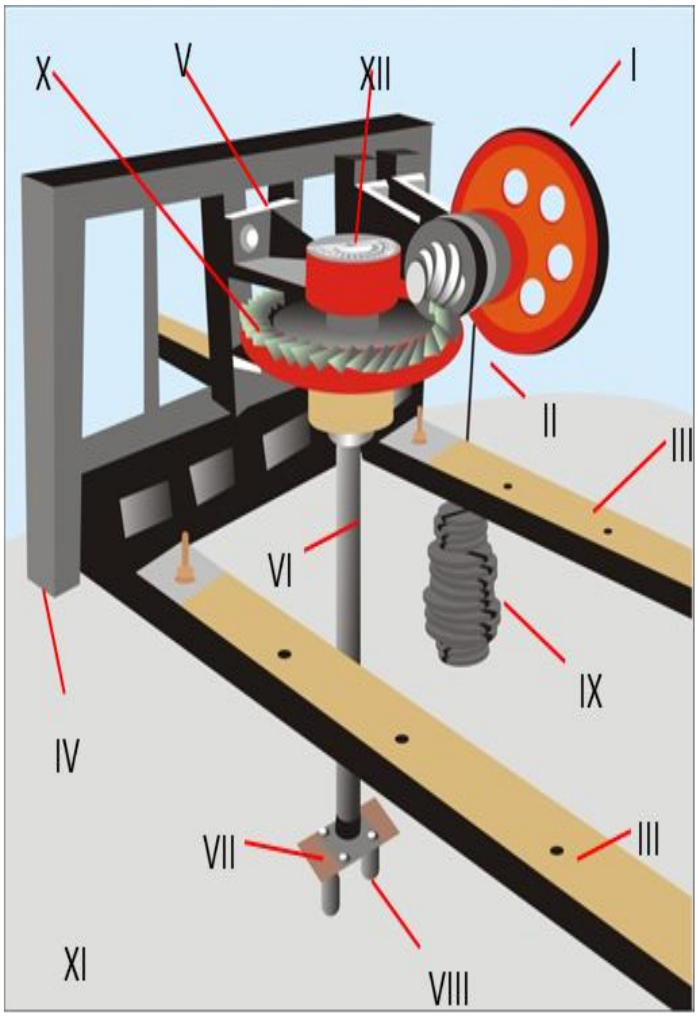

Figure 3.1 Test set-up fabricated to impart torque on pile groups (i, j)

The pile group subjected to torsional loads at the centre simultaneously deploy lateral and torsional resistance of the individual pile. The piles in a group have been represented by (p-y) and (τ-θ) curves. Therefore, the governing fourth and second-order differential equilibrium equations (Poulos and Davis 1980, Chow 1985) for lateral displacement (y) and twist angle (θ) of the pile are expressed as follows:

$$-E_P I_P \left(\frac{\partial^4 y}{\partial z^4}\right) + k_h\, y = 0 \tag{3.1}$$

$$-G_P J_P \left(\frac{\partial^2 \theta}{\partial z^2}\right) + k_\theta\, \theta = 0 \tag{3.2}$$

where E_p and G_p are the elastic and shear modulus of the pile shaft, respectively; I_p and J_p are the second moment and polar second moment of the area of the pile section, respectively; $G_P J_P$ is the torsional rigidity of the pile; z is the depth; k_h and k_θ are the modulus of subgrade reaction for lateral and torsional loading, respectively.

The numerical pile group model is shown in Figure 3.2a. When the torsional load is applied, the individual pile in a pile group is subjected to the lateral load, bending moment, and torsional load. Every pile in a pile group is assumed as an elastic beam that has been divided into n-segments (Figure 3.2b). Using the Galerkin element method (Hutton 2004), an approximation of the displacement field $\delta(z)$, is expressed as follows:

$$\delta(z) = N_1(z)\,\delta_1 + N_2(z)\,\delta_2 + N_3(z)\,\delta_3 + N_4(z)\,\delta_4 + N_5(z)\,\psi_5 + \tag{3.3}$$

$$+N_6(z)\,\psi_6 + N_7(z)\,\psi_7 + N_8(z)\,\psi_8 + N_9(z)\,\theta_9 + N_{10}(z)\,\theta_{10}$$

$$= [N]\{\theta\}$$

$$[N] = [N_1\ N_2\ N_3\ N_4\ N_5\ N_6\ N_7\ N_8\ N_9\ N_{10}] \tag{3.4}$$

$$\{\delta\} = \{\delta_1 \delta_2\ \delta_3\ \delta_4\ \psi_5\ \psi_6\ \psi_7\ \psi_8\ \theta_9\ \theta_{10}\} \tag{3.5}$$

where N_m are the shape functions and are used for interpolation $\delta(z)$ using its nodal values.

$$N_1 = N_2 = 1 - 3\varsigma^2 + 2\varsigma^3 \tag{3.6}$$

$$N_3 = N_4 = 3\varsigma^2 - 2\varsigma^3 \tag{3.7}$$

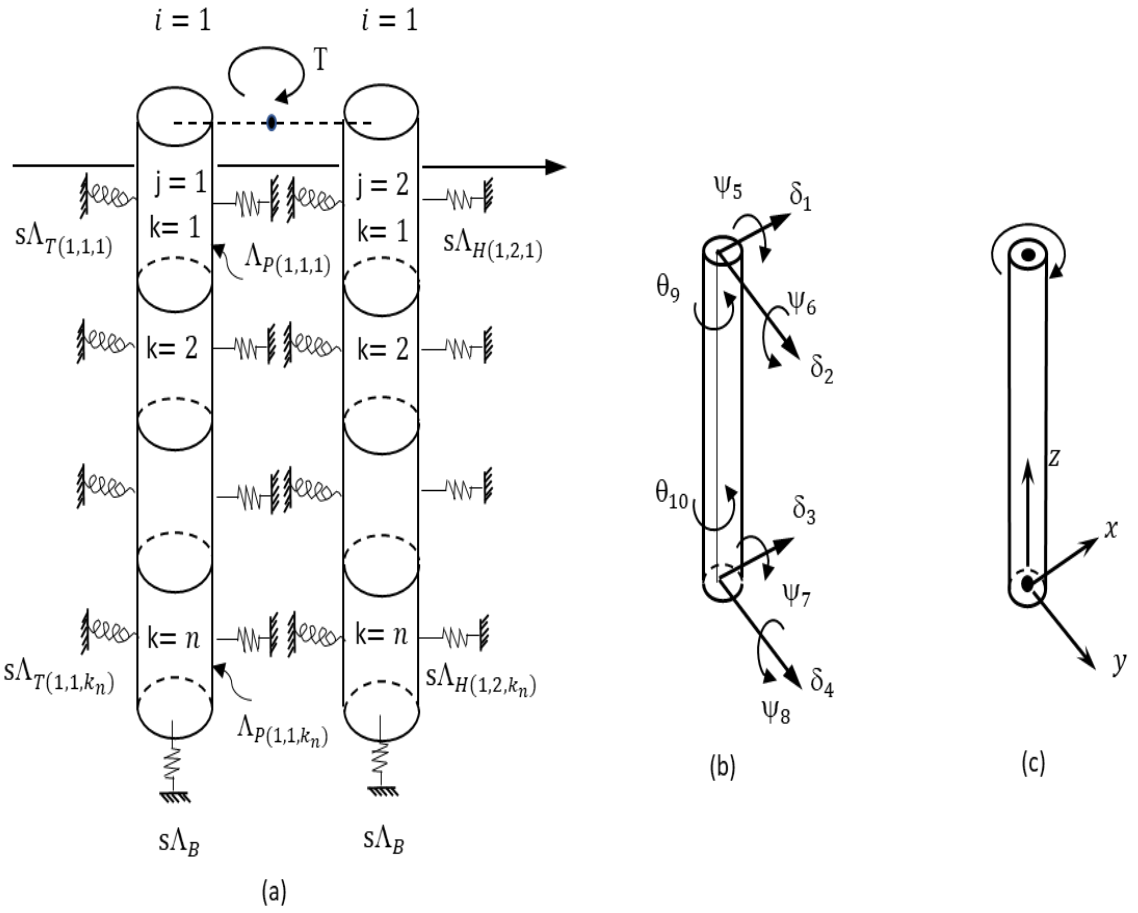

Figure 3.2(a) Pile group subjected to torsional loads with pile stiffness ($\Lambda_{P(i,j,k_n)}$), soil torsional spring ($s\Lambda_{T(i,j,k_n)}$), soil lateral spring ($s\Lambda_{H(i,j,k_n)}$) and base soil spring ($s\Lambda_B$) at node (b) The pile element, node and degree of freedom for the torsional loads are represented by four translational ($\delta_1, \delta_2, \delta_3, \delta_4$), four rotational ($\psi_5, \psi_6, \psi_7, \psi_8$), and two torsional ($\theta_9$ and θ_{10}) (c) twist about z-axis

$$N_5 = N_6 = L(\varsigma - 2\varsigma^2 + \varsigma^3) \tag{3.8}$$

$$N_7 = N_8 = L\,\varsigma^2(\varsigma - 1) \tag{3.9}$$

where $\varsigma = \frac{z}{L}$. The nodal values $\{\delta_1 \delta_2\, \delta_3\, \delta_4\, \psi_5\, \psi_6\, \psi_7\, \psi_8\, \theta_9\, \theta_{10}\}$ are the unknowns and are determined from the global equation system. The Galerkin residual equation for the finite element of length L is expressed as follows:

$$\int_0^L N_m(z)\left[\frac{d^2}{dz^2}\left(EI\frac{d^4\delta}{dz^4}\right)\right]=0 \qquad m=1,2,5,6; n=3,4,7,8 \tag{3.10}$$

Integrating by parts and rearranging Eq. (10), the pile element matrix (Mehra and Trivedi 2021) is expressed as follows:

$$[\Lambda_{PP}]=EI\int_0^L \frac{d^2N_m}{dz}\frac{d^2N_n}{dz}dz \tag{3.11}$$

Similarly, considering the torsional element (Figure 3.2 c), the pile element matrix is expressed as follows:

$$[\Lambda_{PT}]=GJ\int_0^L \frac{dN_m}{dz}\frac{dN_n}{dz}dz \qquad m=9; n=10 \tag{3.12}$$

$$[N]=[N_9\ N_{10}] \tag{3.13}$$

$$\{\theta\}=\{\theta_9\ \theta_{10}\} \tag{3.14}$$

$$N_9=1-\frac{Z}{L};\ N_{10}=\frac{Z}{L} \tag{3.15}$$

3.3.2 Soil Zone

The hyperbolic representation of stress-strain curves is a convenient and useful means of representing the nonlinearity of the soil stress-strain behaviour. Moreover, it is further supported by the nonlinear finite element to use a hyperbolic relationship. The nonlinear relation for the soil in the near field is assumed with the hyperbolic correlation (Duncan and Chang 1970) between τ and γ, and is expressed as follows:

$$\tau = \frac{\gamma}{\frac{1}{G_s} + \frac{R_f}{\tau_u}\gamma} \tag{3.16}$$

where G_s is the initial shear modulus; R_f is the reduction factor varies between 0.8 to 1 (Randolph 2003); τ and τ_u are the shear stress and ultimate shear stress of the soil respectively, and γ is the shear strain. A lumped mass of soil in the near field has been assumed to be morphed and imposed on each pile node. Each node has been attached with two springs (a lateral translational spring; and a torsional spring). The base springs have been attached at the end to model the soil response at the base. The initial stiffness of the torsional spring (Mehra and Trivedi, 2021) at a node has been related to parameters inside the yield surface and is expressed as follows:

$$\left[s\Lambda_{T_e}\right] = k_\theta \int_0^L \frac{dN_m}{dz}\frac{dN_n}{dz}dz \tag{3.17}$$

The resulting stiffness of the torsional spring at each node has been related to the yield flow parameters and is expressed as follows:

$$\left[s\Lambda_{Tf}\right] = f\left(\mathrm{s}\Lambda_{\mathrm{Te}}, \mathrm{s}\Lambda_{\mathrm{Tp}}\right) = (k_\theta f(G_{se})) \int_0^L \frac{dN_m}{dz}\frac{dN_n}{dz}dz \tag{3.18}$$

where $k_\theta = \pi D_p^2 G_{se} L$, $(s\Lambda_{T_e})$ = stiffness as long as $f = 0$, $(s\Lambda_{T_p})$ = flow-controlled stiffness, D_p is the pile diameter, G_{se} is the equivalent shear modulus of the soil at a node (Mehra and Trivedi 2021). Similarly, the initial and resulting stiffness of the lateral translational spring at a node is expressed as follows:

$$\left[s\Lambda_{H_e}\right] = k_h \int_0^L \frac{dN_m}{dz}\frac{dN_n}{dz}dz \tag{3.19}$$

$$\left[s\Lambda_{Hf}\right] = f\left(\mathrm{s}\Lambda_{\mathrm{He}}, \mathrm{s}\Lambda_{\mathrm{Hp}}\right) = \left(k_h\, f(G_{se})\right) \int_0^L \frac{dN_m}{dz}\frac{dN_n}{dz}dz \tag{3.20}$$

where $k_h = \frac{P}{y}$, $P\ and\ y$ are the lateral soil reaction per unit length of the pile and lateral displacement of the pile respectively. The pile base spring is modelled using the bearing capacity theory (Poulos 1975). The torsional base spring is not considered in the present analysis as its contribution to the response of long piles is insignificant (Poulos 1975).

3.4 Torsional Energy and Energy Zones

Torsional energy is a potential active area among scientists, engineers, and practitioners. The immense complexities of the soil-pile group interaction system are yet to be resolved and modelled adequately with field applications. In the present study, the torsional energy-induced twist response of a pile group is captured using a numerical program. The torsional energy zones are divided into the near and far-field zones. The soil element is considered linear elastic in the far fields while it tends to accumulate plastic deformations in the near fields. The interaction between lateral resistances of piles in the group has been considered using Mindlin's (1936) solution. The effect of lateral movement of a pile on the lateral behaviour of other piles in a group or the shadowing effect (Brown et al. 1988) is present in torsionally loaded pile groups as observed during the tests. However, the interaction effects in pile groups subjected to torsion or lateral loading are significantly different as the directions and magnitudes of lateral movements of piles in a group subjected to torsion are varied. The interaction between the torsional resistance of the piles in a group (k_{TT}) is negligible (Poulos 1975). The interaction between the torsional and lateral resistance of

piles in a group has been considered through Randolph's (1981) analytical solution for torsionally loaded single piles. The distance from the centre of the pile shaft to a point in the same soil layer is $r(r \geq D_p/2)$, the circumferential soil displacement of a point δ_c $(i = 1; j = 1; k = 1)$ which is expressed as follows:

$$\delta_{c_{(1,1,1)}} = \frac{\tau D_P^2}{8 G_S r} \tag{3.21}$$

Assuming the torsional shear stresses are lumped at the corresponding pile node, the induced circumferential displacement at the adjacent pile $(i = 1; j = 2; k = 1)$ is expressed as follows;

$$\delta_{c_{(1,2,1)}} = \frac{T_{(1,1,1)}}{4\pi G_s s L_1} \tag{3.22}$$

where s is the centre-to-centre spacing between the two piles; L_1 is the thickness of the corresponding soil layer (pile element length) and lumped torque at a node $i = 1;\ j = 1; k = 1$ is expressed as follows:

$$T_{(1,1,1)} = \frac{\pi \tau D_S^2 L_1}{2} \tag{3.23}$$

Therefore, stiffness at a node $(i = 1; j = 2; k = 1)$ due to the lateral constituent of soil deformation due to unit torsional load at a node $(i = 1; j = 1; k = 1)$ on another pile is expressed as follows:

$$k_{HT} = k_{TH} = \frac{T_{(1,1,1)}}{\delta_{c_{(1,2,1)}}} = 4\pi G_S s L_1 \tag{3.24}$$

where, k_{TH}, is the stiffness at a node $(i = 1; j = 2; k = 1)$ of a torsional constituent of soil deformation due to unit lateral load at a node $(i = 1; j = 1; k = 1)$ on another pile. The far field is characterized by the distance of soil elements from the centre of the pile group. A negligible energy effect is considered for the far field. The near fields are normally associated with high energy concentration while far fields are largely elastic. The equilibrium equation for pile-soil element related to yield flow parameters considering Eq. (3.1-3.24) is expressed as follows:

$$\{\mathrm{T}\} = \begin{bmatrix} EI\int_0^L \frac{d^2N_m}{dz}\frac{d^2N_n}{dz}dz + GJ\int_0^L \frac{dN_m}{dz}\frac{dN_n}{dz}dz + \\ \left(k_\theta + k_\theta f(G_{se})\right)\int_0^L \frac{dN_m}{dz}\frac{dN_n}{dz}dz + \\ \left(k_h + k_h f(G_{se})\right)\int_0^L \frac{dN_m}{dz}\frac{dN_n}{dz}dz + k_{HT} + k_{TH} \end{bmatrix}\{\delta\} \tag{3.25}$$

$$\{\delta, \psi, \theta\} = \left\{\delta_1\delta_2\delta_3\delta_4\psi_5\psi_6\psi_7\psi_8\theta_9\theta_{10}\right\} \tag{3.26}$$

$$\{\mathrm{T}\} = \left\{\ P_{mx}P_{my}\ P_{nx}\ P_{ny}\ M_{mx}\ M_{my}\ M_{nx}\ M_{ny}\ T_m\ \ T_n\right\} \tag{3.27}$$

From the assembled group stiffness matrix and known load vector, overall equilibrium equations have been formulated. The load-deformation relationship of the pile-soil group system is expressed as follows:

$$\{\mathrm{T}\} = [\Lambda_P]\{d_p\} + [s\Lambda]\{\mathrm{d_s}\} \tag{3.28}$$

Where $[\Lambda_p]$ and $[s\Lambda]$ are the global stiffness matrix of all the elements of the pile groups and soil respectively; $\{d_p\}$ and $\{d_s\}$ are the vector of deformations at pile nodes and soil respectively; {T} is the torque applied on the pile group. Eq. 3.28 has been solved for unknown nodal displacements by Gauss elimination. The torsional energy of the pile group

is equal to the work done by the external torsional load inclusive of the plastic energy. Therefore, the torsional energy, E_T, of the pile-soil system is expressed as follows:

$$E_T = \left\{[\Lambda_P]\{d_p\} + [s\Lambda]\{\mathrm{d_s}\}\right\}.\{\theta\} \tag{3.29}$$

$$E_T = \left\{\begin{bmatrix} EI\int_0^L \frac{d^2N_m}{dz}\frac{d^2N_n}{dz}dz + GJ\int_0^L \frac{dN_m}{dz}\frac{dN_n}{dz}dz + \\ \left(k_\theta + k_\theta f(G_{se})\right)\int_0^L \frac{dN_m}{dz}\frac{dN_n}{dz}dz + \\ \left(k_h + k_h f(G_{se})\right)\int_0^L \frac{dN_m}{dz}\frac{dN_n}{dz}dz + k_{HT} + k_{TH} \end{bmatrix}\{\delta\}\right\}.\{\theta\} \tag{3.30}$$

3.5 Numerical Simulation and Validation

Three-dimensional finite element modelling acts as a valuable mechanism of load transfer from the pile to the surrounding soil, especially for pile groups. Therefore, several constitutive models have been executed with varying initial soil moduli to capture the torque-twist relationship for pile groups. The analysis has been executed using the numerical scheme shown in Eq. (3.1-3.30). The input parameters for numerical analysis of pile groups (1,1; 1,2; 1,3; 2,2) have been considered (Table 3.1).

Table 3.1 Input parameters for numerical analysis of pile groups

Pile group parameters	Pile groups (1,2) (1,3), (2,2)
Young modulus of pile material (E_p, GPa)	*210*
Poisson's ratio (μ_p)	*0.3*
Unit weight (γ_p, kN/m^3)	*78*
Diameter (D_p, mm)	*40*
Length (L_p, mm)	*650*
Pile-to-pile spacing (S_p, mm)	*3D_P*

The Mohr-Coulomb failure criterion has been adopted for the soil with instantaneous and maximum uniform initial shear modulus respectively ($G_{max} = 19.23$ MPa). The input parameters for the soil domain have been defined (Table 3.2).

Table 3.2 Input parameters for numerical analysis of soil

Parameter	Sand deposit
Initial shear modulus ratio (G_s/G_{max})	*0.1-1*
Maximum shear modulus considered (G_{max}, MPa)	*19.23*
Initial Poisson's ratio (μ_s)	*0.3*
Constant volume friction angle $(\emptyset_c$, degrees)	*30*
Dilation angle $(\emptyset_d$, degrees)	*14*
Friction coefficient between pile (master) and soil (slave)	*0.36*

The soil has been selected such that the flow potential for the yield surface is a hyperbolic function in the meridional stress plane and the smooth elliptic function in the deviatoric stress plane respectively (Menetrey and Willam 1995; Mehra and Trivedi 2021). The tetrahedral element has been considered for modelling pile groups (1,2; 1,3; 2,2) as shown in Figure 3.3 (a). The view of pile group (2,2) considers kinematic coupling constraint to incorporate the torsional loading effect in the computational model inclusive of the radial motion as shown in Figure 3.3 (b).

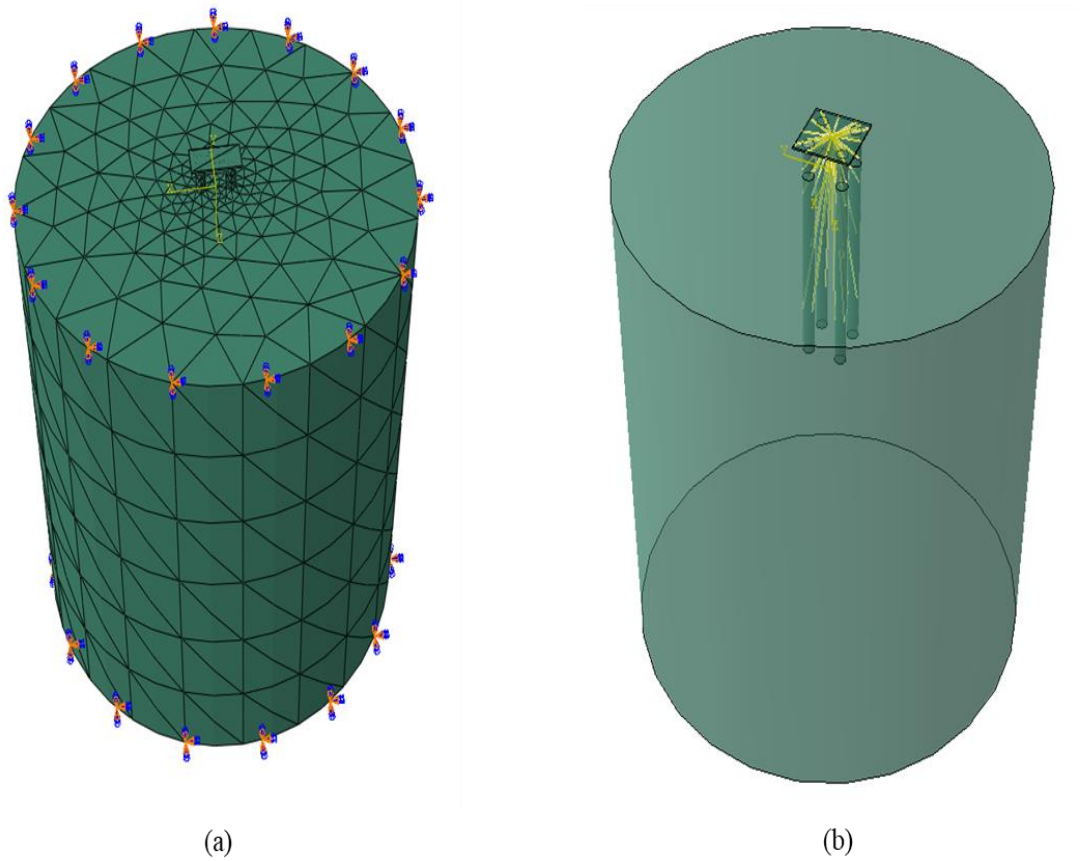

Figure 3.3(a) A numerical model for the soil-pile group considering tetrahedral elements and boundary conditions, (b) a view of the (2,2) pile group considering kinematic coupling constraint to incorporate the torsional loading effect in the computational model

The group of coupling nodes are constrained to the reference node using kinematic coupling constraint. A coarse and fine mesh has been considered for the soil and pile groups respectively. The colour scheme is selected to represent the magnitude of displacement, whereas the intensified colour schemes are for maximum displacement in cavity and heave zones respectively (Figure 3.4).

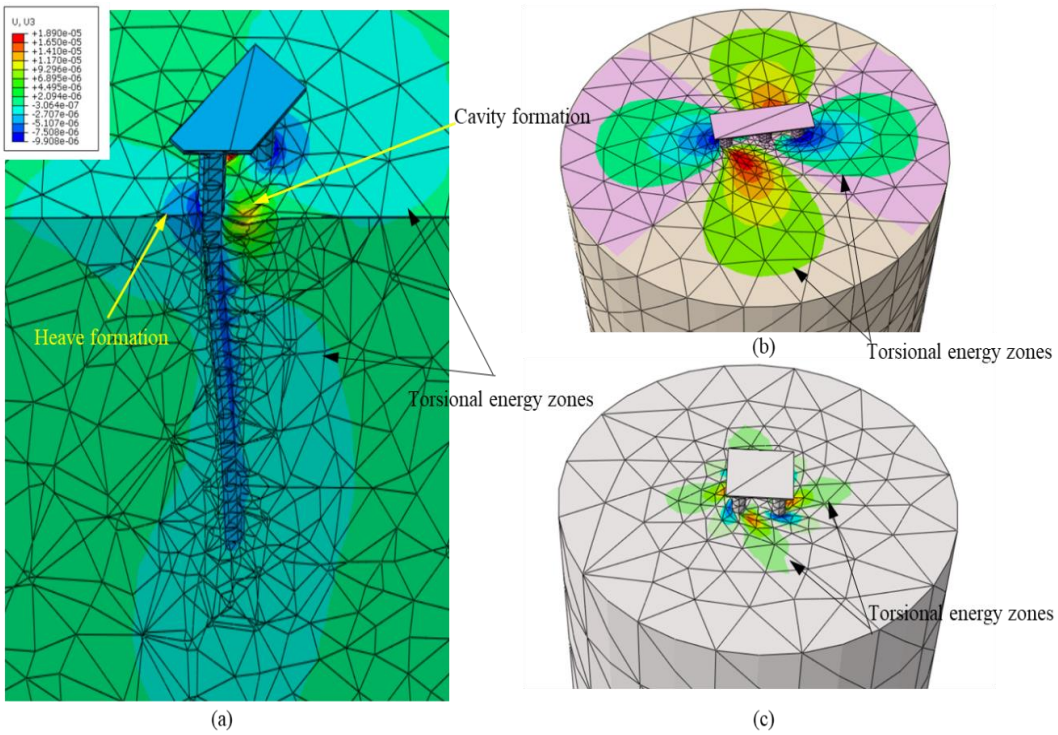

Figure 3.4(a) Sectional view of the pile group (1,2), (b) top view of the pile group (1,3), (c) top view of the pile group (2,2). The colour scheme is selected to represent the magnitude of displacement, where the red and blue colour schemes are for maximum displacement in cavity and heave zones respectively. The colour separators are used to distinguish the torsional energy zones

The program "PGTORQUE" is developed and computation is performed. The flowchart is described in Figure 3.5.

3.6 Results and Discussions

The torque-twist relationship of pile groups is an effort-some process. Having the plot between the normalized applied torque and twist rigidity factor for pile groups, we can predict the torque-twist relationship for the pile groups based on the experimental output of the torque-twist of a single pile. The variation of the normalized applied torque and pile group head twist has been shown in Figure 3.6-3.9.

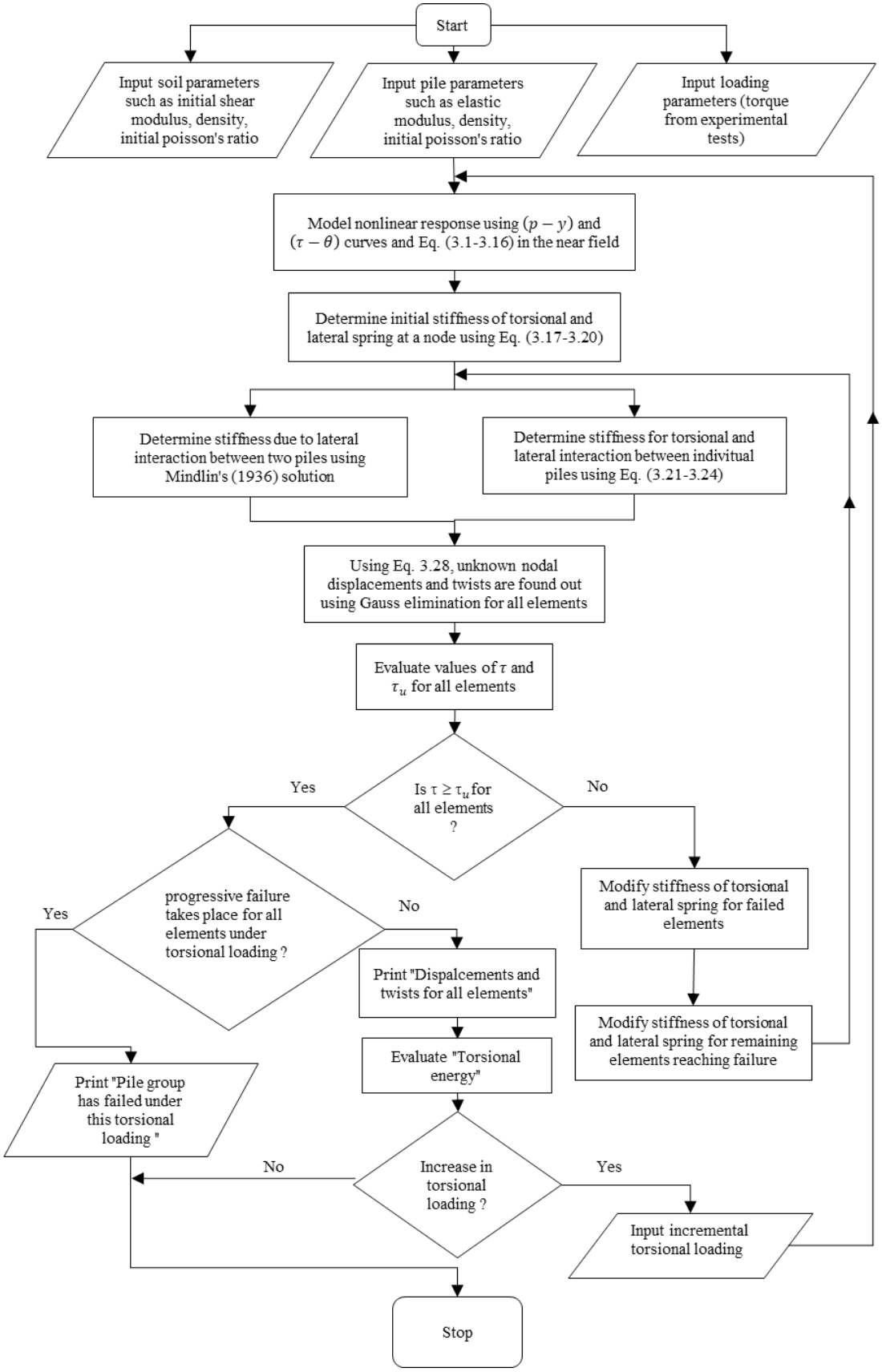

Figure 3.5 Flowchart for computation program "PGTORQUE"

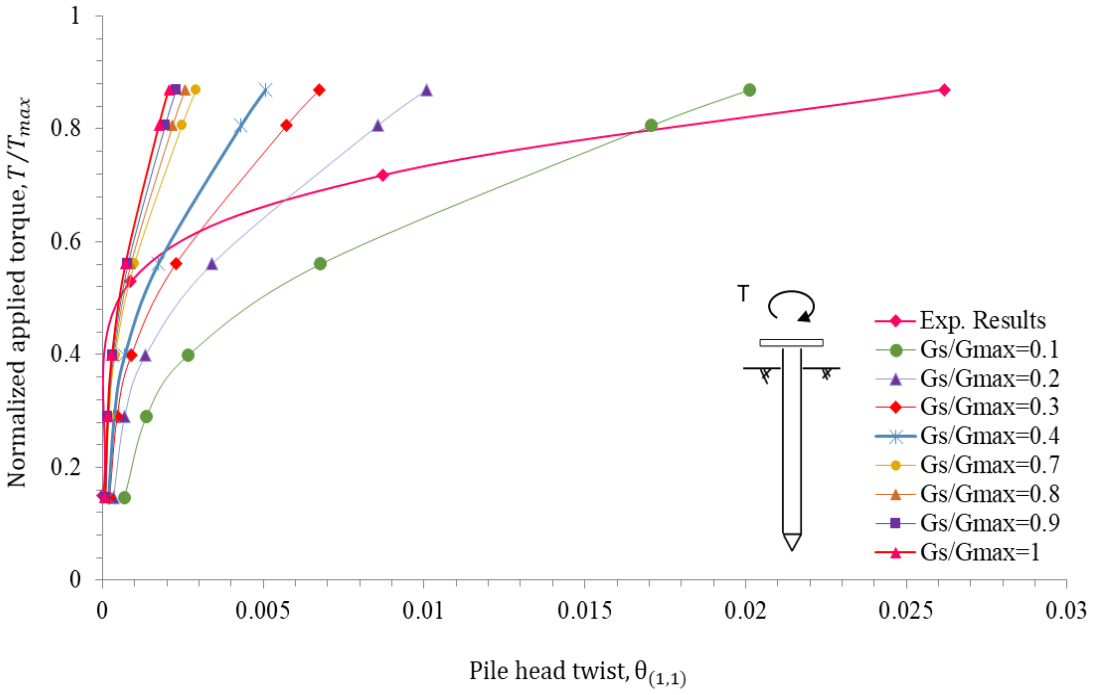

Figure 3.6 Variation of normalized applied torque with pile head twist for sand characterised by initial shear modulus ratio ranging from 0.1 to 1 for a single pile

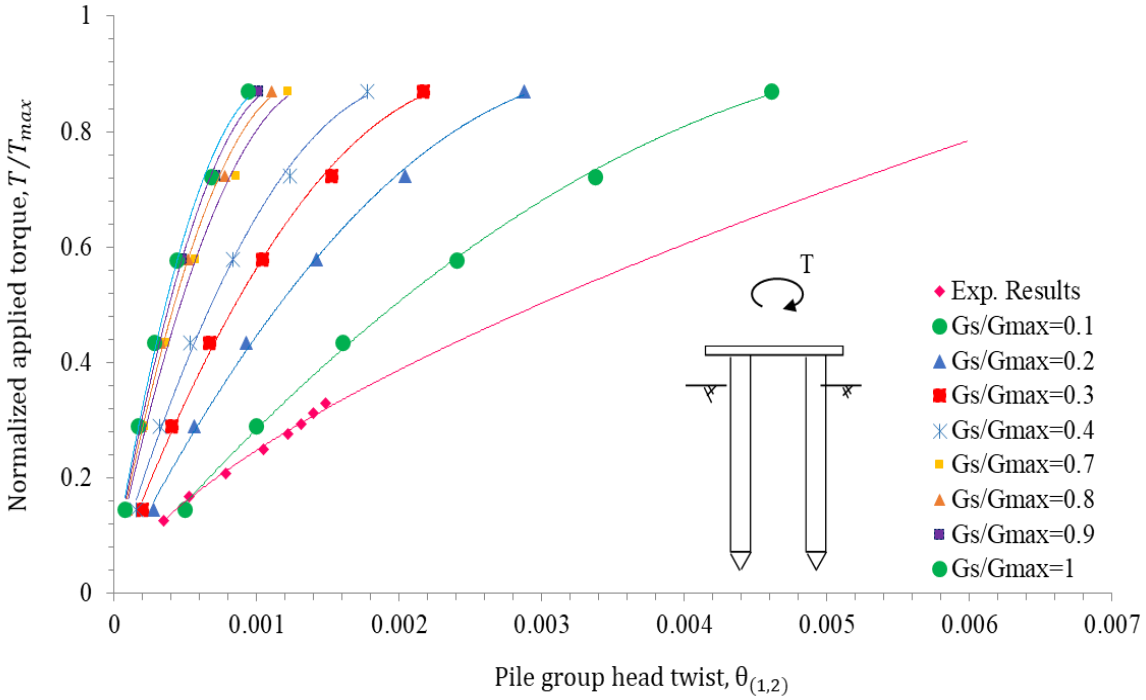

Figure 3.7 Variation of normalized applied torque with pile group head twist for sand characterised by initial shear modulus ratio ranging from 0.1 to 1 for pile group (i =1, j=2) compared with the experimental results

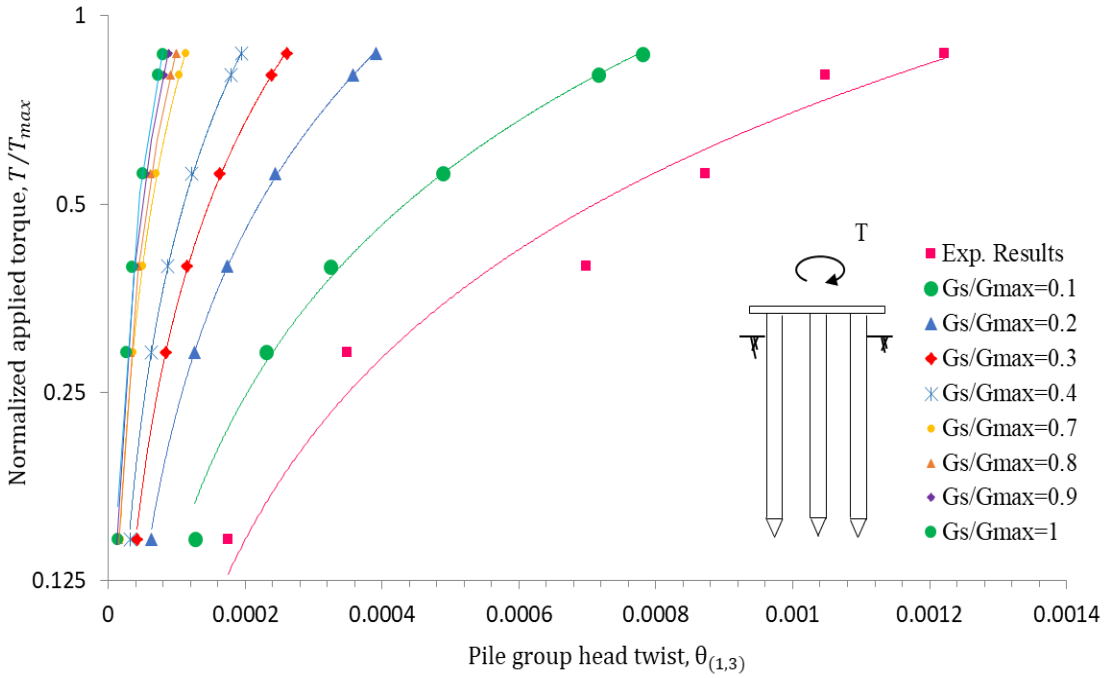

Figure 3.8 Variation of normalized applied torque with pile group head twist for sand characterised by initial shear modulus ratio ranging from 0.1 to 1 for pile group (i =1, j=3) compared with the experimental results

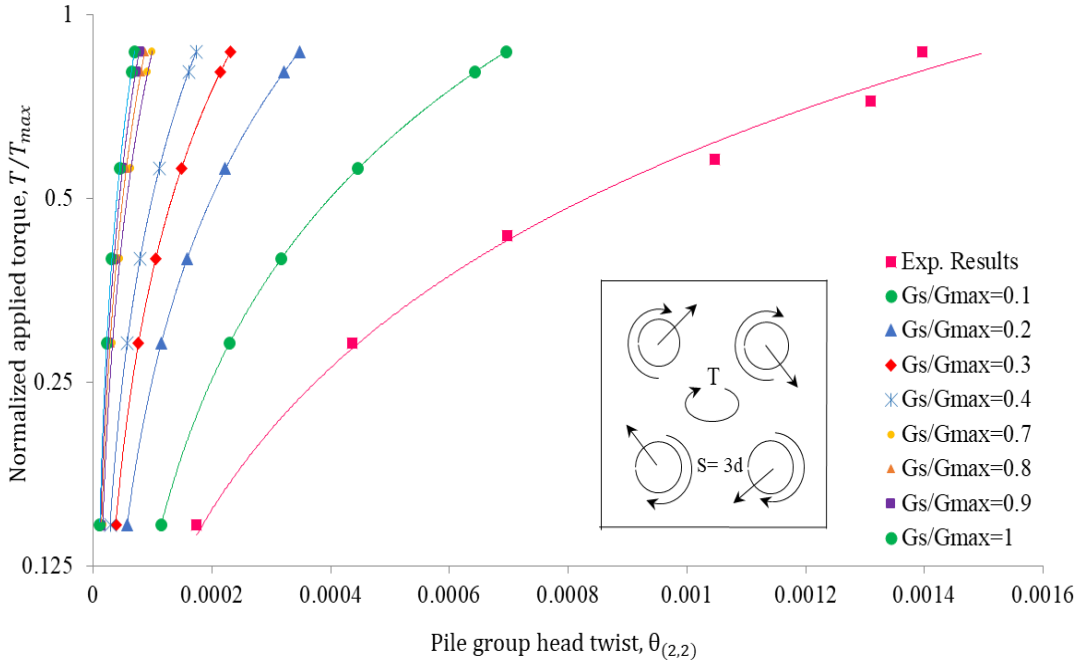

Figure 3.9 Variation of normalized applied torque with pile group head twist for sand characterised by initial shear modulus ratio ranging from 0.1 to 1 for pile group (i =2, j=2) compared with the experimental results

The normalized applied torque is defined by the instantaneous torque (T) to the maximum torque ($T_{max} = 100$ N-m) obtained from the model test. The three-dimensional finite element modelling has utilized the experimental results on the sand. The application of torque in the numerical model is described by the stiffness matrix of the pile elements in the pile group and soil such that cavity and heave formation of soil takes place in terms of displacement in three-dimensional space *(x, y, z)* in relation to the diameter of pile. A sample visual output of the numerical program for pile group (1,2; 1,3; 2,2) clearly shows the displacements with heave and cavity formations at the surface of the soil which has been presented in Figure 3.4 (a, b, c).

This output validates the simultaneous occurrence of heave and cavity formations of varying magnitude at the surface of the soil. The heave and cavity deformations are further classified as heave dominant deformation *(HDD;* $U^c < U^h$ *)* and cavity dominant deformation *(CDD;* $U^c > U^h$*)* has been shown in Table 3.3. As U^c/U^h is less than one, there is a greater heave deformation in the direction of the twist and smaller cavity deformation against the direction of the twist while U^c/U^h greater than one, there is a lesser heave deformation in the direction of the twist and a greater cavity deformation against the direction of the twist. The plots of normalized applied torque and twist rigidity factor characterised by torsional energy zones are shown in Figure (3.10-3.12) for a wide-ranging initial shear modulus ratio to show a distinct behaviour comprising of initial energy zone, transitional energy zone and flow energy zone which has been classified in Table 3.4. Similarly, the plots of normalized applied torque and displacement rigidity factor characterised by torsional energy zones are shown in Figure (3.13-3.15).

Table 3.3 Range of parameters for displacement in cavity dominant zones for pile groups

Pile group (i, j)	Normalized applied torque (T/T_{max})	Shear modulus ratio (G_s/G_{max})	Displacement direction	Displacement ratio in cavity zone $\left(\frac{U^c}{D_p}\right)x10^{-4}$	Displacement ratio in heave zone $\left(\frac{U^h}{D_p}\right)x10^{-4}$	U^c/U^{h*}
(1,2)	*0.1-1*	*0.1-0.4*	U_z	*0.7-7.80*	*0.67-4.7*	*1.03-1.66*
		0.7-1		*0.12-4.73*	*0.12-2.48*	*1.02-1.91*
(1,3)	*0.1-1*	*0.1-0.4*	U_z	*0.50-0.87*	*0.5-0.81*	*1.0-1.07*
		0.7-1		*0.07-0.46*	*0.07-0.34*	*1.0-1.36*
(2,2)	*0.1-1*	*0.1-0.4*	U_z	*0.21-0.32*	0.195-0.288	*1.08-1.11*
		0.7-1		*0.01-0.13*	0.028-0.121	*1.11-1.10*

U^c/U^h>1, cavity dominant; $U^c/U^h = 1$, cavity balances heave displacement; U^c/U^h<1, heave dominant

The flow energy zone corresponds to the flow potential on the yield surface of the flow-controlled soil. The flow potential is captured as a hyperbolic function of stresses in the meridional stress plane and the smooth elliptic function in the deviatoric stress plane (Mehra and Trivedi 2021). The extent of the energy concentration as marked by the coloured separators in Figure 3.4 (b-c) has been incorporated into the zone of the energy content displayed in Figure (3.10-3.13). These plots signify the excess torsional energy required to mobilise the group compared to the single pile. The pictorial representations are based upon the assumption of the tetrahedral shape of finite elements. However, if the shape of the element is other than the assumed, the extent of the energy concentration may not change significantly for the results shown in Figure 3.4 (a-c).

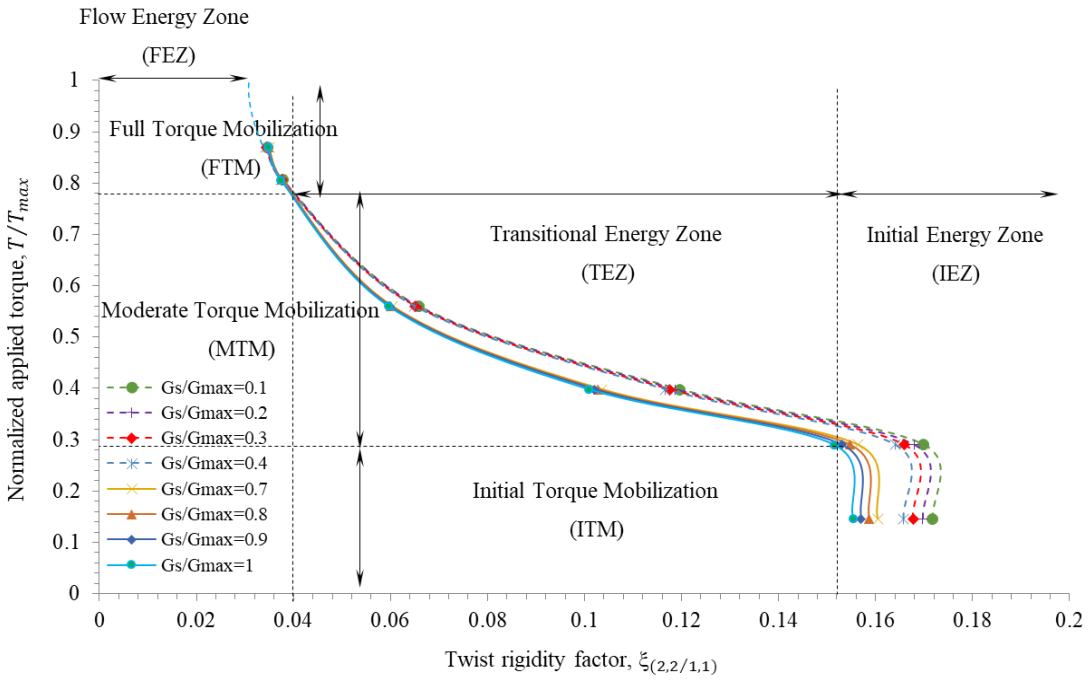

Figure 3.10 Variation of normalized applied torque with twist rigidity factor defined by a ratio of twist angle of the pile group (2,2 and 1,1) for sand characterised by different torsional energy zones

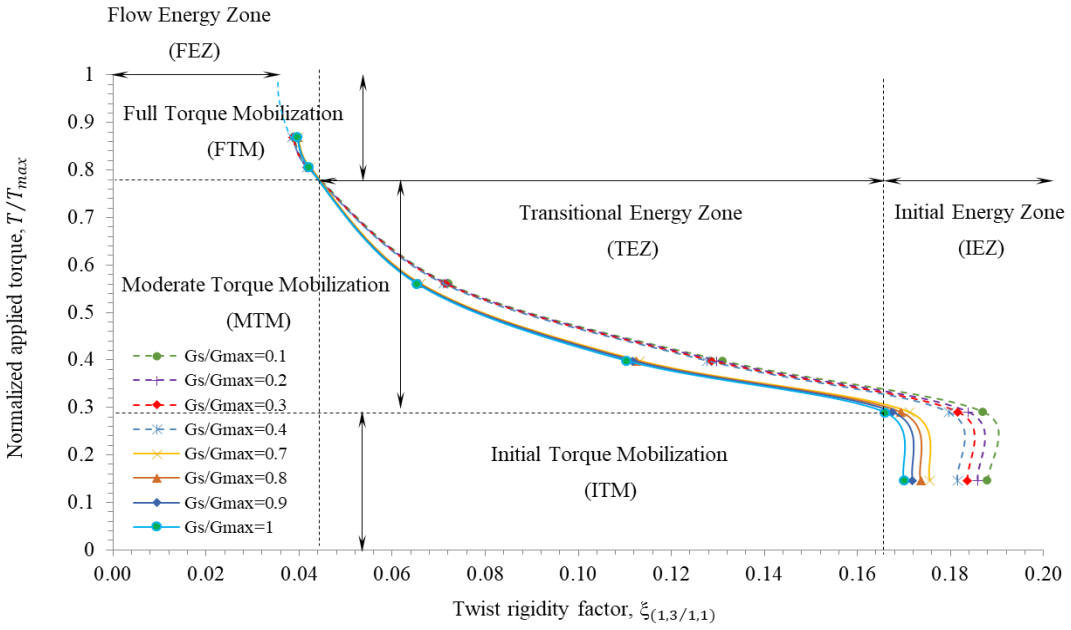

Figure 3.11 Variation of normalized applied torque with twist rigidity factor defined by a ratio of twist angle of the pile group (1,3 and 1,1) for sand characterised by different torsional energy zone

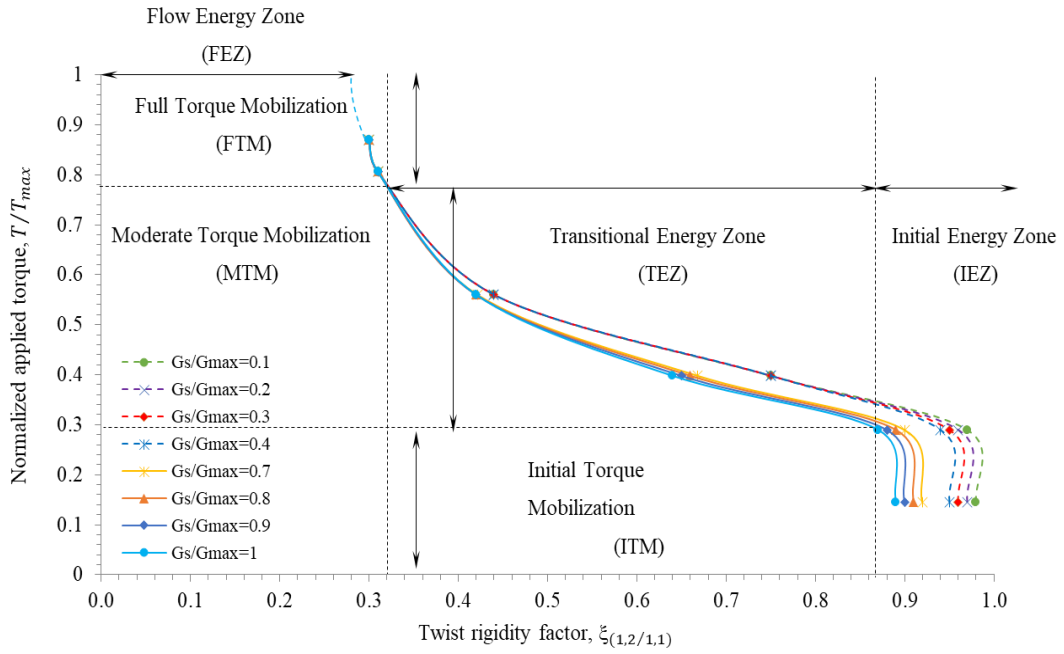

Figure 3.12 Variation of normalized applied torque with twist rigidity factor defined by a ratio of twist angle of pile group (1,2 and 1,1) for sand characterised by different torsional energy zones

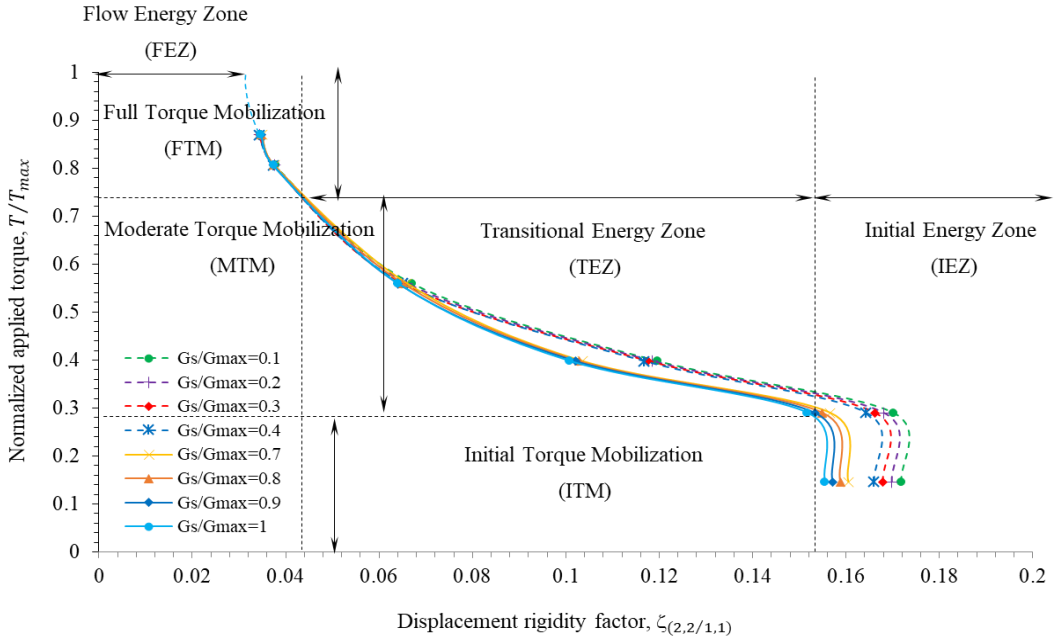

Figure 3.13 Variation of normalized applied torque with displacement rigidity factor defined by a ratio of resultant displacement of pile group (2,2 and 1,1) for sand characterised by different torsional energy zones

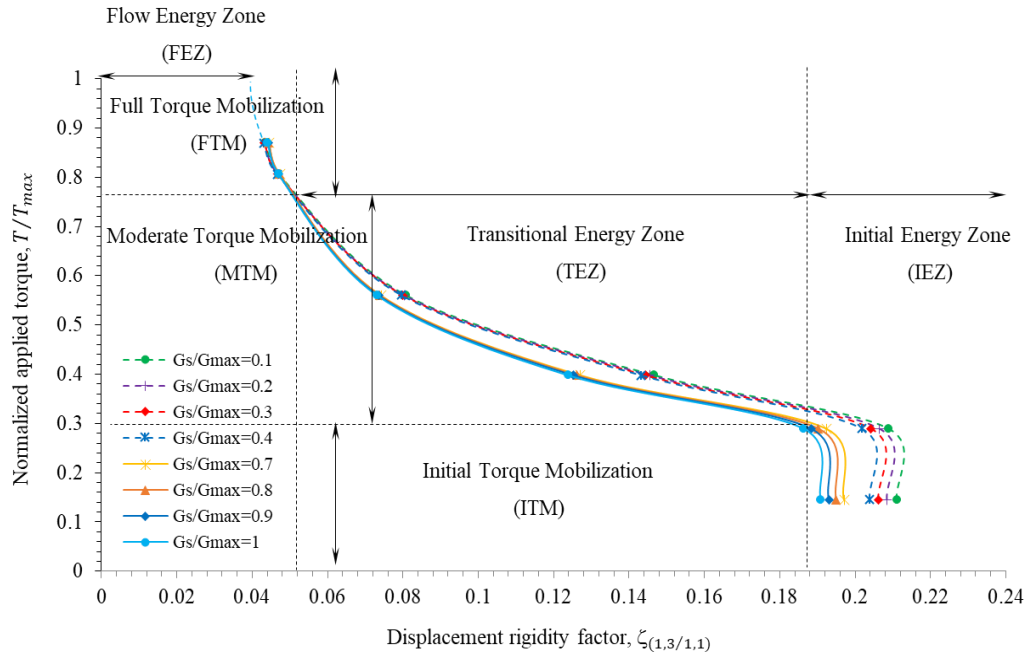

Figure 3.14 Variation of normalized applied torque with displacement rigidity factor defined by a ratio of resultant displacement of pile group (1,3 and 1,1) for sand characterised by different torsional energy zones

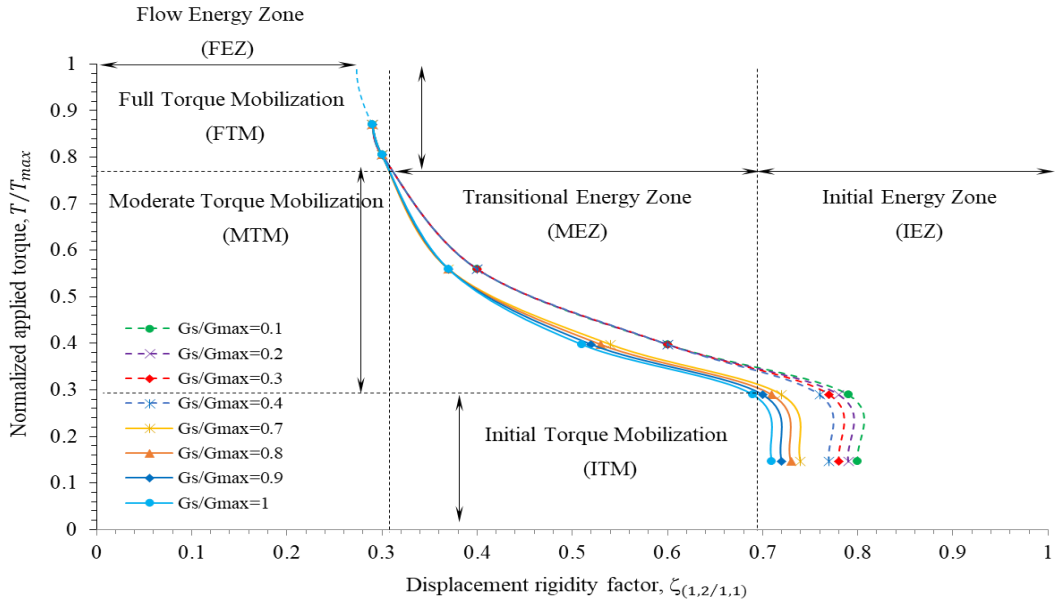

Figure 3.15 Variation of normalized applied torque with displacement rigidity factor defined by a ratio of resultant displacement of pile group (1,2 and 1,1) for sand characterised by different torsional energy zones

Table 3.4 Classification of torsional energy zones corresponding to twist and displacement rigidity factors

Pile group (i, j)	Torque mobilization level*	Shear modulus ratio (G_s/G_{max})	Twist rigidity factor (ξ)	Displacement rigidity factor (ζ)	Torsional energy zones*
	ITM		$0.172 - 0.164$	$0.172 - 0.164$	IEZ
	MTM	0.1	$0.164 - 0.037$	$0.164 - 0.037$	TEZ
	FTM		$0.037 - 0.034$	$0.037 - 0.034$	FEZ
(2,2)	ITM		$0.160 - 0.151$	$0.160 - 0.152$	IEZ
	MTM		$0.151 - 0.037$	$0.152 - 0.037$	TEZ
	FTM	1	$0.037 - 0.035$	$0.037 - 0.035$	FEZ
	ITM		$0.188 - 0.180$	$0.211 - 0.202$	IEZ
	MTM	0.1	$0.180 - 0.042$	$0.202 - 0.047$	TEZ
	FTM		$0.042 - 0.039$	$0.047 - 0.043$	FEZ
(1,3)	ITM		$0.176 - 0.166$	$0.197 - 0.186$	IEZ
	MTM		$0.166 - 0.042$	$0.186 - 0.047$	TEZ
	FTM	1	$0.042 - 0.039$	$0.047 - 0.044$	FEZ
	ITM		$0.89 - 0.90$	$0.71 - 0.72$	IEZ
	MTM	0.1	$0.90 - 0.31$	$0.72 - 0.30$	TEZ
	FTM		$0.31 - 0.30$	$0.30 - 0.29$	FEZ
	ITM		$0.95 - 0.97$	$0.77 - 0.79$	IEZ
(1,2)	MTM		$0.97 - 0.31$	$0.79 - 0.30$	TEZ
	FTM	1	$0.31 - 0.30$	$0.30 - 0.29$	FEZ

*****ITM-Initial Torque Mobilization — IEZ-Initial Energy Zone

MTM-Moderate Torque Mobilization — TEZ-Transitional Energy Zone

FTM-Full Torque Mobilization — FEZ-Flow Energy Zone

The torque-twist behaviour has been classified into three zones namely initial torque mobilization (ITM; $T/T_{max} \leq 0.3$), moderate torque mobilization (MTM; $T/T_{max} = 0.3 - 0.8$), full torque mobilization (FTM; $T/T_{max} \geq 0.8$) as shown in Table 3.5.

Table 3.5 Energy parameters due to twist and displacement

Pile group (i, j)	c_θ''	c_θ'	c_θ	c_d''	c_d'	c_d
(2,2)	-15.473	65.168	50.146	-18.782	62.586	56.014
(1,3)	-7.751	17.814	6.514	-11.539	25.267	8.099
(1,2)	-5.109	14.776	5.858	-7.630	18.891	6.691

The torsional energy due to progressive twist is expressed as follows:

$$[E_T^\theta] = \begin{bmatrix} \xi_p^2 & \xi_p & 1 \end{bmatrix} \begin{bmatrix} c_\theta'' \\ c_\theta' \\ c_\theta \end{bmatrix} \tag{3.32}$$

where c_θ'', c_θ' and c_θ are energy parameters due to twist (Table 5). Similarly, the torsional energy due to progressive displacement is expressed as follows:

$$[E_T^d] = \begin{bmatrix} \zeta_p^2 & \zeta_p & 1 \end{bmatrix} \begin{bmatrix} c_d'' \\ c_d' \\ c_d \end{bmatrix} \tag{3.33}$$

where c_d'', c_d' and c_d are energy parameters due to displacement (Table 3.6). The torsional energy due to progressive twist and displacement for pile groups in the sand is shown (Figure 3.16-3-17). The percentage of torsional energy due to twist is the area covered by normalized applied toque and twist rigidity factor plot when progressive twist varies between 0 to 1.

Table 3.6 Energy components for pile groups (2,2; 1,3; 1,2)

Pile groups configuration	Energy component, η_θ, due to progressive twist	Energy component $(1-\eta_\theta)$ due to progressive displacement
(2,2)	0.462−0.464	0.535−0.538
(1,3)	0.431−0.445	0.555−0.571
(1,2)	0.472−0.50	0.50−0.528

Similarly, the percentage of torsional energy due to displacement is the area covered by normalized applied torque and displacement rigidity factor plot when progressive displacement varies between 0 to 1. Accordingly, the torsional resistance (Kong and Zhang 2009) corresponds to the component of energy associated with applied torque while the remaining energy is associated with lateral resistance. Therefore, the total energy can be expressed as follows:

$$[E_T] = \eta_\theta . [E_T^\theta] + (1-\eta_\theta) . [E_T^d] \tag{3.34}$$

The component of energy as associated with a twist is denoted by η_θ. The η_θ is 0.464, 0.431 and 0.50 for pile groups (2,2; 1,3; 1,2) for the progressive twist, respectively (Table 3.6). Similarly, the components of the energy for progressive displacement are 0.536, 0.569 and 0.50 for pile groups (2,2; 1,3; 1,2) respectively (Table 3.6).

3.7 Conclusions

- The torque-twist relationship for the pile group is a necessary design step; therefore, the study is required to capture the behaviour of the pile group relative to the single pile.

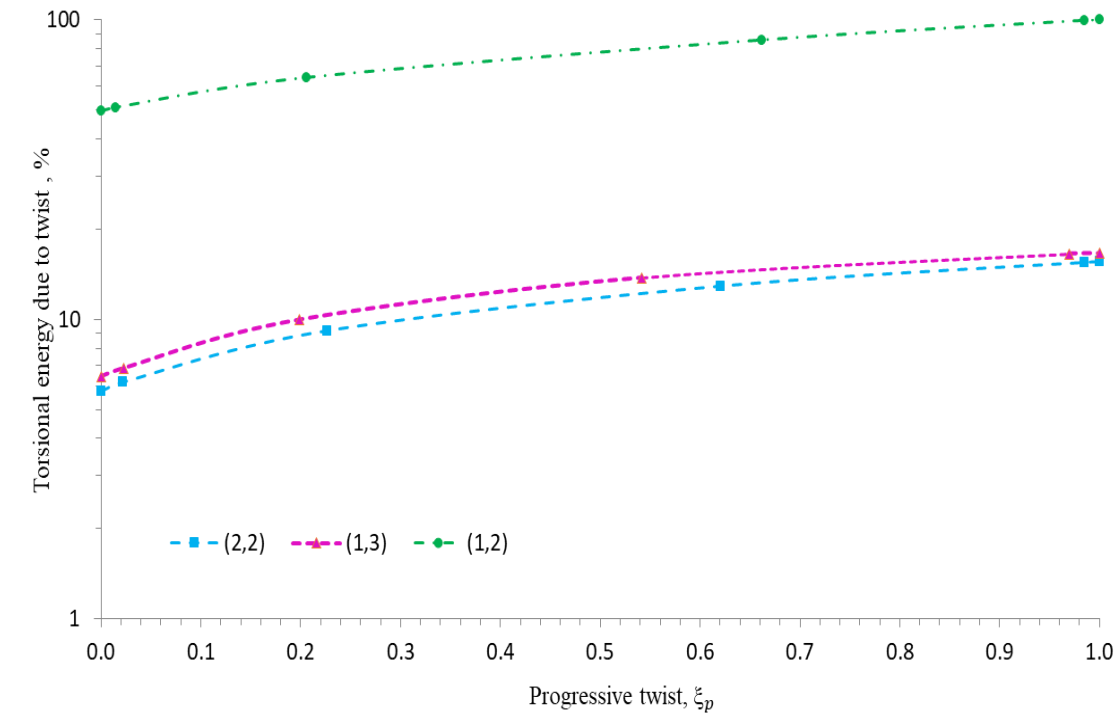

Figure 3.16 Variation of torsional energy due to progressive twist for pile groups (1,2; 1,3; 2,2) in sand

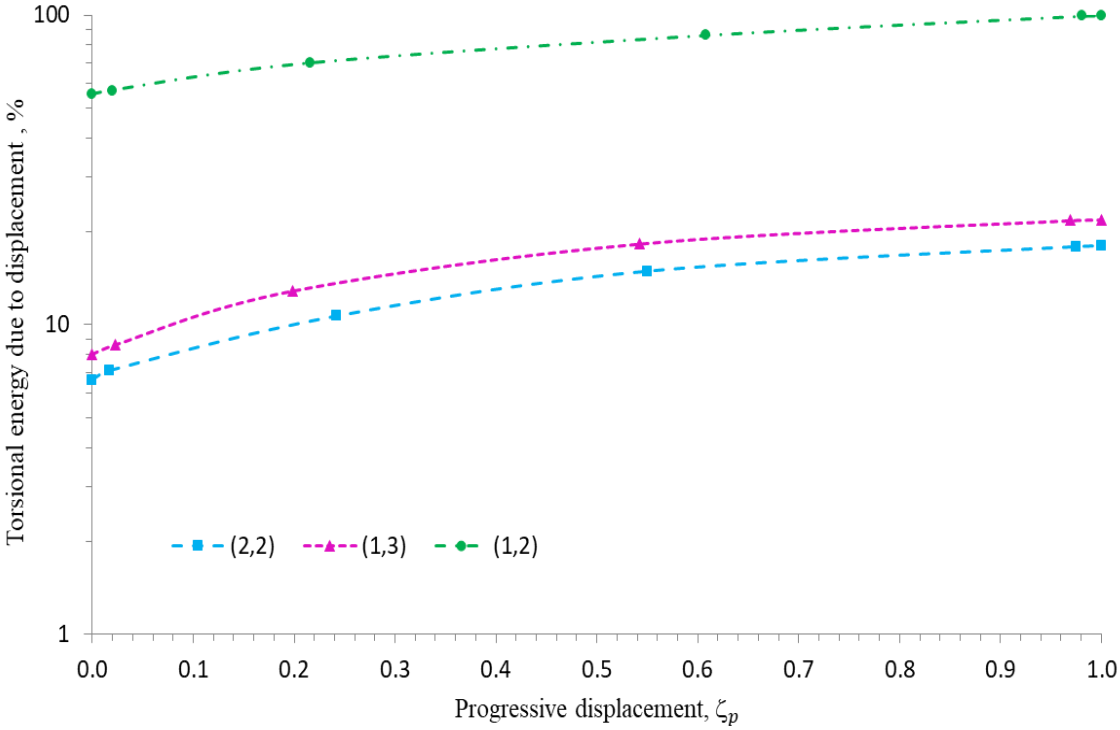

Figure 3.17 Variation of torsional energy due to progressive displacement for pile groups (1,2; 1,3; 2,2) in sand

The plot between the normalized applied torque and twist rigidity factor has been evaluated to predict the torque-twist relationship for the pile groups using the experimental output of the single pile.

- As a result of twisting, the torsional energy zones are set into the soil and there is the formation of a heave and cavity around the pile group. The heave and cavity formations have been captured using displacement ratios.
- The torque−twist behaviour has been classified into three zones namely, initial torque mobilisation (LTM), moderate torque mobilisation (MTM), and full torque mobilisation (FTM) characterised by different torsional energy zones. The group behaviour may be limited to either of the classified segments of normalized applied torque and twist rigidity factor depending upon the magnitude of the torsional loading.
- There is a remarkable difference among the torque-twist behaviour of the single pile and pile groups at the initial stages of the torque application while at ultimate values, the modulus ratio less than 0.7 has no effect on the twist rigidity factor for soils undergoing cavity and heave formation simultaneously.
- The torsional energy and twist rigidity parameters were evaluated for a range of initial shear modulus ratios of the soil. The twist rigidity decreases significantly with an increase in the normalised torsional loads.
- It has been observed that the torsional energy of the pile group (1,2) is significantly higher than pile groups (1,3; 2,2). The torsional energy is obtained in the range of 5.7%~15.6%, 6.4%~16.6% and 49.6%~100% for pile groups (2,2; 1,3; 1,2) respectively.
- A classification for torque mobilisation based upon torsional energy zones associated with twist rigidity and displacement rigidity factor has been suggested to set the limits of the pile groups relative to a single pile.

- The soil element around the pile group behaves as linear elastic ($\xi_p \sim 0, \zeta_p \sim 0$), transitional ($\xi_p > 0, \zeta_p > 0$), and fully plastic ($\xi_p \sim 1, \zeta_p \sim 1$).
- The component of energy resulting from torsional force and moments for progressive twist (η_θ) and progressive displacement ($1\text{-}\eta_\theta$) are obtained in the range (0.43~0.50) and (0.50~0.57), respectively.

References

Basile, F. (2010). "Nonlinear Analysis of Torsionally Loaded Pile Groups." Soils and Foundations, 50(2), 337-340.

Brown, D. A., Morrison, C., and Reese, L. C. (1988). "Lateral load behavior of pile group in sand." J. Geotech. Eng., 114(11), 1261-1276.

Chow, Y. K. (1985). "Torsional response of piles in nonhomogeneous soil." Journal of Geotechnical Engineering, 111(7), 942-947.

Dutt, R. N., & O'Neill, M. W. (1983). "Torsional behavior of model piles in sand." In Geotechnical practice in offshore engineering (pp. 315-334). ASCE.

Duncan, J. M., and Chang, C. Y. (1970). "Nonlinear analysis of stress and strain in soils." J. Soil Mech. & Founds. Div.

Georgiadis, M. (1987). Interaction between torsional and axial pile responses. International journal for numerical and analytical methods in geomechanics, 11(6), 645-650.

Guo, W.D. and Randolph, M.F. (1996). "Torsional response of piles in non-homogeneous media." Comput. Geotech., 19(4), 265-287.

Guo, W. D., Chow, Y. K., & Randolph, M. F. (2007). "Torsional piles in two-layered nonhomogeneous soil." International Journal of Geomechanics, 7(6), 410-422.

Hache, R.A.G., and Valsangkar, A.J. (1988). "Torsional resistance of single pile in layered soil." J. Geotech. Eng. 10.1061/ (ASCE) 0733-9410(1988)114:2(216), 216-220.

Hutton, D. V. (2004). Fundamentals of finite element analysis. McGraw-Hill.

Kong, L.G. (2006). "Behavior of pile groups subjected to torsion." PhD Thesis, Hong Kong University of Science and Technology, Hong Kong, 339p.

Kong, L.G. and Zhang, L.M. (2008). "Experimental study of interaction and coupling effects in pile groups subjected to torsion," Canadian Geotechnical Journal, 45, 1001-1017.

Kong, L. G., and Zhang, L. M. (2009). "Nonlinear analysis of torsionally loaded pile groups." Soils and foundations, 49(2), 275-286.

Kong, L. G., Zhang, Z. C., and Chen, Y. M. (2020). "Nonlinear analysis of pile groups subjected to combined lateral and torsional loading." Journal of Zhejiang University SCIENCE A, 21(3), 179-192.

Mindlin, R.D. (1936). "Force at a point in the interior of a semi-infinite solid." Physics, 7, 195-202.

Menetrey, P., & Willam, K. J. (1995). "Triaxial failure criterion for concrete and its generalization." Structural Journal, 92(3), 311-318.

Mehra, S. (2011). "Experimental study on model pile groups subjected to torque." ME Thesis,University of Delhi, India.

Militano, G., and Rajapakse, R.K.N.D. (1999). "Dynamic response of a pile in a multi-

layered soil transient torsional and axial loading." Geotechnique 49 (1), 91-109.

Mehra, S. and Trivedi, A. (2018). "Experimental studies on model single pile and pile groups subjected to torque." Proceedings of China-Europe Conference, Geotech. Engg., 10.1007/978-3-319-97115-5_24, pp 997-1000.

Mehra, S. and Trivedi, A. (2018). "Analysis and simulation of cyclic torque application on pile groups." Proceeding of 12th International Super Pile World, Nanjing, Jiangsu, China, pp 277-282.

Mehra, S., and Trivedi, A. (2021). "Pile Groups Subjected to Axial and Torsional Loads in Flow−Controlled Geomaterial." Int. J. Geomech., 21(3), 04021002.

O' Neill (1964). "Determination of the pile-head torque-twist relationship for a circular pile embedded in clay soil." M.S. Thesis, University of Texas, Austin, Texas.

Trivedi, A, and Sud VK (2005): "Ultimate bearing capacity of footings on coal ash." Granular Matter, 7 (4) 203-212.

Perkins, S.W., and Madson, C.R. (2000) "Bearing capacity of shallow foundations on sand: A relative density approach". J. Geotech. and Geoenv. Eng., ASCE, Vol. 126(6): 521–529.

Poulos, H.G. (1975). "Torsional response of piles." J. Geotech. Eng., 101(10), 1019-1035.

Poulos, H.G., and Davis, E.H. (1980). "Pile foundation analysis and design." Wiley, New York.

Randolph, M. F. (1981). "Piles subjected to torsion." J. Geotech. Eng. Div., 107(8), 1095-1111.

Rajapakse, R.K.N.D. (1988). "A torsion load transfer problem for a class of non-homogenous elastic solids." Int. J. of Solids and Structures, 24(2), 139-151.

Reese, L.C and Van Impe, W.F. (2001). "Single pile and pile group under lateral loading." A.A. Balkema, Rotterdam.

Randolph, M. F. (2003). "RATZ: Load transfer mechanism of axially loaded piles." Technical Manual.

Wang, K.H., Zhang, Z.Q., Leo, C.J., and Xie, K.H. (2008). "Dynamic torsional response of an end bearing pile in saturated poroelastic medium." Comput. Geotech. 35 (3), 450-458.

Wu, W.B., Liu, H., El Naggar, M.H., Mei, G.X., and Jiang, G.S. (2016). "Torsional dynamic response of a pile embedded in layered soil based on the fictitious soil pile model." Comput. Geotech. 80, 190-198.

Zheng, C.J., Liu, H.L., Ding, X.M., and Lv, Y. (2014). "Torsional dynamic response of a large-diameter pipe pile in viscoelastic saturated soil." Int. J. Numer. Anal. Methods GeoMech. 38 (16), 1724-1743.

4.0 PILE GROUPS SUBJECTED TO AXIAL AND TORSIONAL LOADS IN FLOW CONTROLLED GEOMATERIAL

This chapter is based on the work that has been listed in Section 1.8 and published in the International Journal of Geomechanics, ASCE. To keep the presentation of the details consistent throughout the thesis, the details are offered here with some layout modifications.

4.1 Introduction

The pile groups have been used as a foundation substructure for large structures such as offshore platforms, wind turbines, high-rise buildings, bridges, railway embankments, traffic, and signal pole structures for several causes, such as wind, earthquake, water current, earth pressure, the effect of moving vehicles or ships, plant, and equipment, etc. These complex structures experience large axial, lateral, and torsional loads. Conventionally, the piles have been analysed for displacement due to axial loads and then for eccentric lateral loading to compute deflections and twists. The main objective of the present work is to investigate the effects of torsional loading on axial pile displacements along with the influence of axial loads on the torsional pile response.

The numerical methods for piles subjected to torsion have been presented by Poulos (1975), Randolph (1981), Chow (1985), Georgiadis (1987), Kong & Zhang (2009), and Mehra & Trivedi (2018, 2019). The single pile subjected to the combined action of axial and torsional has been analysed (Georgiadis 1987; Georgiadis & Saflekou 1990). There have been studies on piles (Vesic 1977; Poulos 1980; Randolph 1981; Anagnostopoulos & Georgiadis 1993; Bowles 1996; Reese & Van Impe 2001), however, the solutions for pile groups subjected to combined axial and torsional load have largely been elusive. Normally, a

subgrade modulus in the three-dimensional model of the pile group may be considered to compute the load-displacement relationship. The soil springs have been assigned to idealize the subgrade of soil reaction in the horizontal direction at several nodes defined along the pile length and at the end to idealize the end-bearing reaction of soil. The modulus of horizontal subgrade reaction increases linearly with depth (Broms 1964) due to overburden alone keeping other parameters constant. However, the subgrade reaction approach doesn't fit well with continuums of geomaterial, and the pile reaction at the point is overtly related to the deflection of that point. Therefore, a novel numerical scheme has been presented to capture the nonlinear pile-soil interaction and flow controlled of geomaterial to make allowance for the yield effects. Based upon the numerical model, a three-dimensional finite element analysis has been performed on pile groups subjected to combined axial and torsional loads in flow controlled geomaterial using a computational program.

The Mohr-Coulomb plasticity has been normally considered for geomaterials. However, it has certain discontinuities on the yield surface with edges at which the yield function is not with the flow. It needs special treatment for the geomaterial in contact with the pile group subjected to combined axial and torsional loads. The flow potential for the yield surface of flow-controlled geomaterial is a hyperbolic function of stresses in the meridional stress plane and the smooth elliptic function in the deviatoric stress plane, respectively (Menetrey & Willam 1995). The load-displacement and torque-twist relation has been presented for several combinations of axial and torsional loads. The load-displacement relationship between LDP and pile groups (1,2 and 2,2) has been validated and compared with the experimental pile load test results (Gong et al 2002 & 2019) and the numerical results (Georgiadis 1987) reported in the literature. The understanding of the pile groups subjected to axial and torsional loads depends heavily and solely on the output of the resultant displacement obtained from the computation methods namely the finite element method.

4.2 Interaction of Pile Group with Geomaterial

Conventionally, the vertical and horizontal soil reactions are considered using the soil model (Terzaghi,1955), where the initial modulus of subgrade reaction for the axial load (k_q) and lateral load (k_h) are expressed as follows:

$$k_q = \frac{q}{\delta} \tag{4.1}$$

$$k_h = \frac{P}{y} \tag{4.2}$$

where q and P are the bearing pressure and lateral soil reaction per unit length of pile, respectively; δ and y represents the axial and lateral displacement, respectively. The pile group subjected to axial and torsional loads at the centre concurrently mobilises the axial, lateral, and torsional resistance of the individual piles in the pile group. The governing second and fourth-order differential equilibrium equations (Poulos & Davis 1980, Chow 1985) for axial displacement (δ), lateral displacement (y), and twist angle (θ) of the pile are expressed as follows:

$$-E_P \frac{\partial^2 \delta}{\partial z^2} + S_f A_p = 0 \tag{4.3}$$

$$-E_P I_P \frac{\partial^4 y}{\partial z^4} + k_h\, y = 0 \tag{4.4}$$

$$-G_P J_P \left(\frac{\partial^2 \theta}{\partial z^2}\right) + k_\theta \theta = 0 \tag{4.5}$$

where E_p and G_p are the elastic modulus and shear modulus of the pile shaft, respectively;

I_p and J_p are the second moment and polar second moment of the area of the pile section, respectively; $G_P J_P$ is the torsional rigidity of the pile; z is the depth; S_f is the unit shaft resistance of the pile; A_P is the perimeter of the pile and k_h and k_θ are the modulus of subgrade reaction for lateral and torsional loading, respectively. Figure 4.1 demonstrates the numerical pile group foundation model in flow controlled geomaterial employed in the present investigation.

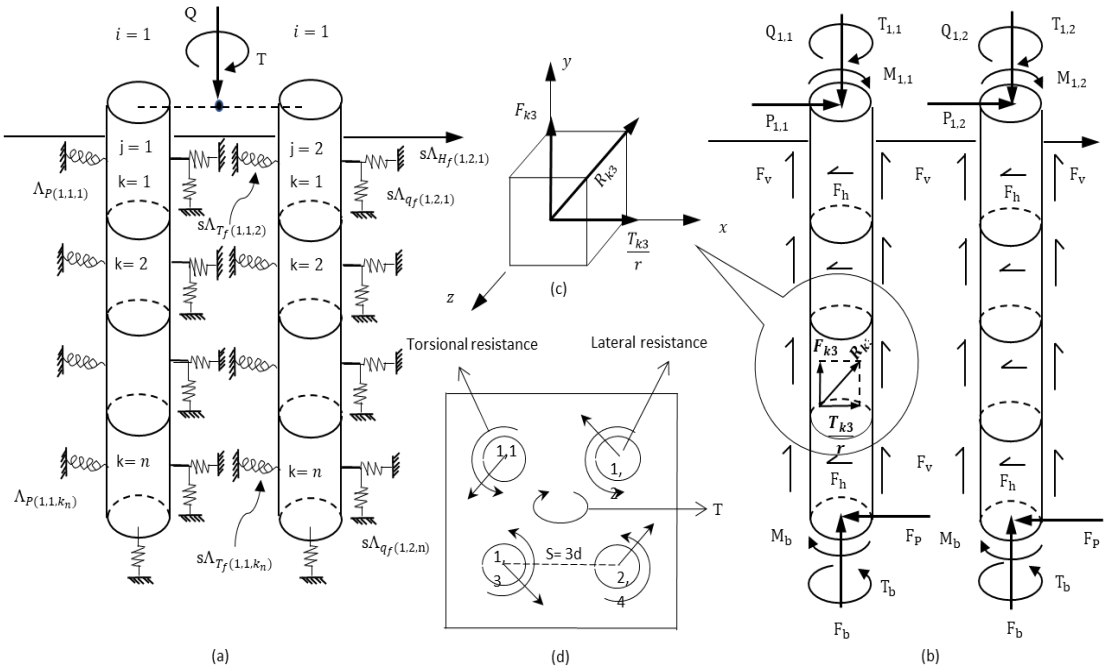

Figure 4.1(a) Numerical model of pile group subjected to combined loads with pile stiffness ($\Lambda_{P(1,1,1)}$), geomaterial axial stiffness ($s\Lambda_{q_f(i,j,k)}$) and geomaterial torsional stiffness ($s\Lambda_{T_f(1,1,k_n)}$) at node (b) Numerical model showing induced bending moment and lateral force at pile head ($M_{1,1}$, $P_{1,1}$) due to the application of torsional loads at the centre of the pile group, where (M_b, F_b, $F_{p,}$ T_b, F_v, F_h) are the moments, vertical, horizontal forces on pile node (c) Resultant force at the 3^{rd} node (R_{k3}) (d) Top view of pile group (2,2) showing lateral and torsional resistance

When the torque is applied, the individual pile in a pile group is subjected to a lateral load, a bending moment, and a torsional load (Figure 4.1b, c, d). The induced bending moments, lateral forces, torsional forces, and soil reactive forces on the pile shaft and pile base have been demonstrated (Figure 4.1b). Every pile in a pile group is assumed as an elastic beam

which has been divided into *n* segments. The pile material is linear, isotropic, and homogenous. The pile material follows Hooke's law for stress−strain relation as a function of I_1. Consider the finite element in axial load (Figure 4.2a) with two nodes and length (L).

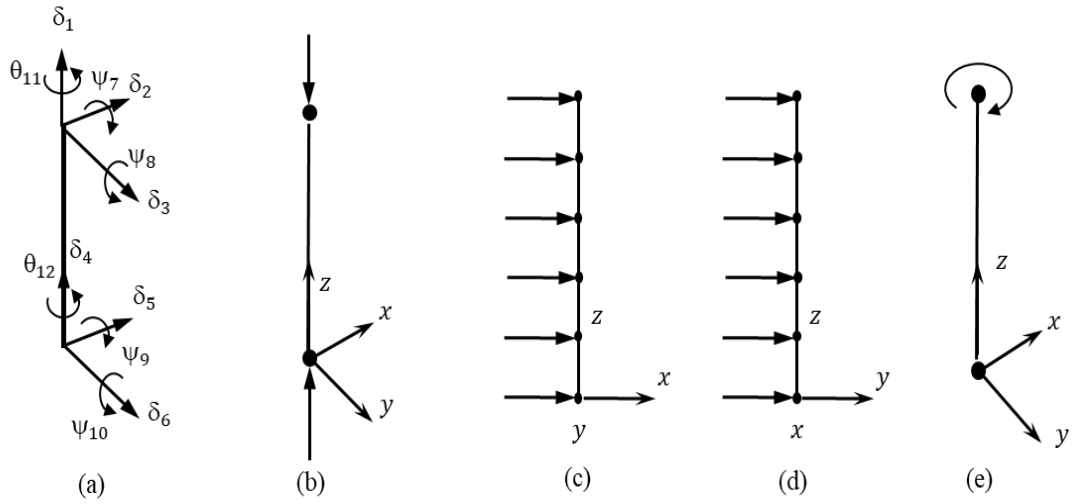

Figure 4.2(a) The definition of pile element, node and degree of freedom represented by six translational ($\delta_1, \delta_2, \delta_3$, δ_4, δ_5 , δ_6), four rotational (ψ_7, ψ_8, ψ_9 , ψ_{10}), and two torsional (θ_{11} and θ_{12}) movements (b) axial load (c) bending in the x-direction (d) bending in the y-direction (d) twist about the z-axis

Using the Galerkin element method (Hutton 2004), the approximation of the displacement field $\delta(z)$ is expressed as follows:

$$\delta(z) = N_1(z)\ \delta_1 + N_4(z)\ \delta_4 = [N]\{\delta\} \tag{4.6}$$

$$[N] = [N_1\ N_4] \tag{4.7}$$

$$\{\delta\} = \{\delta_1\ \delta_4\} \tag{4.8}$$

where N_m are the shape functions; $N_1 = 1 - \frac{Z}{L}$, $N_4 = \frac{Z}{L}$ are used for interpolation $\delta(z)$ using its nodal values. The nodal values δ_1 and δ_2 are the unknowns and are determined

from the global equation system. Since the domain of the element is the volume of the element, the Galerkin residual equation is expressed as follows:

$$\iiint N_m(z)\left(E\frac{d^2\delta}{dz^2}\right)dV = \int_0^L N_m\left(E\frac{d^2\delta}{dz^2}\right)A\,dz = 0 \qquad m = 1,4 \tag{4.9}$$

where $dV = A\,dz$ and A is the constant cross−sectional area of the element. Integrating by parts and rearranging Eq. (4.9), the pile element matrix is expressed as follows:

$$[\Lambda_{\mathrm{PA}}] = \mathrm{A}E\int_0^L \frac{dN_m}{dz}\frac{dN_n}{dz}dz = \left[N_m\,AE\,\frac{d\delta}{dz}\right]_0^L \tag{4.10}$$

The pile element matrix in the combined matrix form is expressed as follows:

$$[\Lambda_{\mathrm{PA}}] = AE\int_0^L \begin{bmatrix} \frac{dN_1}{dz}\frac{dN_1}{dz} & \frac{dN_1}{dz}\frac{dN_4}{dz} \\ \frac{dN_1}{dz}\frac{dN_4}{dz} & \frac{dN_4}{dz}\frac{dN_4}{dz} \end{bmatrix} d\delta \begin{Bmatrix}\delta_1 \\ \delta_4\end{Bmatrix} = \begin{Bmatrix}F_1 \\ F_4\end{Bmatrix} \tag{4.11}$$

Similarly, considering the element in bending (Figure 4.2b-d), the pile element matrixes are expressed as follows:

$$[\Lambda_{\mathrm{PP}}] = EI\int_0^L \frac{d^2N_m}{dz}\frac{d^2N_n}{dz}dz \quad m = 2,3,5,6,7,8,9,10 \tag{4.12}$$

where
$$[N] = [N_2\ N_3\ N_5\ N_6 N_7\ N_8\ N_9\ N_{10}] \tag{4.13}$$

$$\{\delta,\psi\} = \{\delta_2\ \delta_3\ \delta_5\ \delta_6\ \psi_7\psi_8\psi_9\psi_{10}\} \tag{4.14}$$

Similarly, considering the torsional element (Figure 4.2d), the pile element matrix is expressed as follows:

$$[\Lambda_{PT}] = GJ \int_0^L \frac{dN_m}{dz}\frac{dN_n}{dz}dz \qquad m = 11,12 \tag{4.15}$$

where $$[N] = [N_{11}\ N_{12}] \tag{4.16}$$

$$\{\theta\} = \{\theta_{11}\ \theta_{12}\} \tag{4.17}$$

4.3 Response of Flow Controlled Geomaterial

The elastic analysis assumes that the soil in the near field always adheres to the pile. However, the soil has a limited ability to take tension, significant deformation will likely occur near the top of the pile. This deformation and local yield are the main causes of the nonlinear behaviour of soil even at low load levels. A lumped mass of soil in the near field has been assumed to be morphed and imposed on each pile node which may change its position in space on the application of combined loads. Each node has been attached with three springs (a vertical shear axial spring, a lateral translation spring, and a torsional spring) of flow controlled geomaterial. The lateral loads are mobilised due to the application of torsional loads. The base springs have been attached at the end to model the geomaterial response at the base. Assumptions for flow controlled geomaterial are expressed as follows:

a) The behaviour of geomaterial is elastic inside the yield surface. Isotropic hardening is assumed for the initial behaviour of the Mohr−Coulomb yield surface to quantify cohesion as a special case.
b) The flow controlled geomaterial follows a law for stress-strain relation as a function of I_1, J_2, J_3 and has an onset of nonlinearity at $\varepsilon_{ij}^{p} > 0$.
c) The shear criterion has an onset of controlled granular flow, which intersects Mohr-Coulomb as a special case, has a smooth yield surface such that, $f = 0$.

d) The flow controlled geomaterial follows a plastic stress-strain relation defined by a chain rule such that, $\frac{\partial f}{\partial \sigma_{ij}} \partial \sigma_{ij} > 0$.

e) The smooth flow potential for geomaterial has a hyperbolic shape with a constant eccentricity in the meridional stress plane and a piecewise elliptic shape in the deviatoric stress plane.

The yield function $f(\sigma_{ij,}\ \varepsilon_{ij}^{p})$ is such that $f = 0$ to define the yield surface (Yu 2007) and is expressed as follows:

$$f = 0 \quad \text{and} \ \frac{\partial f}{\partial \sigma_{ij}} \partial \sigma_{ij} > 0 \tag{4.18}$$

ε_{ij}^{p} is varied with loading such that $d\varepsilon_{ij}^{p} \neq 0$, and the consistency condition guarantees the yield surface is carried along with the stress point such that,

$$\partial f = \frac{\partial f}{\partial \sigma_{ij}} \partial \sigma_{ij} + \frac{\partial f}{\partial \varepsilon_{ij}^{p}} d\varepsilon_{ij}^{p} = 0 \tag{4.19}$$

The direction of plastic strain increment, $d\varepsilon_{ij}^{p}$ is expressed as follows:

$$d\varepsilon_{ij}^{p} = \partial \lambda \frac{\partial g}{\partial \sigma_{ij}} \tag{4.20}$$

where $\partial \lambda$, $\frac{\partial g}{\partial \sigma_{ij}}$ are positive scalar and linearly dependent gradients, respectively.

$$\partial \lambda = \frac{\frac{\partial f}{\partial \sigma_{kl}}}{\frac{\partial f}{\partial \varepsilon_{pq}^{p}} \frac{\partial g}{\partial \varepsilon_{pq}^{p}}} \partial \sigma_{kl} \tag{4.21}$$

The total strain is expressed as follows:

$$d\varepsilon_{ij} = d\varepsilon_{ij}^{e} + d\varepsilon_{ij}^{p} = \left[E_{ijkl} + \frac{\frac{\partial f}{\partial \sigma_{kl}} \frac{\partial g}{\partial \sigma_{ij}}}{\frac{\partial f}{\partial \varepsilon_{pq}^{p}} \frac{\partial g}{\partial \sigma_{pq}}} \right] \partial \sigma_{kl} \tag{4.22}$$

The geomaterial has been modelled with a torsional and axial pair of springs at each node. The initial stiffness of the torsional spring at a node has been related to parameters inside the yield surface and is expressed as follows:

$$[s\Lambda_{Te}] = k_{\theta} \int_{0}^{L} \frac{dN_m}{dz} \frac{dN_n}{dz} dz \tag{4.23}$$

The resulting stiffness of the torsional spring at each node has been related to the yield flow parameters and is expressed as follows:

$$\left[s\Lambda_{Tf}\right] = f\left(\mathrm{s}\Lambda_{\mathrm{Te}}, \mathrm{s}\Lambda_{\mathrm{Tp}}\right) = (k_{\theta} f(G_{se})) \int_{0}^{L} \frac{dN_m}{dz} \frac{dN_n}{dz} dz \tag{4.24}$$

where $k_{\theta} = \pi D_p^2 G_{se} L$, $(s\Lambda_{T_e})$ is the stiffness as long as $f = 0$, $(s\Lambda_{T_p})$ is the flow controlled stiffness, D_p is the pile diameter, G_{se} is the equivalent shear modulus of the soil at a node and is expressed as follows:

$$G_{se} = f(f, g) = f\left(\frac{\frac{\partial f}{\partial \sigma_{kl}} \frac{\partial g}{\partial \sigma_{ij}}}{\frac{\partial f}{\partial \varepsilon_{pq}^{p}} \frac{\partial g}{\partial \sigma_{pq}}} \right) \tag{4.25}$$

The initial stiffness of the axial spring at a node is expressed as follows:

$$[s\Lambda_{qe}] = k_q \int_0^L \frac{dN_m}{dz}\frac{dN_n}{dz}dz \tag{4.26}$$

where k_q is computed from the convectional bearing capacity methods. The resulting stiffness of the axial spring at each node related to yield flow parameters is expressed as follows:

$$[s\Lambda_{qf}] = f(\mathrm{s}\Lambda_{\mathrm{qe}}, \mathrm{s}\Lambda_{\mathrm{Tp}}) = (k_q\, f(G_{se})) \int_0^L \frac{dN_m}{dz}\frac{dN_n}{dz}dz \tag{4.27}$$

Similarly, the initial and resulting stiffness of the lateral translational spring at a node is expressed as follows:

$$[s\Lambda_{He}] = k_h \int_0^L \frac{dN_m}{dz}\frac{dN_n}{dz}dz \tag{4.28}$$

$$[s\Lambda_{Hf}] = f(\mathrm{s}\Lambda_{\mathrm{He}}, \mathrm{s}\Lambda_{\mathrm{Hp}}) = (k_h\, f(G_{se})) \int_0^L \frac{dN_m}{dz}\frac{dN_n}{dz}dz \tag{4.29}$$

The pile base spring is modelled using the bearing capacity theory (Poulos 1975). The torsional base spring is not considered in the present analysis as its contribution to the response of long piles is insignificant (Poulos 1975). The correct yield criterion for any frictional material would be a function of first stress invariants. If the stress state lies on the single yield surface, then the Mohr-Coulomb yield function for sand (Yu 2007) is expressed as follows:

$$f = \sigma_3 - \sigma_1 + (\sigma_3 + \sigma_1)\sin\emptyset \tag{4.30}$$

The plastic potential has been obtained using the dilation angle $\emptyset_d$ (Yu 2007) and is expressed as follows:

$$g = \sigma_3 - \sigma_1 + (\sigma_3 + \sigma_1) \sin \emptyset_d \tag{4.31}$$

Frictional geomaterials are normally treated corresponding to the Mohr-Coulomb failure criterion. However, the Mohr−Coulomb plasticity has certain discontinuities on the yield surface with edges at which the yield function is not with the flow, which needs special treatment for the pile group subjected to combined axial and torsional loads involving axisymmetric loading conditions. In the present analysis, the flow potential, g, for the Mohr-Coulomb yield surface has been chosen as a hyperbolic function in the meridional stress plane and the smooth elliptic function in the deviatoric stress plane (Menetrey and Willam,1995) and is expressed as follows:

$$g = \sqrt{(\in \mathrm{c} \tan \emptyset_d)^2 + (R_{mw} q)^2} - p \tan \emptyset_d \tag{4.32}$$

where $R_{mw}(\Theta, \mathrm{e}) =$ (4.33)

$$\frac{4(1-e^2)cos^2\Theta+(2\mathrm{e}-1)^2}{2(1-e^2)\cos\Theta+(2e-1)\sqrt{4(1-e^2)cos^2\Theta+5e^2-4e}} R_{mc}\left(\frac{\pi}{3}, \emptyset\right)$$

and $$R_{mc}\left(\frac{\pi}{3}, \emptyset\right) = \frac{3 - \sin \emptyset}{6 \cos \emptyset} \tag{4.34}$$

where $\emptyset_d$ is the dilation angle measured in the plane at high confining pressure; c is the initial cohesion yield stress; Θ is the deviatoric polar angle; ϵ is the meridional eccentricity that defines the rate at which the hyperbolic function approaches the asymptote (the flow potential tends to a straight line in the meridional stress plane as the meridional eccentricity

tends to zero); e is the deviatoric eccentricity. A constant value has been considered for the meridional eccentricity, ϵ and the deviatoric eccentricity, e is calculated as follows:

$$e = \frac{3 - \sin \emptyset}{3 + \sin \emptyset} \tag{4.35}$$

where, $\emptyset$ is the Mohr-Coulomb friction angle.

4.4 Equilibrium Equation

The pile groups have been connected by a rigid pile cap to have a fixed head connection. The twist of the pile cap should be equal to the twist of all pile heads. The individual piles in the pile group have been represented by $q - z$, $p - y$, and $\tau - \theta$ curves. The far-field soil-pile interactions have been considered linear elastic and predicted using analytical solutions. The interaction between lateral resistances of individual piles has been considered using Mindlin's (1936) solution and the interactions between the torsional and lateral resistance of individual piles have been considered through Randolph's (1981) solution. The equilibrium equation for pile-soil element considering Eq. (4.1-4.35) is expressed as follows:

$$\{F\} = \Big[AE \int_0^L \frac{dN_m}{dz}\frac{dN_n}{dz}dz + EI \int_0^L \frac{d^2N_m}{dz}\frac{d^2N_n}{dz}dz + GJ \int_0^L \frac{dN_m}{dz}\frac{dN_n}{dz}dz + \left(k_\theta + k_\theta f(G_{se})\right)\int_0^L \frac{dN_m}{dz}\frac{dN_n}{dz}dz + \left(k_q + k_q f(G_{se})\right)\int_0^L \frac{dN_m}{dz}\frac{dN_n}{dz}dz + \left(k_h + k_h f(G_{se})\right)\int_0^L \frac{dN_m}{dz}\frac{dN_n}{dz}dz\Big]\{\delta\} \tag{4.36}$$

$$\{\delta, \psi, \theta\} = \{\delta_1 \delta_2 \delta_3 \delta_4 \delta_5 \delta_6 \psi_7 \psi_8 \psi_9 \psi_{10} \theta_{11} \theta_{12}\} \tag{4.37}$$

$$\{F\} = \{\, Q_{mx}\ Q_{nx}\ P_{mx}\ P_{my}\ P_{nx}\ \ P_{ny}\ M_{mx}\ M_{my}\ M_{nx}\ M_{ny}\ T_m\ \ T_n\} \tag{4.38}$$

Using Eq. (4.1-4.38), the stiffness matrix of the pile and geomaterial is assembled in the global stiffness matrix.

4.5 Group Assembly of Stiffness Matrix

The load−deformation relationship of the pile−geomaterial group system is expressed as,

$$\{F\} = [\Lambda_P]\{d_p\} + [s\Lambda]\{\mathrm{d_s}\} \tag{4.39}$$

where $[\Lambda_p]$ and $[s\Lambda]$ are the global stiffness matrix of all the elements of the pile groups and soil, respectively; $\{d_p\}$ and $\{d_s\}$ are the vector of deformations at pile nodes and soil, respectively; {F} is the external loads applied on the pile groups. From the assembled group stiffness matrix and known load vector, overall equilibrium equations have been formulated. Eq. 4.39, has been solved for unknown nodal displacements by Gauss elimination. After the computation of the nodal displacements, the stiffness matrix of each element has been recalled to compute the internal forces within the element. Based upon the aforesaid idealizations, three-dimensional finite element modelling of pile groups has been performed. The numerical modelling uses the tangent stiffness method computed from the model configuration and calculates the displacement correction for small load increments to get the updated model configuration. The method then calculates the model's internal forces for its updated configuration. The difference between the total applied load and the updated model internal forces are the force residual for the step. The residue signifies the nonlinearity of the pile-soil interaction.

4.6 Resultant Force and Displacement

The individual pile shaft in the pile group has been subjected to an axial and tangential force (Figure 4.1b, d). The resultant has been computed as the square root of the sum of

squares of the axial and tangential force. The resultant force (Georgiadis 1987) at the pile shaft subjected to combined load is expressed as follows:

$$F_m = \sqrt{\left[Q_m^2 + \left(\frac{T_m}{r}\right)^2\right]} \tag{4.40}$$

where $F_m, Q_m \; and \; \frac{T_m}{r}$ are the resultant force, axial force, and torsional force at each node, respectively; r is the pile radius. Similarly, the resultant node displacement (Georgiadis 1987) at the pile shaft is expressed as follows:

$$u_m = \sqrt{\left[\delta_{\mathrm{m}}^2 + \left(\frac{D_p \theta_m}{2}\right)^2\right]} \tag{4.41}$$

where $u_m, \delta_m \; and \; \theta_m$ are the resultant displacement, axial displacement, and twist at each node, respectively; D_p is the pile diameter.

4.7 Three-dimensional Analysis Considering Continuum of Geomaterial

Three-dimensional finite element modelling is a convenient and reliable approach to account for the continuity of the soil mass and the nonlinearity of the pile-soil interactions. The equivalent perimeter surface area has been considered for the numerical model of pile groups (1,2; 2,2) and large-diameter piles. The equivalent perimeter is the circumference of the circle that encloses the pile group which plays a role to mobilise torque around the pile group. The input parameters for the three-dimensional numerical analysis of pile groups have been considered as shown in Table 4.1. Table 4.1 shows an equivalent perimeter of pile groups which is effective against axial loads. The purpose of this equivalent perimeter is to designate the phenomenon of deformation taking place initially

against the axial loads, however, the application of torsional loads over and above would trigger further deformations.

Table 4.1 Input parameters for numerical analysis of LDP (large diameter pile) and pile groups with reference to the equivalent perimeter

Pile group parameters	LDP	(1,2)	(2,2)
Young modulus of pile material (E_p, GPa)	*210*	*210*	*210*
Poisson's ratio (μ_p)	*0.3*	*0.3*	*0.3*
Unit weight (γ_p, kN/m^3)	*78*	*78*	*78*
Diameter, (D_p, m)	*1.6*	*0.8*	*0.4*
Length (L_p, m)	*50*	*50*	*50*
Pile-to-pile spacing (S_p)	–	$3D_p$	$3D_p$
Equivalent perimeter (m)	*5.03*	*5.03*	*5.03*

The geomaterial continuum has been divided into several volume elements. Each element consists of nodes and each node has several degrees of freedom. The three-dimensional analysis has been performed using the numerical model captured by Eq. (4.1-4.41). The strain hardening model using the Mohr-Coulomb failure criterion has been adopted for the geomaterial with a single layer. The geomaterial has been selected such that the flow potential for the yield surface is a hyperbolic function in the meridional stress plane and the smooth elliptic function in the deviatoric stress plane, respectively. The computational program considers a peak value of the angle of internal friction $\emptyset_{max}$, a function of internal friction angle $\emptyset_s$ and angle of dilation $\emptyset_d$ (Trivedi 2015; Zhao and Cai 2010). The four nodded nonlinear tetrahedron shapes (C3D4) have been considered for pile groups (1,2; 2,2) as shown in Figure 4.3 that could capture the interlocking effects in terms of strength

parameters. A relatively fine mesh was adopted for the pile groups and a coarser mesh was adopted for the geomaterial.

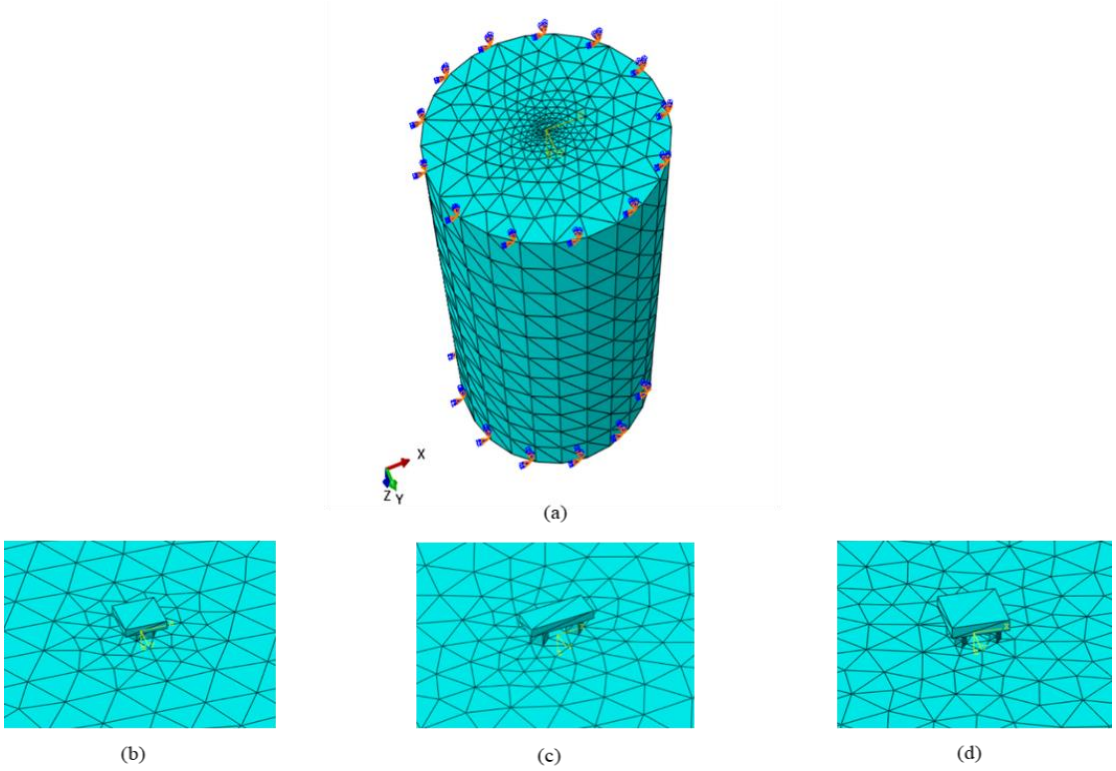

Figure 4.3(a) Three-dimensional numerical model with the continuum of geomaterial divided into a number of volume elements (b, c, d) part view of large diameter pile (LDP), pile group (1,2) and pile group (2,2) respectively

The boundary conditions have been considered at the exterior surface of the soil cylinder fixed in longitudinal (x), transverse (y), and vertical (z) directions to model the confinement of the soil at $40\mathrm{D_p}$ (Figure 4.3) where D_p is the diameter of the individual pile. Using three-dimensional finite element analysis, several constitutive models have been executed to model the pile-soil interaction for different combinations of load sets. The input parameters for three-dimensional numerical analysis for geomaterial have been defined in Table 4.2. The interaction between the pile and the geomaterial has been defined using tangential and normal contact behaviour. The master surface is represented by the exterior surface of the pile and the slave surface by the interior surface of the geomaterial. The tangential contact

between the surfaces of the geomaterial and the pile has been defined using a friction coefficient of 0.36.

Table 4.2 Input parameters for numerical analysis of geomaterial

Parameter	Geomaterial
Range of initial modulus of elasticity (MPa)	*25-160*
Effective unit weight (γ_s, kN/m^3)	*16*
Initial Poisson's ratio (μ_s)	*0.3*
Effective friction angle ($\emptyset_s$, degrees)	*30*
Dilation angle ($\emptyset_d$, degrees)	*6-14*

The free-standing pile group (Poulos & Davis 1980) in which the pile cap is not in contact with the underlying soil has been selected to examine the behaviour of pile groups. To arrive at the nonlinear response, the loading must be specified as a function of time and incremental time. The approximate equilibrium configuration has been determined at the end of each time increment by splitting the simulation into multiple time increments. A workable solution for each time increment has been found after multiple iterations using the Newton technique.

4.8 Results, Discussion, and Validation

In designing pile foundations to resist axial and torsional loads, the criterion for design in the majority of cases is not the ultimate axial and torsional capacity of the piles, but the maximum displacement and twist of the piles. The allowable deflection and twist may be relatively large for temporary structures, but only small movements and twists can be tolerated in such structures as tied abutments to bridges or in the foundation of tall structures (Rajapakse 2016). The three-dimensional finite element numerical model of pile

groups (1,2; 2,2) and LDP have been executed in a computational program (Abaqus) to capture real soil behaviour. Due to the combined loads, the individual pile stresses the soil in the near field. The soil particles further away from piles are less stressed and settle less. The axial load-displacement and torque-twist relations for combined axial and torsional loads have been analysed. Fig. 4.4 (a, b, c) shows the typical view of the pile group section, and the top view of the pile group (2,2; 1,2), respectively.

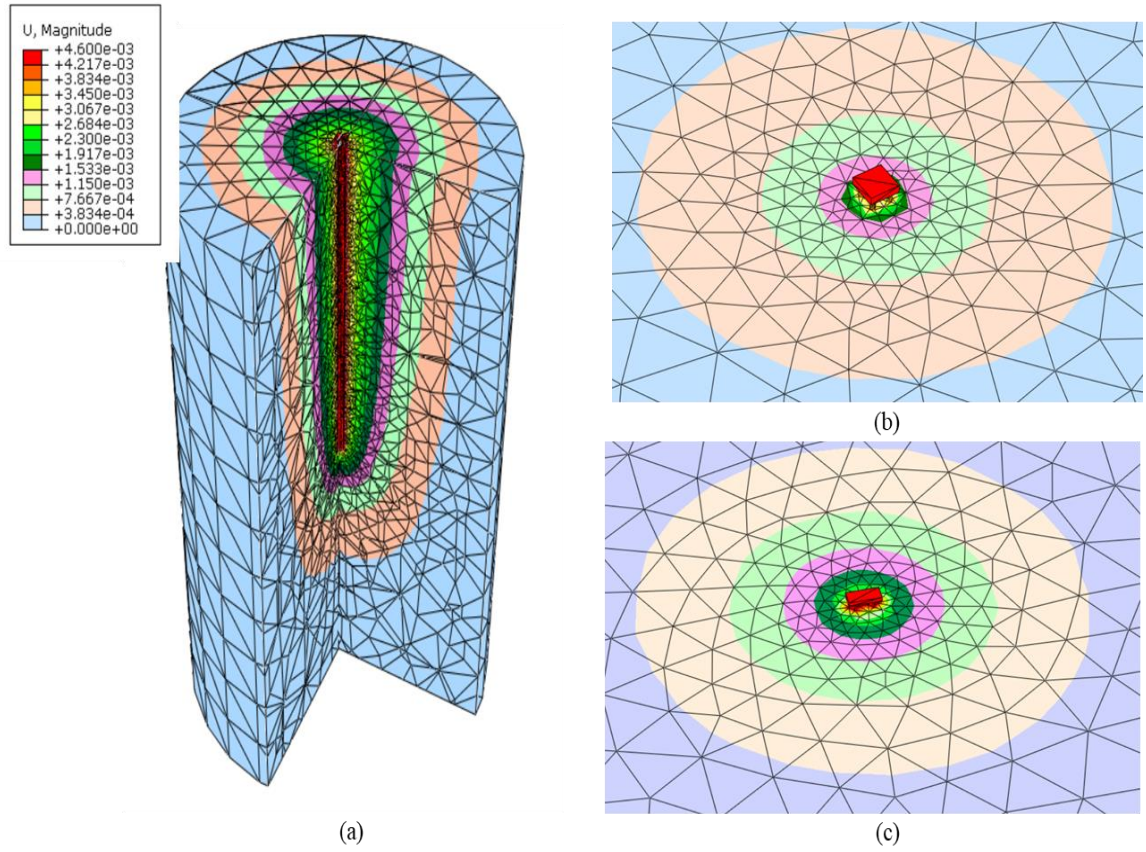

Figure 4.4(a) A typical view of the pile group section (b, c) the top view of the pile group (2,2; 1,2) respectively. The colour scheme is selected to represent the magnitude of displacement which reduces outwardly, where the red colour scheme is selected for the highest displacement and the blue colour scheme is for the lowest displacement

The colour scheme is selected to represent the magnitude of displacement which reduces outwardly, where the red colour scheme is selected for the highest displacement and the blue colour scheme is for the lowest displacement. The variation of normalized axial load and normalized pile head displacement in a flow controlled geomaterial captured for

varying normalized applied torque for LDP of diameter 1.6 m and initial modulus of elasticity 25 MPa (Figure 4.5). The normalized axial load has been described as the ratio of the instantaneous axial load to the maximum axial load considered during the analysis. Similarly, normalized pile head displacement has been described as the ratio of the instantaneous displacement to the maximum displacement considered during the analysis.

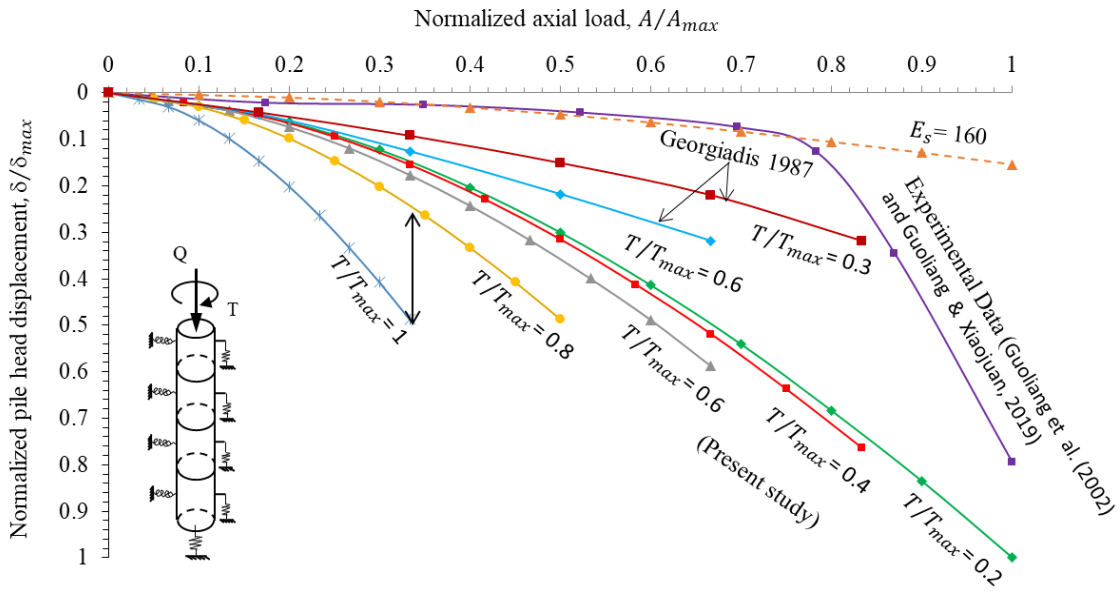

Figure 4.5 Variation of normalized axial load with normalized pile head displacement in a flow controlled geomaterial captured for varying normalized applied torque for large diameter pile of dia. 1.6 m and initial modulus of elasticity as 25 MPa (present study), the numerical study (pile diameter, wall thickness, length and unit shaft resistance is 1.52 m, 37 mm, 50 m and 50 kN/m^2, respectively, the experimental data and the large diameter pile without torsional load (LDP-WT) with an initial modulus of elasticity (160 MPa)

The results obtained from the present three-dimensional numerical investigation have been validated with the experimental pile load test reported in the literature (Figure 4.5); the LDP of 1.6 m tested at Chizhou Yangtse River Bridge, China for a bridge foundation for the pile length of 49 m (Gong et al 2002 & 2019). The variation of normalized axial load and normalized pile head displacement in a flow controlled geomaterial captured for varying normalized applied torque for LDP of diameter 1.6 m and initial modulus of elasticity 25 MPa (Figure 4.5). The normalized axial load has been described as the ratio of the

instantaneous axial load to the maximum axial load considered during the analysis. Similarly, normalized pile head displacement has been described as the ratio of the instantaneous displacement to the maximum displacement considered during the analysis. The results obtained from the present three-dimensional numerical investigation have been validated with the experimental pile load test reported in the literature (Figure 4.5); the LDP of 1.6 m tested at Chizhou Yangtse River Bridge, China for a bridge foundation for the pile length of 49 m (Gong et al 2002 & 2019). Initially, the numerical model shows good agreement with the test results, however, the slope of the experimental curve increases sharply due to the controlled displacement flow of the geomaterial immediately after transient yield conditions preceded by the initial displacement region.

The present investigation results have been also validated and compared with the numerical model (Georgiadis 1987) and a good agreement has been achieved; the numerical model considered pile diameter, wall thickness, length, unit shaft resistance, undrained shear strength and shear modulus as 1.52 m, 37 mm, 50 m, 50 kN/m^2, 100 kN/m^2 and 5 MN/m^2, respectively. The resultant displacement increases in a range of 19% to 235%; 20% to 140%; and 20% to 246% for the LDP and pile group (1,2; 2,2) as normalized applied torque and normalized axial load applied in the range 0.6 to 1 and 0.33 to 0.67, respectively (Figure 4.5, 4.6, 4.7). The variation of normalized applied torque at pile head with normalized pile head twist in a flow controlled geomaterial for large diameter pile and pile groups (1,2; 2,2) has been presented (Figure 4.8, 4.9, 4.10). The normalized applied torque has been described as the ratio of the instantaneous torque to the maximum torque considered for investigation. Similarly, a normalized pile head twist has been described as the ratio of the instantaneous twist to the maximum twist obtained during the analysis.

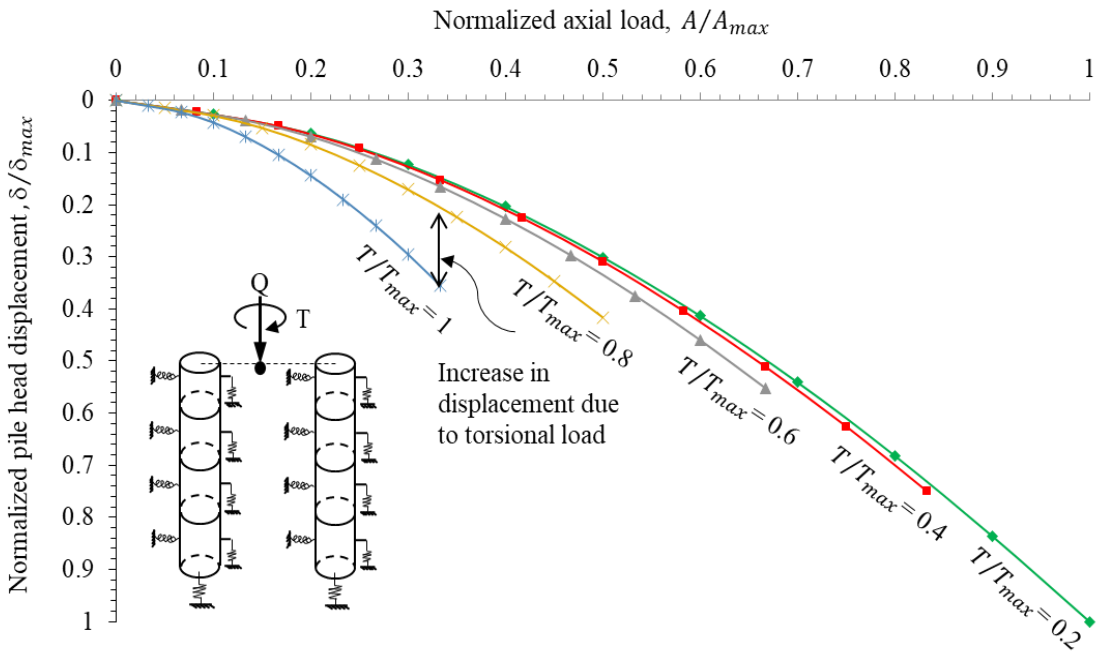

Figure 4.6 Variation of normalized axial load with normalized pile head displacement in a flow controlled geomaterial captured for varying normalized applied torque for pile group (1,2). The diameter of the pile and initial modulus of geomaterial is 0.8 m and 25 MPa respectively

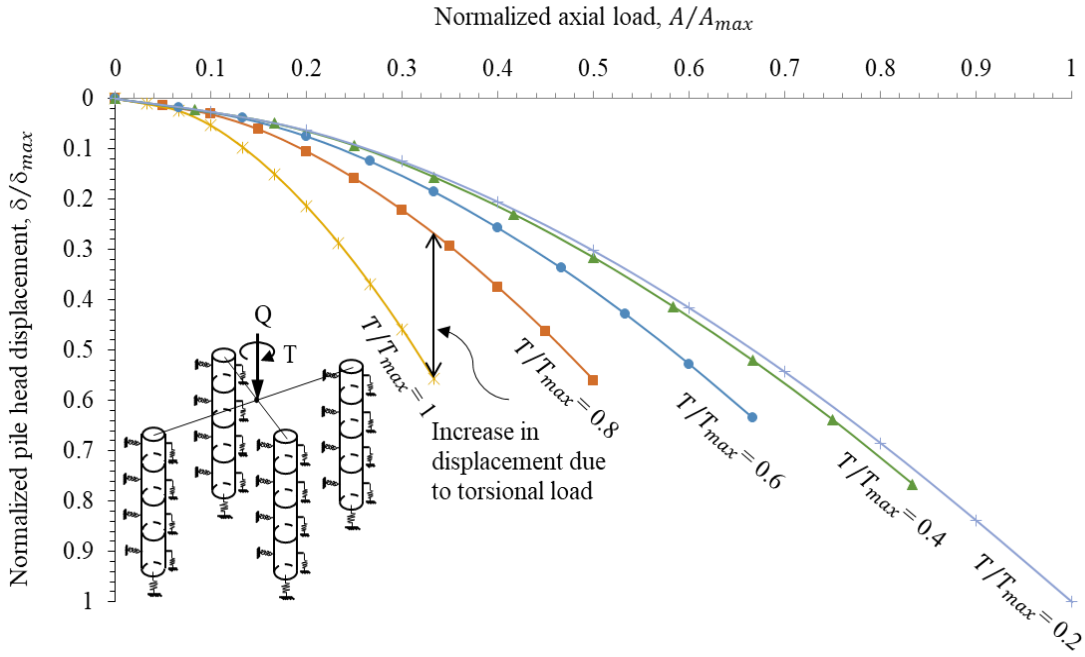

Figure 4.7 Variation of normalized axial load with normalized pile head displacement in a flow controlled geomaterial captured for varying normalized applied torque for pile group (2,2). The diameter of the pile and initial modulus of geomaterial are 0.4 m and 25 Mpa respectively

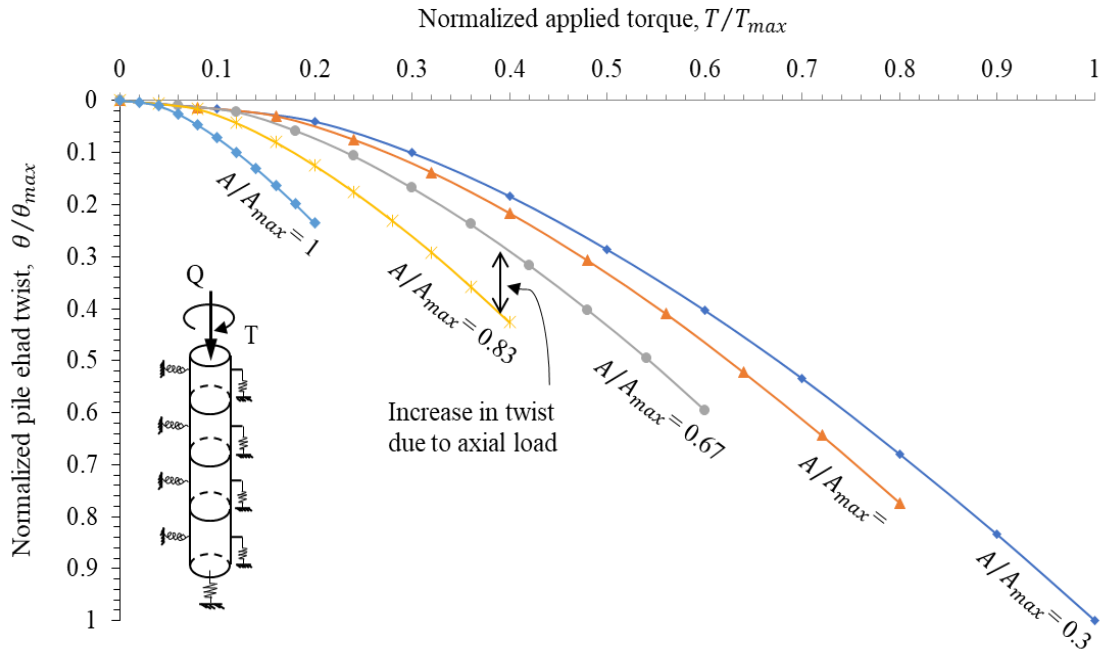

Figure 4.8 Variation of normalized applied torque with normalized pile head twist in a flow controlled geomaterial captured for varying normalized axial load for large diameter pile (LDP) of dia. 1.6 m and initial modulus of elasticity of geomaterial 25 MPa

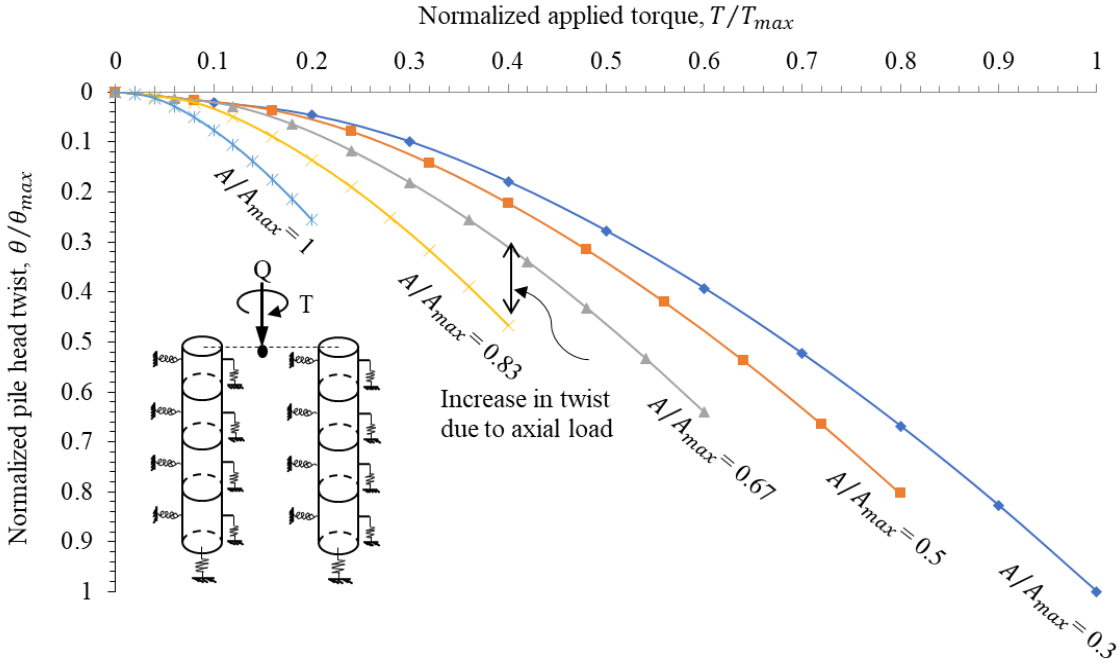

Figure 4.9 Variation of normalized applied torque with normalized pile head twist in a flow controlled geomaterial captured for varying normalized axial load for pile group (1,2). The diameter of the pile and initial modulus of geomaterial is 0.8 m and 25 MPa respectively

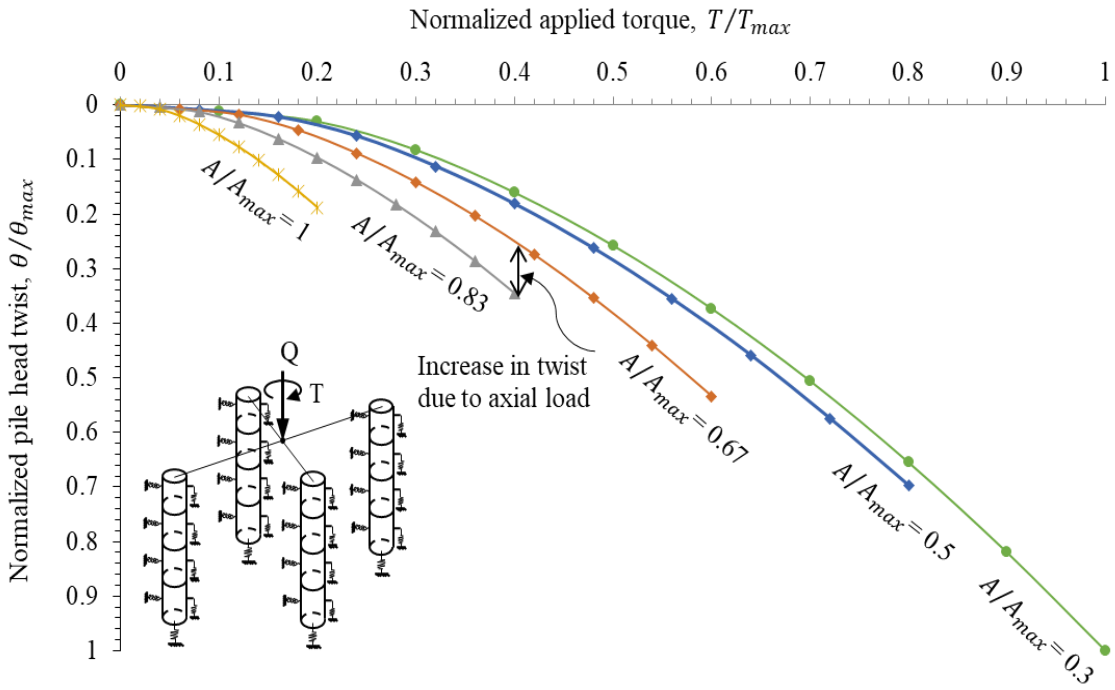

Figure 4.10 Variation of normalized applied torque with normalized pile head twist in a flow controlled geomaterial captured for varying normalized axial load for pile group (2,2). The diameter of the pile and initial modulus of geomaterial is 0.4 m and 25 MPa respectively

The twist increases in a range of 18% to 530%; 30% to 474%; and 22% to 651% for LDP and pile group (1,2; 2,2) as the normalized axial load and normalized applied torque in the range 0.5 to 1 and 0.2 to 0.8, respectively. The relationship between the normalized axial load and normalized displacement has been expressed in matrix form as follows:

$$[\delta/\delta_{max}] = [(Q/Q_{max})^2 \quad Q/Q_{max} \quad 1]\begin{bmatrix} C_T'' \\ C_T' \\ C_T \end{bmatrix} \tag{4.42}$$

where $C_T^{"}, C_T', and\ C_T$ are the twist parameters which depend upon the plastic strain and dilation angle.

Similarly, normalized pile head twist and normalized applied torque relationship have been expressed in matrix form as follows:

$$[\theta/\theta_{max}] = [(T/T_{max})^2 \quad T/T_{max} \quad 1]\begin{bmatrix} C_Q'' \\ C_Q' \\ C_Q \end{bmatrix} \tag{4.43}$$

where $C_Q^{"}, C_Q', and\ C_Q$ are the displacement parameters which depend upon plastic strain and dilation angle. Figure (4.11-4.12) shows the variation of displacement and twist parameters with normalized applied torque and normalized axial load, respectively. The region of initial twist (RIT), the region of a twist at yield (RYT) and the region of flow-controlled twist (RFT) have been classified for normalized applied torque ranges $(0-0.2;\ 0.2-0.6;\ 0.6-1)$, respectively (Figure 4.11). Similarly, the region of initial displacement (RID), the region of displacement at yield (RYD) and the region of flow-controlled displacement (RFD) have been classified for normalized axial load ranges $(0.3;\ 0.4-0.6;\ 0.8-1)$, respectively (Figure 4.12).

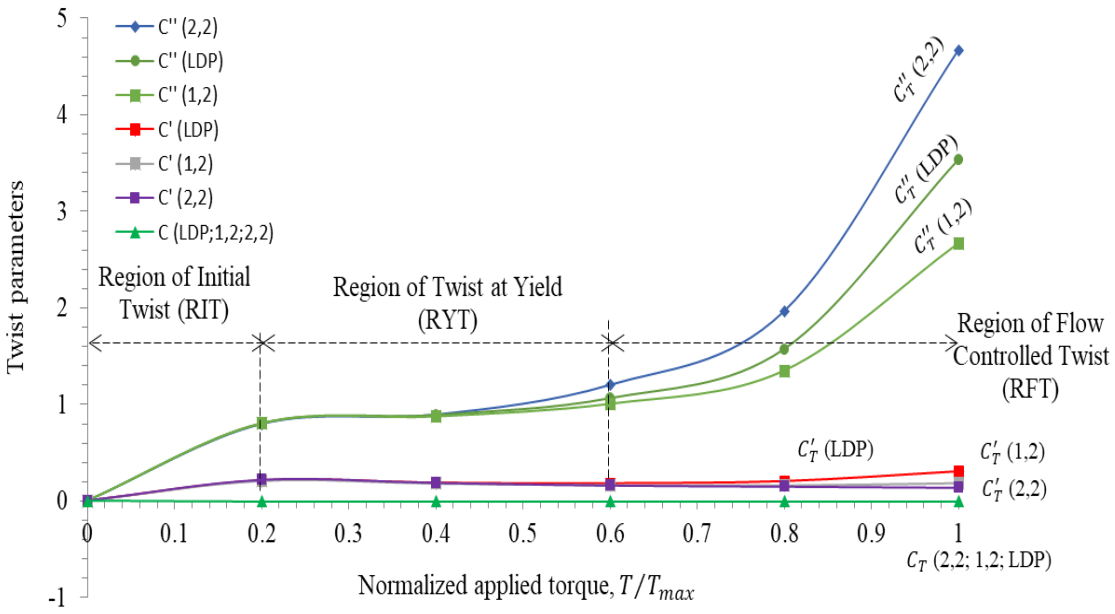

Figure 4.11 Variation of twist parameters $(C_T^{"}, C_T',\ C_T)$ with normalized applied torque for large diameter pile (LDP) and pile groups (1,2; 2,2)

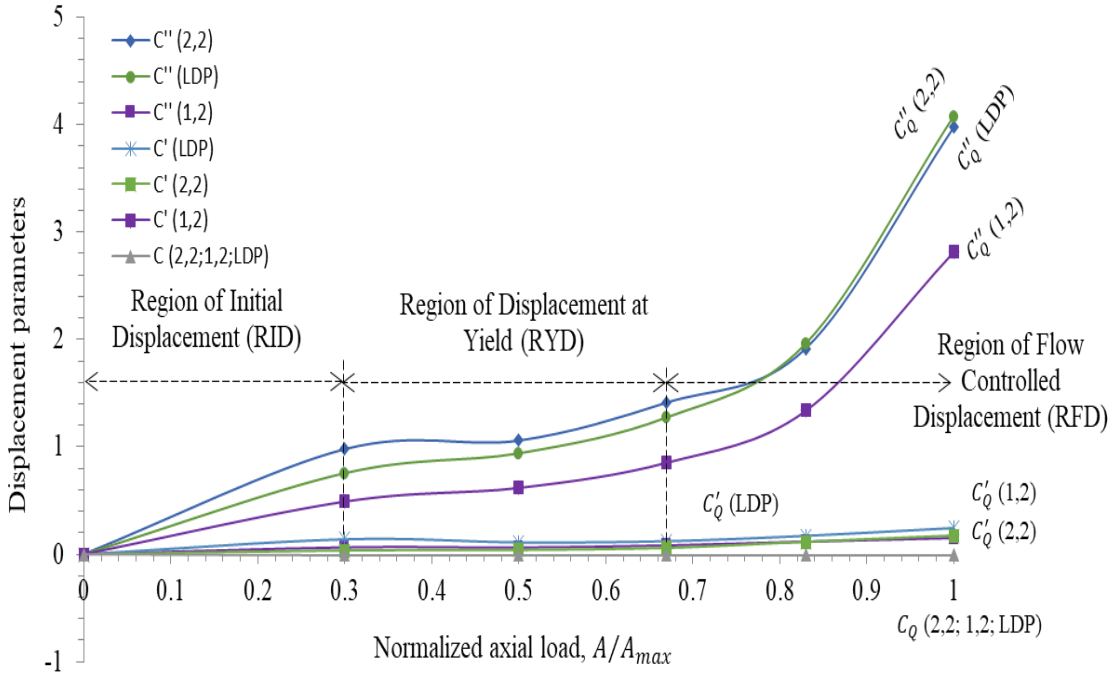

Figure 4.12 Variation of displacement parameters $(C_Q^{"}, C_Q', C_Q)$ *with normalized applied torque for large diameter pile (LDP) and pile groups (1,2; 2,2)*

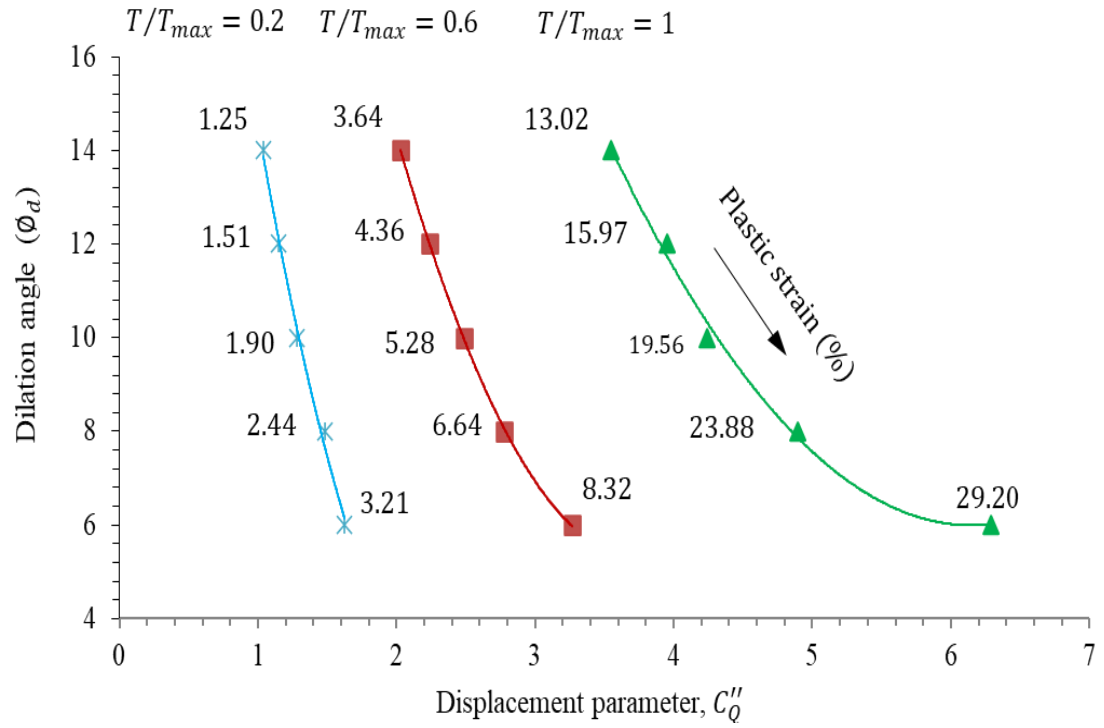

Figure 4.13 Variation of displacement parameter with dilation angle and plastic strain captured for $T/T_{max} = 0.2 - 1$, A/A_{max} *=0.33*

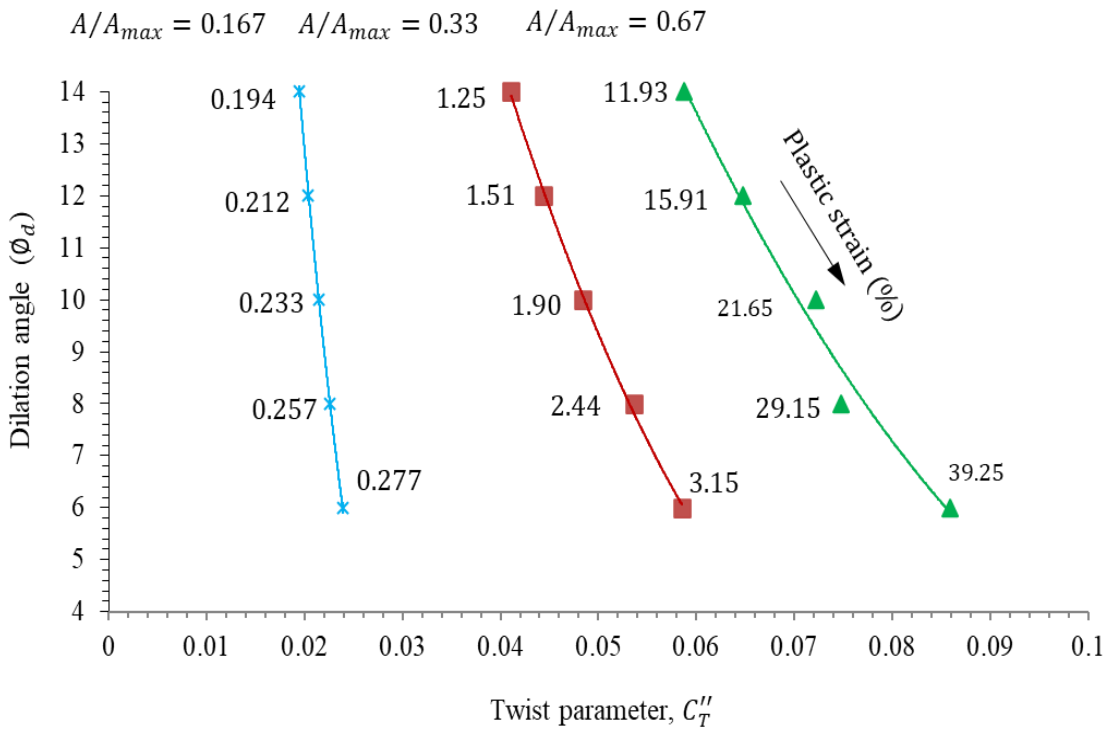

Figure 4.14 Variation of twist parameter with dilation angle and plastic strain captured for $A/A_{max} = 0.167 - 0.67,\ \ T/T_{max} = 0$

The variation of displacement and twist parameters with dilation angle and plastic strain has been captured (Figure 4.13-14). The displacement and twist parameter increases with a decrease in the angle of dilation. The plastic strain increases with an increase in displacement and twist parameters. The load-displacement and torque-twist relationships have been classified in Table 4.3 and Table 4.4 according to displacement and twist parameters for various pile groups. The variation of normalized axial load and normalized pile head displacement was captured for dilation angles 6^0 to 14^0. The axial displacement decreases with an increase in the angle of dilation. Such a decrease in displacement is due to the increase in the confinement of geomaterial (Bolton 1986). The effect of increasing the dilation angle on axial displacement reduces when the normalized applied torque has been decreased from 1 to 0.6 (Figure 4.15). Similarly, the effect of increasing the dilation angle on twist reduces when the normalized axial load has been decreased from 0.67 to 0.167 (Figure 4.16).

Table 4.3 Classification of twist parameters

Pile layout	T/T_{max}	C_T''	C_T'	C_T	Classification*
(2,2)	0.8-1.0	1.96-4.67	0.15-0.14	-0.001	RFT
	0.4-0.6	0.89-1.20	0.19-0.16	-0.001	RYT
	0.2	0.79	0.22	-0.001	RIT
(1,2)	0.8-1.0	1.35-2.67	0.19-0.16	-0.0006	RFT
	0.4-0.6	0.87-1.0	0.16-0.182	-0.0004	RYT
	0.2	0.80	0.21	-0.0050	RIT
LDP	0.8-1.0	1.57-3.53	0.20-0.30	-0.002	RFT
	0.4-0.6	0.88-1.06	0.18-0.19	-0.003	RYT
	0.2	0.80	0.21	-0.005	RIT

Table 4.4 Classification of displacement parameters

Pile layout	Q/Q_{max}	C_Q''	C_Q'	C_Q	Classification*
(2,2)	0.83-1.0	1.92-3.98	0.12-0.17	-0.005	RFD
	0.50-0.67	1.06-1.41	0.04-0.06	-0.005	RYD
	0.30	0.98	0.04	-0.005	RID
(1,2)	0.83-1.0	1.34-2.82	0.12-0.15	-0.003	RFD
	0.50-0.67	0.62-0.85	0.06-0.08	-0.003	RYD
	0.30	0.49	0.06	-0.002	RID
LDP	0.83-1.0	1.96-4.07	0.17-0.25	-0.005	RFD
	0.50-0.67	0.94-1.28	0.11-0.12	-0.006	RYD
	0.30	0.754	0.14	-0.012	RID

*LDP-large diameter pile, RFT-Regions of flow-controlled twist, RYT-Regions of twist at yield, RIT-Regions of initial twist, RFD-Regions of flow-controlled displacement, RYD-Regions of displacement at yield, RID-Regions of initial displacement

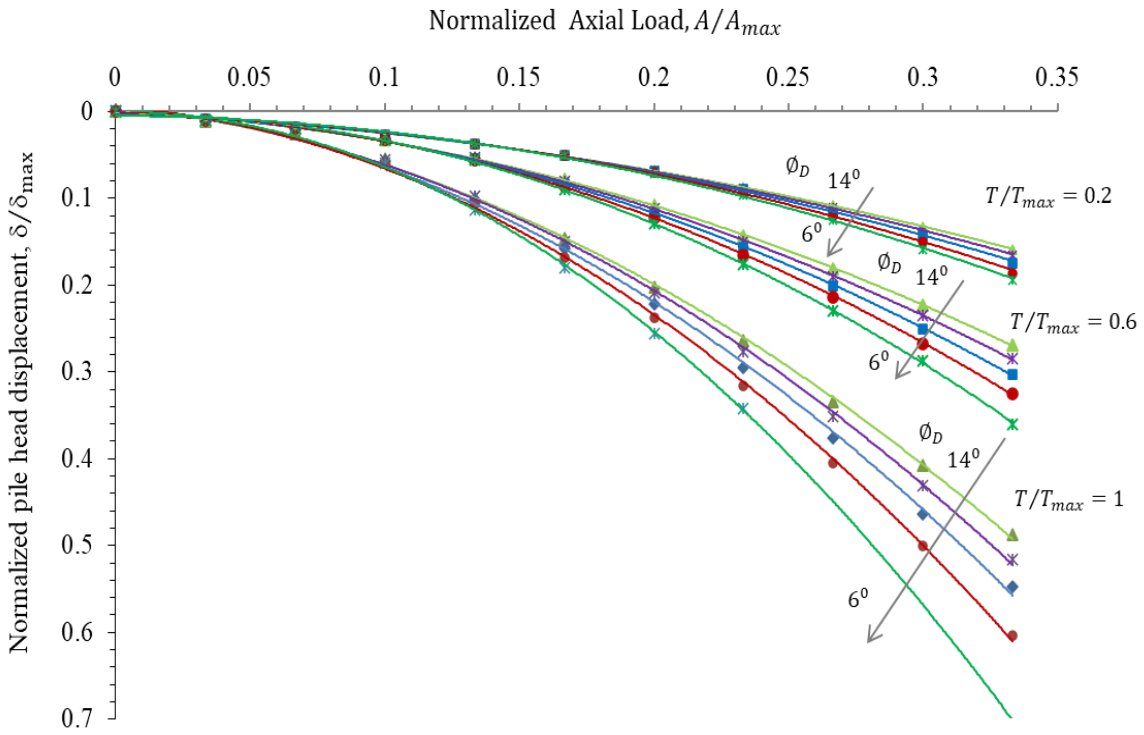

Figure 4.15 Variation of normalized axial load and normalized pile head displacement captured for $\emptyset_D = 6^0$ *to* 14^0

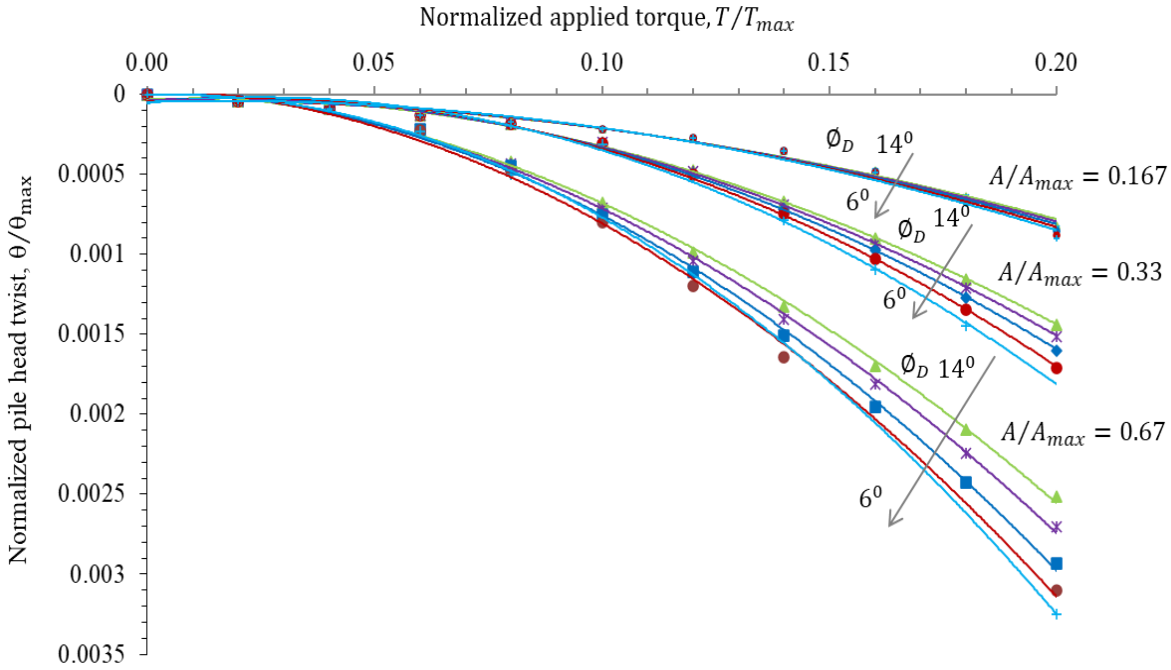

Figure 4.16 Variation of normalized applied torque and normalized pile head twist captured for $\emptyset_D = 6^0$ *to* 14^0

The comparison of the large diameter pile (LDP) and pile groups (1,2; 2,2) has been presented (Figure 4.17). The (1,2) pile group shows the highest resistance to the torsional load.

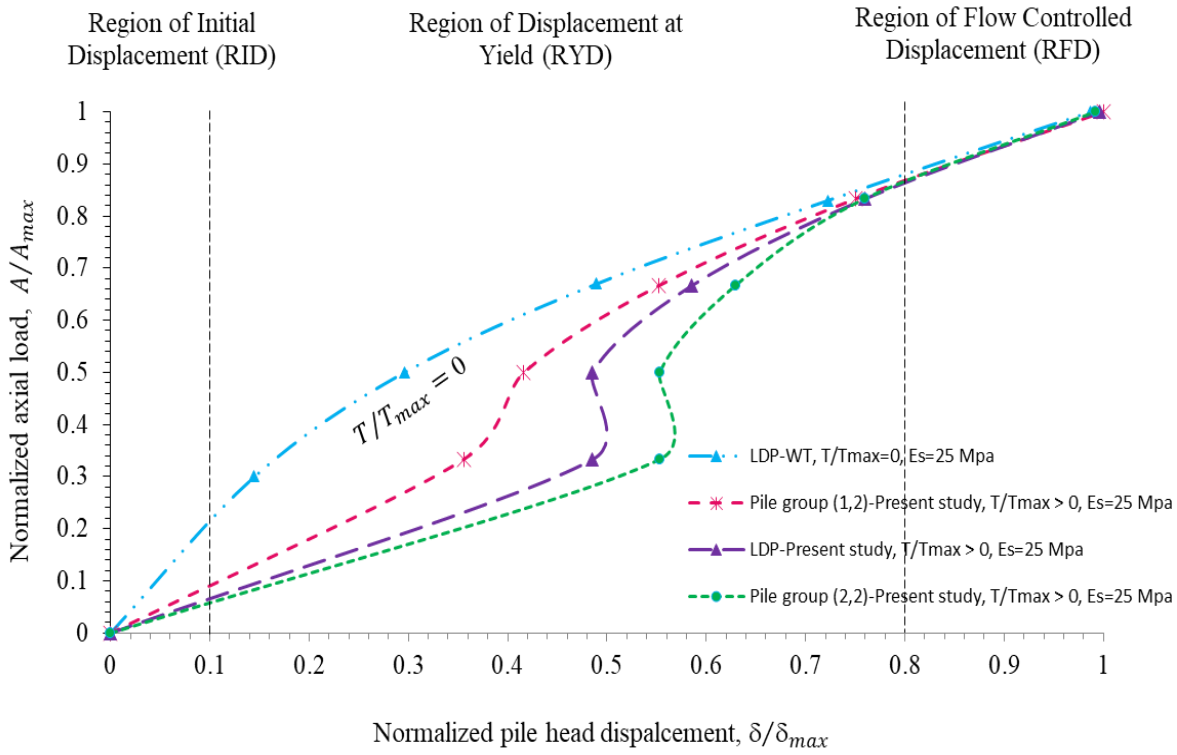

Figure 4.17 The comparison of the A/A_{max} of the large-diameter pile (LDP) and pile groups (1,2; 2,2) in the present study, the large-diameter pile without torsional load (LDP-WT) for initial modulus of elasticity 25 Mpa

4.9 Conclusions

- The coupling effect of axial load on torsional pile response conversely can be studied with a nonlinear three-dimensional finite-element analysis, while the conventional subgrade reaction method of pile analysis cannot consider this interaction.
- In designing pile groups to resist combined axial and torsional loads, the criterion for design is not the ultimate capacity but the displacement and twist of piles. The resultant displacement and twist should be considered while designing pile groups subjected to combined loads.

- The three-dimensional numerical model on the LDP (large diameter pile) and pile groups (1,2; 2,2) has been compared with the result of the experimental pile load test reported by Gong et al (2002 & 2019). Initially, the numerical model shows good agreement with the test results, however, the slope of the experimental curve increases sharply due to the flow of the geomaterial in the field test (in the absence of a flow-controlled regime) immediately after yield conditions preceded by initial displacement region. The results are in good agreement with the numerical solutions presented by Georgiadis (1987).
- The resultant displacement increases on the application of the torsional load for the LDP and pile groups (1,2; 2,2). The resultant displacement increases in a range of 19% to 235%; 20% to 140%; and 20% to 246% for the LDP and pile group (1,2; 2,2), respectively, the normalized applied torque and normalized axial load applied in the range 0.6 to 1 and 0.33 to 0.67, respectively.
- The twist increases with an increase in axial load. The twist increases in a range of 18% to 530%; 30% to 474%; and 22% to 651%, respectively, and the normalized axial load and normalized applied torque are in the range of 0.5 to 1 and 0.2 to 0.8, respectively.
- The twist parameters ($C_T^{"}, C_T', C_T$) and displacement parameters ($C_Q^{"}, C_Q', C_Q$), which depends upon the plastic strain and dilation angle have been classified and recommended for designing piles for displacement and twist.

References

Anagnostopoulos, C., & Georgiadis, M. (1993). "Interaction of axial and lateral pile responses." *J. Geotech. Eng.,* 119(4), 793-798.

Bolton, M. D. (1986). "The strength and dilatancy of sands." *Geotechnique*, 36(1), 65-78.

Bowles, L. E. (1996). *Foundation analysis and design*. McGraw-Hill.

Broms, B. B. (1964). "Lateral resistance of piles in cohesionless soils." *J. Soil Mech. Found. Div.,* 90(3), 123-158.

Chow, Y. K. (1985). "Torsional response of piles in nonhomogeneous soil." Journal of Geotechnical Engineering, 111(7), 942-947.

Georgiadis, M. (1987). "Interaction between torsional and axial pile responses." *Int. J. numerical and analytical methods in geomechanics,* 11(6), 645-650.

Georgiadis, M., & Saflekou, S. (1990). "Piles under axial and torsional loads." *Comput. Geotech.,* 9(4), 291-305.

Guoliang, D., Weiming, G., Lin, J., & Qinzhong, Y. (2002). "Static loading test of a self-balanced approach to a pile in the Yangtze River." *In Advances in Building Technology,* 695-701. Elsevier.

Guoliang, D., & Xiaojuan, L. (2019). "The Statistical Study on Bearing Capacity of the Self-Balanced Loading Test." *Int. Symposium on Testing and Technology for Bearing Capacity of Deep Foundation, Delhi,* ISBN:978-93-5391-519-3, 19-20.

Hutton, D. V. (2004). *Fundamentals of finite element analysis*. McGraw-Hill.

Kong, L. G., & Zhang, L. M. (2009). "Nonlinear analysis of torsionally loaded pile groups." *Soils and Foundations,* 49(2), 275-286.

Mehra, S. & Trivedi, A. (2018). "Experimental studies on model single pile and pile groups subjected to torque." *Proceedings of China-Europe Conference, Geotech. Engg.,* 10.1007/978-3-319-97115-5_24, 997-1000.

Mehra, S. & Trivedi, A. (2018). "Analysis and simulation of cyclic torque application on pile groups." *Proceeding of 12th International Super Pile World, Nanjing, Jiangsu, China,* 277-282.

Mehra, S & Trivedi, A. (2019). "Deep foundations subjected to combined axial and torsional loads." *Int. Symposium on Testing and Technology for Bearing Capacity of Deep Foundation, Delhi,* ISBN:978-93-5391-519-3, 19-20.

Menetrey, P., & Willam, K. J. (1995). "Triaxial failure criterion for concrete and its generalization." *Structural Journal,* 92(3), 311-318.

Mindlin, R. D. (1936). "Force at a point in the interior of a semi-infinite solid." *Physics,* 7(5), 195-202.

Poulos, H. G., & Davis, E. H. (1980). *Pile foundation analysis and design*, Wiley, New York.

Poulos, H. G. (1975). “Torsional response of piles.” *J. Geotech. Geoenviron. Eng.,* 101(10), 1019-1035.

Rajapakse, R. A. (2016). *Pile Design and construction rules of thumb*. Butterworth-Heinemann.

Randolph, M. F. (1981). “The response of flexible piles to lateral loading.” *Geotechnique*, 31(2), 247-259.

Randolph, M. F. (1981). “Piles subjected to torsion.” *J. Geotech. Eng.,* 107(8), 1095-1111.

Reese, L.C & Van Impe, W.F. (2001). “Single pile and pile group under lateral loading.” *A.A. Balkema, Rotterdam.*

Terzaghi, K. (1955). “Evaluation of coefficients of subgrade reaction.” *Geotechnique* 5(4) 297-326.

Trivedi, A. (2015). “Computing in-situ strength of rock masses based upon RQD and modified joint factor: Using pressure and damage sensitive constitutive relationship.” *J. Rock Mech. Geotech. Eng.,* 7(5), 540-565.

Trivedi, A. & Mehra, S. (2018). “Development and application of deep foundations in India.” *Proceedings of 12th Super Pile World, Nanjing, Jiangsu, China,* 71-86.

Vesic, A. S. (1977). *Design of pile foundations*. NCHRP Synthesis of highway practice, (42). http://onlinepubs.trb.org/Onlinepubs/nchrp/nchrp_syn_42.pdf.

Yu, H. S. (2007). *Plasticity and geotechnics (Vol. 13).* Springer Science & Business Media.

Zhao, X. G., & Cai, M. (2010). “A mobilized dilation angle model for rocks.” *J. Rock Mech. Mining Sciences*, 47(3), 368-384.

Appendix A-4

(a) Pile stiffness matrix with two elements and three nodes

$$\{\delta, \psi, \theta\} = \{\delta_1 \delta_2 \delta_3 \delta_4 \psi_5 \psi_6 \theta_7 \theta_8\} \tag{A4.1}$$

$$\{N\} = \{N_1 N_2 N_3 N_4 N_5 N_6 N_7 N_8\} \tag{A4.2}$$

$$\Lambda_P = AE \int_0^L \begin{bmatrix} \frac{dN_1}{dz}\frac{dN_1}{dz} & \frac{dN_1}{dz}\frac{dN_2}{dz} \\ \frac{dN_1}{dz}\frac{dN_2}{dz} & \frac{dN_2}{dz}\frac{dN_2}{dz} \end{bmatrix} dz + GJ \int_0^L \begin{bmatrix} \frac{dN_7}{dz}\frac{dN_7}{dz} & \frac{dN_7}{dz}\frac{dN_8}{dz} \\ \frac{dN_7}{dz}\frac{dN_8}{dz} & \frac{dN_8}{dz}\frac{dN_8}{dz} \end{bmatrix} dz + EI \int_0^L \begin{bmatrix} \frac{dN_3}{dz}\frac{dN_3}{dz} & \frac{dN_3}{dz}\frac{dN_4}{dz} & \frac{dN_3}{dz}\frac{dN_5}{dz} & \frac{dN_3}{dz}\frac{dN_6}{dz} \\ \frac{dN_4}{dz}\frac{dN_3}{dz} & \frac{dN_4}{dz}\frac{dN_4}{dz} & \frac{dN_4}{dz}\frac{dN_5}{dz} & \frac{dN_4}{dz}\frac{dN_6}{dz} \\ \frac{dN_5}{dz}\frac{dN_3}{dz} & \frac{dN_5}{dz}\frac{dN_3}{dz} & \frac{dN_5}{dz}\frac{dN_5}{dz} & \frac{dN_5}{dz}\frac{dN_6}{dz} \\ \frac{dN_6}{dz}\frac{dN_3}{dz} & \frac{dN_6}{dz}\frac{dN_4}{dz} & \frac{dN_6}{dz}\frac{dN_5}{dz} & \frac{dN_6}{dz}\frac{dN_6}{dz} \end{bmatrix} dz \tag{A4.3}$$

Carrying out the differentiation and integration, the global stiffness matrix is expressed as,

$$\Lambda_P = \begin{bmatrix} \frac{A_1E_1}{L_1} & 0 & 0 & 0 & \frac{-AE_1}{L_1} & 0 & 0 & 0 & 0 & 0 & 0 & 0 \\ 0 & \frac{12E_1I_1}{L_1^3} & \frac{6E_1I_1}{L_1^2} & 0 & 0 & \frac{-12E_1I_1}{L_1^3} & \frac{6E_1I_1}{L_1^2} & 0 & 0 & 0 & 0 & 0 \\ 0 & \frac{6E_1I_1}{L_1^2} & \frac{4E_1I_1}{L_1} & 0 & 0 & \frac{-6E_1I_1}{L_1^2} & \frac{2E_1I_1}{L_1} & 0 & 0 & 0 & 0 & 0 \\ 0 & 0 & 0 & \frac{G_1J_1}{L_1} & 0 & 0 & 0 & \frac{-G_1J_1}{L_1} & 0 & 0 & 0 & 0 \\ \frac{-AE_1}{L_1} & 0 & 0 & 0 & \frac{A_1E_1}{L_1}+\frac{A_2E_2}{L_2} & 0 & 0 & 0 & \frac{-A_2E_2}{L_2} & 0 & 0 & 0 \\ 0 & \frac{-12E_1I_1}{L_1^3} & \frac{-6E_1I_1}{L_1^2} & 0 & 0 & \left(\frac{12E_1I_1}{L_1^3}+\frac{12E_2I_2}{L_2^3}\right) & \left(\frac{-6E_1I_1}{L_1^2}+\frac{6E_2I_2}{L_2^2}\right) & 0 & 0 & \frac{-12E_2I_2}{L_2^3} & \frac{6E_2I_2}{L_2^2} & 0 \\ 0 & \frac{6E_1I_1}{L_1^2} & \frac{2E_1I_1}{L_1} & 0 & 0 & \left(\frac{-6E_1I_1}{L_1^2}+\frac{6E_2I_2}{L_2^2}\right) & \left(\frac{4E_1I_1}{L_1}+\frac{4E_2I_2}{L_2}\right) & 0 & 0 & \frac{-6E_2I_2}{L_2^2} & \frac{2E_2I_2}{L_2} & 0 \\ 0 & 0 & 0 & -\frac{G_1J_1}{L_1} & 0 & 0 & 0 & \frac{G_1J_1}{L_1}+\frac{G_2J_2}{L_2} & 0 & 0 & 0 & \frac{-G_2J_2}{L_2} \\ 0 & 0 & 0 & 0 & \frac{A_2E_2}{L_1} & 0 & 0 & 0 & \frac{-A_2E_2}{L_2} & 0 & 0 & 0 \\ 0 & 0 & 0 & 0 & 0 & \frac{-12E_2I_2}{L_2^3} & \frac{-6E_2I_2}{L_2^2} & 0 & 0 & \frac{12E_2I_2}{L_2^3} & \frac{-6E_2I_2}{L_2^2} & 0 \\ 0 & 0 & 0 & 0 & 0 & \frac{6E_2I_2}{L_2^2} & \frac{2E_2I_2}{L_2^2} & 0 & 0 & \frac{-6E_2I_2}{L_2^2} & \frac{4E_2I_2}{L_2} & 0 \\ 0 & 0 & 0 & 0 & 0 & 0 & 0 & -\frac{G_2J_2}{L_2} & 0 & 0 & 0 & \frac{-G_2J_2}{L_2} \end{bmatrix} \tag{A4.4}$$

(b) Soil element stiffness

(b1) Uniform soil with constant subgrade modulus

$$[k_s] = k\,L \begin{bmatrix} \frac{1}{3} & \frac{1}{6} \\ \frac{1}{6} & \frac{1}{3} \end{bmatrix} \tag{A4.5}$$

(b2) Soil with subgrade modulus linearly increasing with depth

$$[k_s] = k\,L \begin{bmatrix} \frac{1}{3} & \frac{1}{6} \\ \frac{1}{6} & \frac{1}{3} \end{bmatrix} + k\,L^2 \begin{bmatrix} \frac{1}{12} & \frac{1}{12} \\ \frac{1}{12} & \frac{1}{4} \end{bmatrix} \tag{A4.6}$$

5 CYCLIC DEGRADATION PARAMETERS OF FLOW-CONTROLLED GEOMATERIAL

This chapter is based on the work that has been listed in Section 1.8 and published in the Applied Sciences and Indian Geotechnical Conference, Springer Nature. To keep the presentation of the details consistent throughout the thesis, the details are offered here with some layout modifications.

5.1 Introduction

The dynamics of pile groups are important due to their applications in machine foundations and structures exposed to cyclic loads such as wind or earthquakes. The response of structures supported by pile groups depends upon the cyclic stiffness and damping generated by geomaterial-pile interaction. Due to complex geomaterial–pile interaction, the dynamics of pile groups are not well understood. There are no readily available methods that could evaluate the response of geomaterial–pile interaction hence the geomaterial stiffness is ignored and only the pile stiffness is considered. The omission of geomaterial–pile interaction makes the analysis of pile groups quite unrealistic (Novak and Sharnouby 1983, 1984). Several analytical and numerical studies on the piles subjected to static lateral and torsional load (Poulos 1975; Randolph 1981a, 1981b; Chow 1985; Georgiadis 1987; Anagnostopoulos and Georgiadis 1993; Guo and Randolph 1996; Kong 2006; Kong and Zhang 2008, 2009; Chen, Kong and Zhang 2016; Kong, Zhang and Chen 2020) are extended to the pile groups in the present work. A series of experiments was reported on single piles and pile groups subjected to torsional loads (Mehra and Trivedi 2018a, 2018b, 2019, 2021). The numerical model was developed for the combined axial and torsional loads in flow-controlled geomaterial for the pile groups (Mehra and Trivedi 2021). The progressive twist, displacements and torsional energy around the pile groups have been presented (Mehra and Trivedi 2023a). The settlements of sand due to the cyclic twisting of

the tube were investigated by Cudmani and Gudehus (2001). The solutions for dynamic analysis of piles (Novak and Howell 1977; Novak and Sharnouby 1984; Long and Vanneste 1994; Ladhane and Sawant 2016; Basack and Nimbalkar 2017) including the literature reported mainly focused on the generic behaviour of pile groups subjected to torsion while the cyclic torsion effect has not been considered. The finite element-finite difference method has been used to evaluate the safety against the liquefaction of a reservoir subjected to cyclic loading (Zhu and Huang 2016).

The design of offshore pile groups requires consideration of the effects of cyclic torsional loading. Therefore, the present paper considers a numerical scheme that provides a framework for the estimation of the behaviour of a pile group in the sand under cyclic torsional loading. Based on a numerical scheme, the three-dimensional finite element analysis has been used to clarify the mechanism of load transfer from the pile to the surrounding geomaterial for the pile groups. The cyclic analysis of the torsionally loaded pile group in the sand is carried out by idealizing the individual pile as beam elements and the geomaterial as nonlinear spring elements. An iterative procedure is adopted and the effect of lateral and torsional load on deflection and twist, respectively, for the pile groups are investigated. Based on the lateral deflection and twist at the end of the first cycle, the degradation factor is evaluated and p-y and τ-θ curves are modified. The results from the numerical analysis work well with the published experimental results on the pile group subjected to two-way cyclic loading. Therefore, regarding the effect of torsional loads on the pile group, the following mechanisms have been investigated, namely, (a) cyclic twist behaviour of the pile group (2,2) in the flow-controlled geomaterial as a result of the torsional loading and (b) the plastic strain and peak shear stress in a flow-controlled geomaterial captured for cyclic torsional loads, which, in turn, is a function of the number of cycles and dilation.

5.2 Cyclic Torsional Load in Relation to Twist and Displacements

A nonlinear numerical scheme is presented to illustrate the behaviour of an individual pile and geomaterial due to the application of a cyclic torsional load at the head of a pile group. In this scheme, the pile is assumed to be elastic and embedded in cohesionless geomaterial. The modified torque-twist relation of a pile under cyclic torsional loading (Timoshenko and Goodier 1970) is expressed as follows:

$$\frac{d^2\theta(z,t)}{dz^2} = \frac{\pi D^2}{2J_P G_P}\tau(z,t) \tag{5.1}$$

where $\theta(z,t)$ is the twist at the pile head; G_P is the shear modulus of the pile shaft; J_P is the polar second moment of the area of the pile section; z is the depth; D is the diameter of the pile; $G_P J_P$ is the torsional rigidity of a pile; $\tau(z,t)$ is the shear stress along the shaft. The basic equation of motion for multi-degree freedom systems is expressed as follows:

$$m\ddot{y} + c_h\dot{y} + k_h y = 0 \tag{5.2}$$

$$m\ddot{\theta} + c_\theta\dot{\theta} + k_\theta\theta = 0 \tag{5.3}$$

where c_h and c_θ are the coefficients of damping for lateral and torsional cyclic loading, respectively; k_h and k_θ are the modulus of subgrade reaction for lateral and torsional cyclic loading, respectively. The modified second and fourth-order differential equilibrium equations for lateral displacement (y) and twist angle (θ) of the pile in the geomaterial, assuming lateral displacement and twist as a function of time are expressed as follows:

$$\rho_s \mathrm{A}\frac{\partial^2 \mathrm{y(z,t)}}{\partial \mathrm{t}^2} + c_h\frac{\partial \mathrm{y(z,t)}}{\partial \mathrm{t}} + k_{hN}\,\mathrm{y}(z,t) = -E_P I_P\frac{\partial^4 \mathrm{y(z,t)}}{\partial z^4} \tag{5.4}$$

$$\rho_s \mathrm{A} \frac{\partial^2 \theta(\mathrm{z,t})}{\partial t^2} + c_\theta \frac{\partial \theta(\mathrm{z,t})}{\partial \mathrm{t}} + k_{\theta N} \theta\,(z,t) = -G_P J_P \frac{\partial^2 \theta(\mathrm{z},t)}{\partial z^2} \tag{5.5}$$

where E_p is the elastic modulus of the pile shaft; I_p is the second-moment area of the pile section; ρ_s is the mass density of geomaterial and N is the number of cycles of torsional loading. Therefore, the differential equation of the geomaterial-pile system due to damped cyclic torsional loads assuming the harmonic motion induced through the pile head is expressed as follows:

$$m \frac{\partial^2 \delta(\mathrm{z,t})}{\partial \mathrm{t}^2} + c_h \frac{\partial \delta(\mathrm{z,t})}{\partial \mathrm{t}} + c_\theta \frac{\partial \delta(\theta,\mathrm{t})}{\partial \mathrm{t}} + k_{hN}\, h(\mathrm{z,t}) + k_{\theta N}\, \theta(z,\mathrm{t}) + E_P I_P \frac{\partial^4 \delta(\mathrm{z,t})}{\partial \mathrm{z}^4} + G_P J_P \frac{\partial^2 \theta\,(\theta,\mathrm{t})}{\partial \mathrm{z}^2} = T_0 e^{iwt} \tag{5.6}$$

where T_0 is the torsional load applied on the centre of the pile group and ω is the natural frequency. Figure 5.1a demonstrates the numerical model of the pile group employed in the present investigation. The loading has been applied as a variation of two-way symmetrical cyclic torsional loading with time (Figure 5.1b). The lateral and torsional resistance in clockwise and anticlockwise directions subjected to cyclic torsional loading for the pile group (2,2) is shown (Figure 5.1c). We consider the finite element in bending (Figure 5.1d). The approximation of the time-dependent displacement field $\delta(z,t)$ using the Galerkin method (Hutton 2004) is expressed as follows:

$$\delta(z,t) = N_1(z)\delta_1(t) + N_2(z)\delta_2(t) + N_3(z)\delta_3(t) + N_4(z)\delta_4(t) + N_5(z)\psi_5(t) + N_6(z)\psi_6(t) + N_7(z)\psi_7(t) + N_8(z)\psi_8(t) + N_9(z)\theta_9(t) + N_{10}(z)\theta_{10}(t) = [N]\{\delta(\mathrm{t})\} \tag{5.7}$$

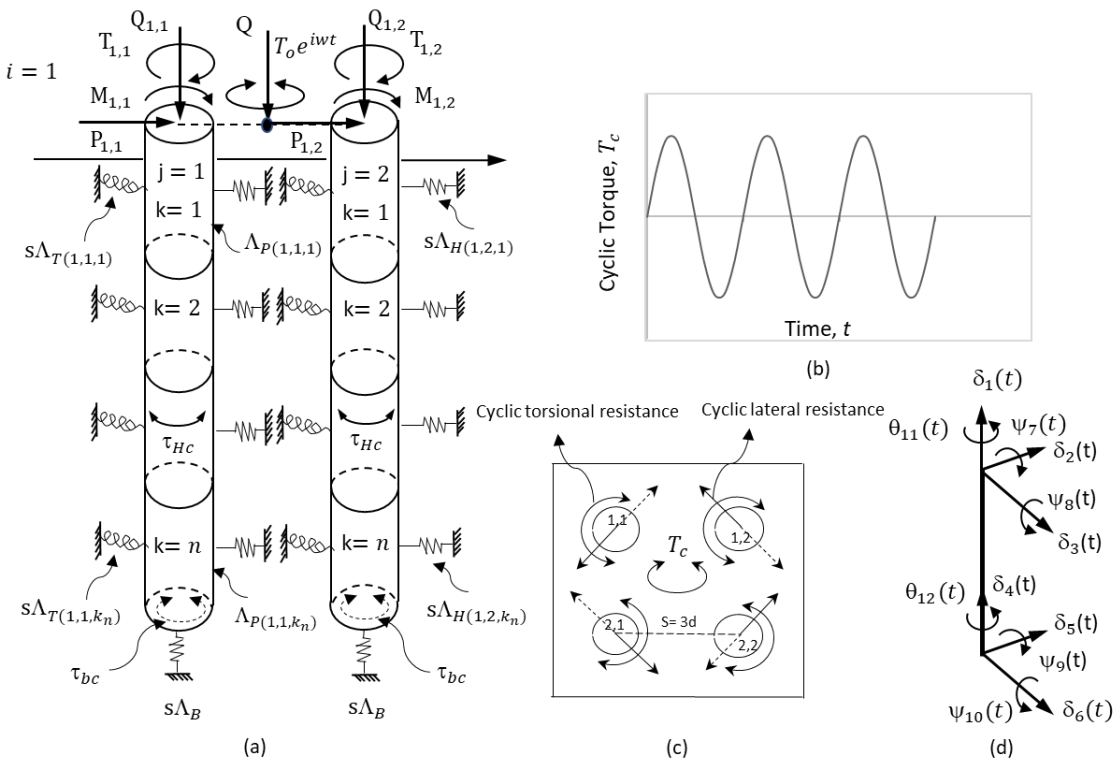

Figure 5.1(a) Pile group (2,2) subjected to cyclic torsional loading at $N = 1$ with initial pile stiffness $(\Lambda_{P(i,j,k_n)})$, initial geomaterial torsional spring $(s\Lambda_{T(i,j,k_n)})$, initial geomaterial lateral spring $(s\Lambda_{H(i,j,k_n)})$, initial base geomaterial spring $(s\Lambda_B)$ at a node and τ_{Hc} and τ_{bc} are the cyclic horizontal and base shear stress, respectively. For the case of pure cyclic torsional load, it is assumed that the value of Q tends to zero, (b) Variation of two-way symmetric cyclic torsional load with time for $N = 3$, (c) The lateral and torsional resistance in clockwise and anticlockwise directions subjected to cyclic torsional loading for pile group (2,2) (d) Six translational $[\delta_1(t), \delta_2(t), \delta_3(t), \delta_4(t), \delta_5(t), \delta_6(t)]$, four rotational $[\psi_7(t), \psi_8(t), \psi_9(t), \psi_{10}(t)]$, and two torsional $[\theta_{11}(t)$ and $\theta_{12}(t)]$ degrees of freedom for a pile element at a node

where,

$$[N] = [N_1\ N_2\ N_3\ N_4\ N_5\ N_6\ N_7\ N_8\ N_9\ N_{10}] \tag{5.8}$$

$$\{\delta(t)\} = \{\delta_1 \delta_2\ \delta_3\ \delta_4\ \psi_5\ \psi_6\ \psi_7\ \psi_8\ \theta_9\ \theta_{10}\}\{t\} \tag{5.9}$$

where, N_m are the shape functions for interpolation $\delta(z,t)$ using its nodal values.

$$N_1 = N_2 = 1 - 3\xi^2 + 2\xi^3;\ N_3 = N_4 = 3\xi^2 - 2\xi^3; \tag{5.10}$$

$$N_5 = N_6 = L\left(\xi - 2\xi^2 + \xi^3\right);\ N_7 = N_8 = L\,\xi^2(\xi - 1) \tag{5.11}$$

The Galerkin residual equation for the finite element of length, *L*, assuming displacements as a function of time is expressed as follows:

$$N_m(z)\int_0^L \left(\rho A\frac{\partial^2\delta(\mathrm{z,t})}{\partial \mathrm{t}^2} + EI\frac{d^4\delta(\mathrm{z,t})}{dz^4}\right)dz = 0 \tag{5.12}$$

Therefore, the pile element matrix in bending assuming displacement as a function of time is expressed as follows:

$$[\Lambda_{\mathrm{PP}}] = \rho A\int_0^L \left(N_m\frac{\partial^2\delta}{\partial \mathrm{t}^2} + N_n\frac{\partial^2\delta}{\partial \mathrm{t}^2}\right)dz + EI\int_0^L \frac{d^2N_m}{dz^2}\frac{d^2N_n}{dz^2}dz \tag{5.13}$$

where, $m = 1,2,5,6;\ n = 3,4,7,8$

Assuming twist as a function of time (Figure 5.1d), the pile element matrix in torsion is expressed as follows:

$$[\Lambda_{\mathrm{PT}}] = \rho A\int_0^L \left(N_m\frac{\partial^2\delta}{\partial \mathrm{t}^2} + N_n\frac{\partial^2\delta}{\partial \mathrm{t}^2}\right)dz + G_P J\int_0^L \frac{dN_m}{dz}\frac{dN_n}{dz}dz \tag{5.14}$$

where, $m = 9;\ n = 10$

$$[N] = [N_9\ N_{10}];\ \{\theta\} = \{\theta_9\ \theta_{10}\}\{t\} \tag{5.15}$$

$$N_9 = 1 - \frac{Z}{L}, N_{10} = \frac{Z}{L} \tag{5.15}$$

5.3 Response of the geomaterial to cyclic torsional loading

The pile group is placed into a homogenous isotropic granular geomaterial medium. The application of cyclic torsional loading on the pile group is resisted by the flow-controlled geomaterial. The stress-strain response of geomaterial is highly nonlinear in all phases of loading. The hyperbolic stress-strain curve (Fahey and Carter 1993) is expressed as follows:

$$\frac{G_s}{G_{max}} = 1 - f_s \left(\frac{\tau}{\tau_{max}}\right)^{g_s} \tag{5.16}$$

where G_s and G_{max} are the initial and maximum shear modulus of geomaterial, respectively; τ and τ_{max} are the current and maximum shear stress, respectively; f_s and g_s are the curve fitting parameters. The parameter f_s controls the magnitude or the extent of degradation whereas the parameter g_s controls the rate of degradation and the curvature of the curve. A two-way torsional load applied at the centre of the pile group varies sinusoidally with time. The torsional and lateral resistances concurrently resist a portion of the applied torsional load (Kong 2006). Therefore, the initial modulus of subgrade reaction for the lateral load, k_h, and torsional load, k_θ, using the nonlinear $p - y$ and $\tau - \theta$ curves are expressed as follows:

$$k_h = \frac{P}{y} \tag{5.17}$$

$$k_\theta = \frac{2T_s}{\pi D^2 L} \tag{5.18}$$

where P and T_s are the lateral and torsional geomaterial reactions per unit length of the pile (L), respectively. In the cyclic torsional analysis of pile groups, the geomaterial degradation has been captured by modifying the geomaterial spring stiffness (lateral translational spring and a torsional spring) after the completion of a number (N) of cycles. Little and Briaud (1988) model calculates the deterioration of the geomaterial reaction modulus, k_h, due to cyclic lateral loading and is expressed as follows:

$$k_{hN} = k_{h1} N^{-\alpha} \tag{5.19}$$

where k_{hN} takes the value of k_h at the N^{th} cycle of load; k_{h1} is the value of the geomaterial lateral reaction modulus for the first cycle of load, and α is the degradation parameter for geomaterial lateral modulus. Similarly, the deterioration of the geomaterial shear modulus, k_θ, due to cyclic torsional loading is expressed as follows:

$$k_{\theta N} = k_{\theta 1} N^{-\beta} \tag{5.20}$$

where $k_{\theta N}$ takes the value of k_θ at the N^{th} cycle of load, $k_{\theta 1}$ is the value of the geomaterial torsional reaction modulus for the first cycle of load and β is the degradation parameter for geomaterial torsional modulus. The degradation parameters for geomaterial lateral reaction modulus, α and geomaterial torsional modulus, β, are expressed as follows:

$$\alpha = \frac{E_c}{E_s};\ \beta = \frac{G_c}{G_s} \tag{5.21}$$

where E_c and E_s are the geomaterial modulus for cyclic and static loading respectively; G_c and G_s are the geomaterial shear modulus for cyclic and static loading respectively. As the angle of the pile twist increases, the mobilised shear stress at the pile shaft will reach the

limiting value and the slip will occur between the pile and the geomaterial. The limiting shaft friction τ_u (Guo and Randolph 1996) can be expressed as follows:

$$\tau_u = A_t z^t \tag{5.22}$$

where, A_t is the constant that determines the magnitude of the shaft friction and t is the corresponding non-homogeneity factor. A correlation between θ_i and τ for an initial no-slip condition (Randolph 1981b) is expressed as follows:

$$\theta_i = \frac{\tau}{2G_s} \tag{5.23}$$

where θ_i is the angle of twist for i^{th} element; τ is the pile-geomaterial interfacial shear stress; G_s is the initial geomaterial modulus.

The lateral spring stiffness at a node has been related to parameters inside the yield surface assuming displacement as a function of time and is expressed as follows:

$$[s\Lambda_{He}] = \rho A \int_0^L \left(N_m \frac{\partial^2 \delta}{\partial t^2} + N_n \frac{\partial^2 \delta}{\partial t^2} \right) dz + c_h \int_0^L \left(N_m \frac{\partial \delta}{\partial t} + N_n \frac{\partial \delta}{\partial t} \right) dz + k_{hN} \int_0^L \frac{dN_m}{dz} \frac{dN_n}{dz} dz \tag{5.24}$$

Similarly, the lateral translational spring stiffness at a node has been related to yield flow parameters assuming displacement as a function of time and is expressed as follows:

$$[s\Lambda_{Hf}] = f(s\Lambda_{He}, s\Lambda_{Hp}) = (k_{hN} f(G_{se})) \int_0^L \frac{dN_m}{dz} \frac{dN_n}{dz} dz \tag{5.25}$$

where $k_{hN} = \frac{P_N}{y_N}$, P_N and y_N are the lateral geomaterial reaction per unit length of the pile and lateral displacement of the pile for N^{th} cycles, respectively; $(s\Lambda_{H_e})$ is the stiffness as long as $f \rightarrow 0$, $(s\Lambda_{H_p})$ is the flow-controlled stiffness and G_{se} is the equivalent shear modulus of the geomaterial (Mehra and Trivedi 2021) at a node and is expressed as follows:

$$G_{se} = f(f,g) = f\left(\frac{\frac{\partial f}{\partial \sigma_{kl}}\frac{\partial g}{\partial \sigma_{ij}}}{\frac{\partial f}{\partial \varepsilon^{p}_{pq}}\frac{\partial g}{\partial \sigma_{pq}}}\right) \tag{5.26}$$

The torsional spring stiffness at a node has been related to parameters inside the yield surface assuming twist as a function of time and is expressed as follows:

$$[s\Lambda_{\theta e}] = \rho A \int_0^L \left(N_m \frac{\partial^2 \delta}{\partial t^2} + N_n \frac{\partial^2 \delta}{\partial t^2}\right) dz + c_\theta \int_0^L \left(N_m \frac{\partial \delta}{\partial t} + N_n \frac{\partial \delta}{\partial t}\right) dz + k_{\theta N} \int_0^L \frac{dN_m}{dz}\frac{dN_n}{dz} dz \tag{5.27}$$

The torsional spring stiffness at each node has been related to the yield flow parameters and is expressed as follows:

$$\left[s\Lambda_{\theta f}\right] = f\left(s\Lambda_{\mathrm{Te}}, s\Lambda_{\mathrm{Tp}}\right) = \left(k_{\theta N} f(G_{se})\right) \int_0^L \frac{dN_m}{dz}\frac{dN_n}{dz} dz \tag{5.28}$$

5.4 Equation of Equilibrium and Group Assembly of Stiffness Matrix

The equation of equilibrium for pile-geomaterial elements considering Eq. (1-28) is expressed as follows:

$$\{F(t)\} = \Big[EI\int_0^L \frac{d^2N_m}{dz^2}\frac{d^2N_n}{dz^2}dz + GJ\int_0^L \frac{dN_m}{dz}\frac{dN_n}{dz}dz + \rho A\int_0^L \Big(N_m\frac{\partial^2\delta}{\partial t^2} + N_n\frac{\partial^2\delta}{\partial t^2}\Big)dz + c_h\int_0^L \Big(N_m\frac{\partial\delta}{\partial t} + N_n\frac{\partial\delta}{\partial t}\Big)dz + c_\theta\int_0^L \Big(N_m\frac{\partial\delta}{\partial t} + N_n\frac{\partial\delta}{\partial t}\Big)dz + k_{hN}\int_0^L \frac{dN_m}{dz}\frac{dN_n}{dz}dz + \big(k_{hN}f(G_{se})\big)\int_0^L \frac{dN_m}{dz}\frac{dN_n}{dz}dz + k_{\theta N}\int_0^L \frac{dN_m}{dz}\frac{dN_n}{dz}dz + (k_{\theta N}f(G_{se}))\int_0^L \frac{dN_m}{dz}\frac{dN_n}{dz}dz\Big]\{\delta\} \quad (5.29)$$

where, $\{\delta, \psi, \theta\} = \{\delta_1\delta_2\delta_3\delta_4\psi_5\psi_6\psi_7\psi_8\theta_9\theta_{10}\}\{t\}$

$$\{F(t)\} = \{\ P_{mx}P_{my}\ P_{nx}\ P_{ny}\ M_{mx}\ M_{my}\ M_{nx}\ M_{ny}\ T_m\ \ T_n\}\{t\}$$

The overall equilibrium equations have been formulated based on the assembled group stiffness matrix and the known load vector is expressed as follows:

$$\{T(t)\} = [\Lambda_P]\{d_p(t)\} + [s\Lambda]\{d_s(t)\} \quad (5.30)$$

where $[\Lambda_p]$ and $[s\Lambda]$ are the global stiffness matrix of all the elements of the pile groups and geomaterial, respectively; $\{d_p(t)\}$ and $\{d_s(t)\}$ are the vector of deformations at pile nodes and geomaterial, respectively; {T(t)} is the cyclic torsional load applied on the pile group. The Gauss elimination has been used to solve Eq. 30, for unknown nodal displacements. The 3D FE modelling of the geomaterial-pile group has been performed based on the aforesaid idealizations.

5.5 Computational Algorithm

The computation is carried out using a pile group cyclic torque computational program (PGCYT). The flowchart is shown in Figure 5.2.

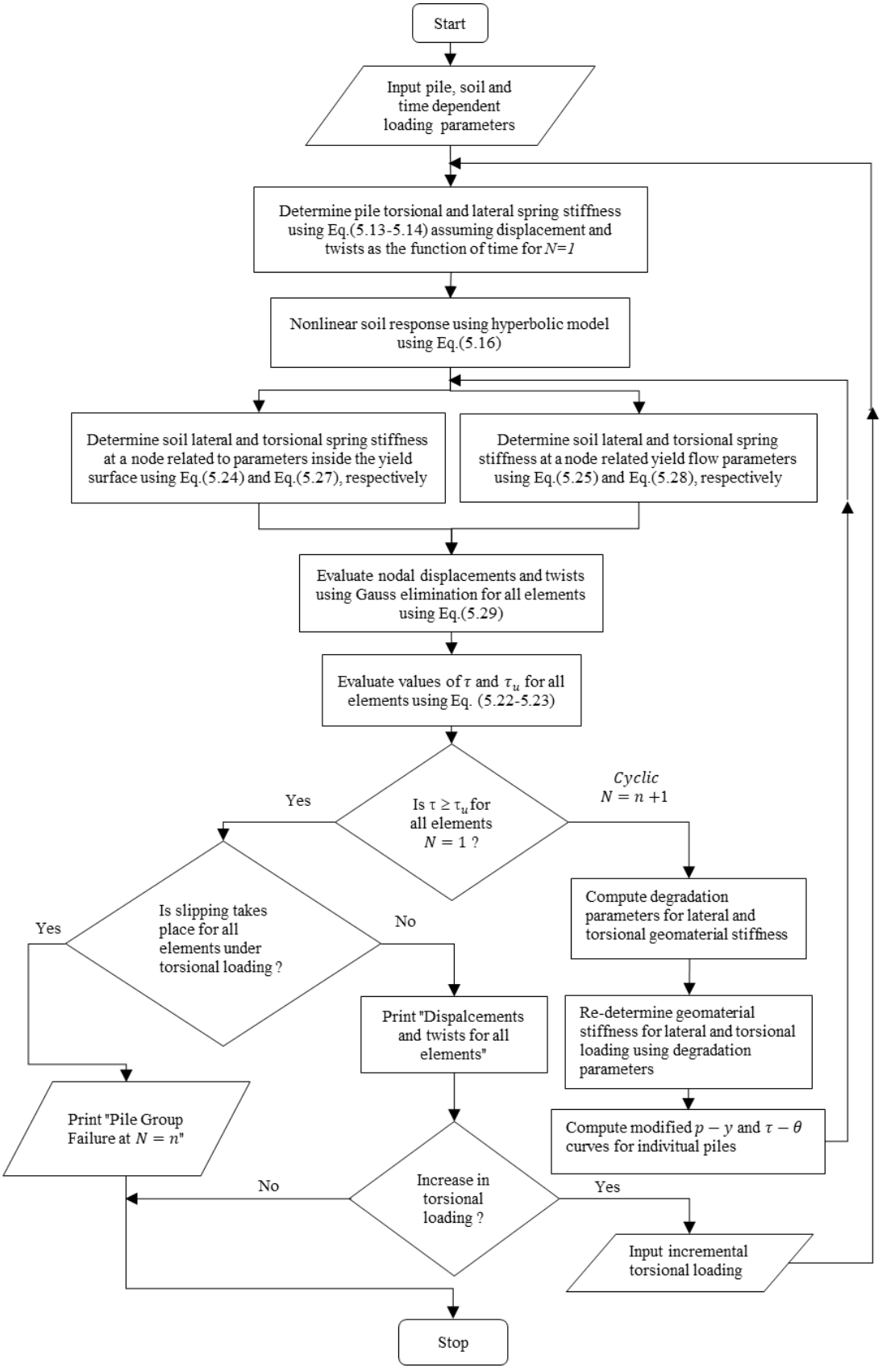

Figure 5.2 Flowchart for computation program "PGCYT"

The step-by-step algorithm for obtaining the cyclic degradation parameter of flow-controlled geomaterial is as follows:

a) Using the input parameters for geomaterial medium, pile group and cyclic loading, the analysis is carried out under cyclic torsional loads.

b) The torsional and lateral spring stiffness of the pile group is determined using Eq. (5.13-5.14) assuming displacement and twists as the function of time for the first cycle (N=1).

c) The stress-strain response of geomaterial is obtained from the hyperbolic model using Eq. (5.16).

d) The lateral and torsional spring stiffness for geomaterial at a node related to parameters inside the yield surface is determined using Eq. (5.24) and Eq. (5.27), respectively.

e) The lateral and torsional spring stiffness for geomaterial at node-related yield flow parameters is determined using Eq. (5.25) and Eq. (5.28), respectively.

f) The nodal displacements and twists are evaluated using Gauss elimination for all elements using Eq. (5.29).

g) The values of τ and τ_u are evaluated for all elements using Eq. (5.22-5.23).

h) The degradation parameter for lateral and torsional geomaterial stiffness has been computed and geomaterial stiffness for lateral and torsional loading.

i) Using reduced values of the geomaterial strength and stiffness, analysis is again carried out following the repeating steps (a-h), and the process is repeated till the required convergence is attained. The distribution of twist, plastic strain and peak shear stress are computed for the pile group.

5.6 Experimental Study on Pile Groups Subjected to Cyclic Torsional Loads

5.6.1 Experimental Test Set-up

A test set-up has been fabricated to impart cyclic torsional loads on pile groups (i, j) as shown in Figure 5.3.

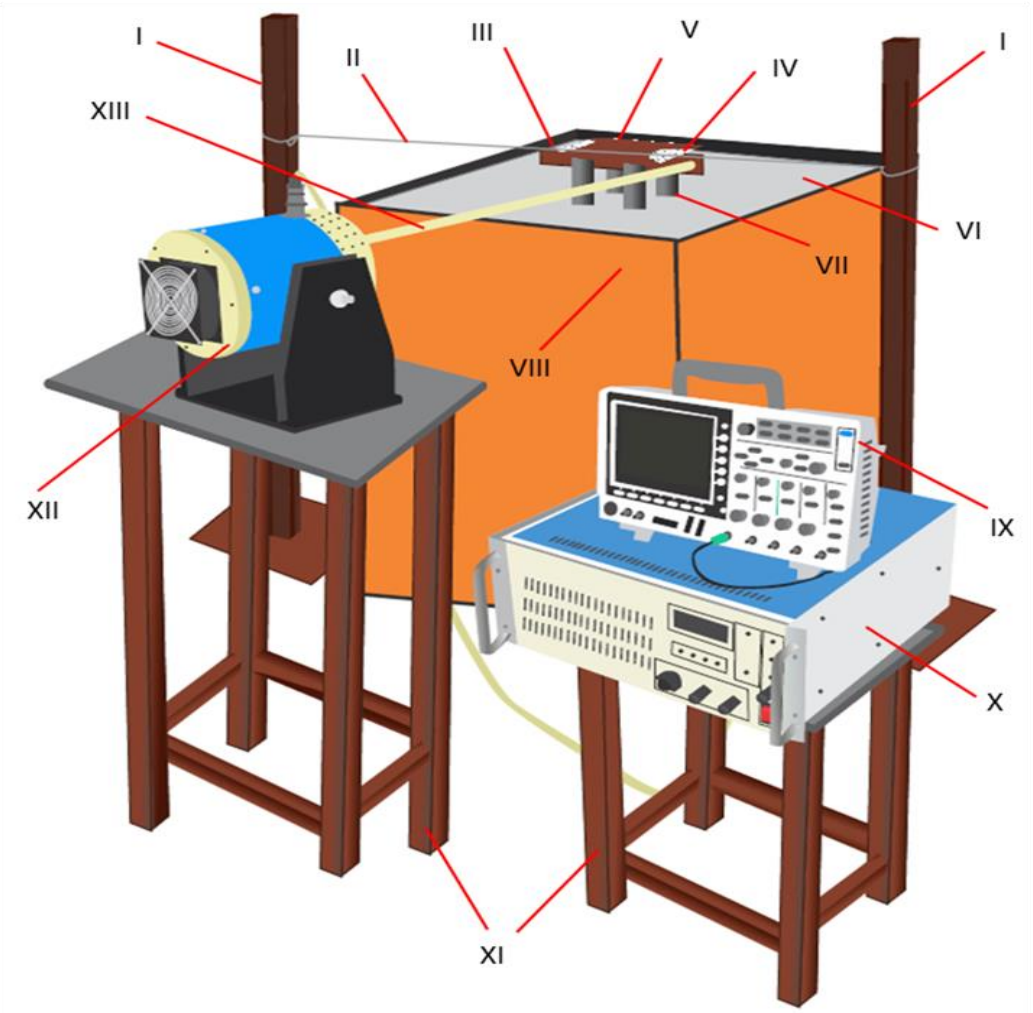

(I)	Stand for connecting thread	(VIII)	Geomaterial chamber
(II)	Connecting thread	(IX)	Oscilloscope
(III)	Measuring scale	(X)	Instrument for controlling frequency and amplitude
(IV)	Measuring protractor scale	(XI)	MS table
(V)	Pile cap	(XII)	Actuator for applying cyclic loading
(VI)	Loose sand	(XIII)	Connecting rod
(VII)	Pile group		

Figure 5.3 Test set-up fabricated to impart cyclic torsional loads on (m, n) pile group

5.6.2 Geomaterial Chamber and Filling Process

The geomaterial chamber was made of steel due to its strength, and durability, and painted to avoid corrosion. The chamber has a length of 900 mm, a breadth of 900 mm, and a depth of 1200 mm. The geomaterial testing chamber provides a controlled environment for conducting experiments to better understand the behaviour of the geomaterial. The well-graded loose sand free from organic matter and debris was deposited into the chamber under controlled conditions as proposed by Cudmani and Gudehas 2001. The soil samples were extracted from different locations within the tank to ensure that the samples were representative of the geomaterial fill throughout the tank depth. The geomaterial sample was weighted and the weight of the sample was recorded in kilograms. The volume of the geomaterial sample was measured and the density was calculated.

5.6.3 Placement of Piles in the Tank

The 2x2 piles were embedded in the geomaterial chamber at the centre to distribute loads more evenly and simulate realistic conditions. The spacing between the piles in a group was kept at three times the diameter of the pile to ensure a more uniform load distribution. The hammer was activated to deliver repeated blows to the pile head, driving it into the ground. The driving process was monitored carefully, recording the number of blows needed to achieve the desired depth.

5.6.4 Experimental Program and Description

The essential components of the test setup include the stand for connecting thread (I and II), a measuring scale and proctor (III and IV), an oscilloscope (IX), an instrument for controlling frequency and amplitude (X), actuator (XII) and connecting rod (XIII). The pile group (VII) with individual steel piles were fabricated. The diameter and length of the individual steel piles were 40 mm and 600 mm respectively. The distance between the

individual piles was kept at $3D_p$, where D_p is the diameter of the individual pile. The pile group was installed in the geomaterial chamber (VII). The loose sand (VI) was deposited into the chamber under controlled conditions. Afterwards, the cyclic torsional load was applied to the pile group while monitoring the twist at the pile cap (V). The cyclic torsional loading was applied through the actuator (Figure 5.3) by way of connecting rod (XII and XIII) and the frequency of loading was controlled by way of (X) in the range of 5-10 Hz. The connecting rod was fixed on the tip of the actuator (XII) and the cyclic torsional loading has been transferred assuming no force dissipation between the components. The actuator and oscilloscope were kept on the rigid MS table (XI). The twist was measured at the pile cap with the number of cycles of torsional loading evaluated for the (2,2) pile group at 40 N-m.

5.7 Numerical Simulation of Pile Group Subjected to Cyclic Torsional Loads

Three-dimensional finite element modelling is a convenient and reliable approach to account for the continuity of the geomaterial mass and the nonlinearity of the geomaterial pile group interaction. The pile group (2,2) input parameters have been considered as shown in Table 5.1. Several trial models have been executed with initial geomaterial modulus and varying dilation $0\text{-}12^0$ (Bolton 1986) to capture the cyclic torque-twist relationship for the pile group. The analysis has been performed using the computational algorithm (PGCYT). The geomaterial continuum has been divided into several volume elements. The tangential contact has been defined to model the interaction behaviour between the pile and the geomaterial using panelty friction formulation having a friction coefficient of 0.36 (Fig. 5.4a-b). The interaction uses the allowable elastic slip which is the fraction of the characteristic surface dimension of 0.005. The eight-node linear brick hexahedral element (C3D8R), with reduced integration, has been considered for modelling pile group (2,2) as shown in Figure 5.4 (c, d) that could capture the interlocking effects in terms of strength

parameters. The master surface is represented by the exterior surface of the pile and the slave surface by the interior surface of the geomaterial. The geomaterial has been selected such that the flow potential for the yield surface is defined by the formulation used by Mehra and Trivedi (2021, 2023a). The yield surface in the front cycle of loading is isotropic and has an onset of nonlinearity at $\varepsilon_{ij}^{p} > 0$. In the reverse cycle, it follows a mixed hardening model necessarily consistent with the hardening rule of a flow-controlled geomaterial. A relatively fine mesh was adopted for the pile group and a coarser mesh was adopted for the geomaterial.

Table 5.1 Pile group and geomaterial parameters

Parameters	**Description**
Young modulus of pile material (E_p, GPa)	210
Poisson's ratio (μ_p)	0.3
Unit weight (γ_p, kN/m^3)	78
Diameter (D_p, mm)	40
Length (L_p, mm)	600
Pile-to-pile spacing (S_p)	$3D_p$
Equivalent perimeter (mm)	50.3
Initial elastic modulus of geomaterial (MPa)	20
Effective unit weight of geomaterial (γ_s, kN/m^3)	16
Initial Poisson's ratio of geomaterial (μ_s)	0.3
Constant volume friction angle ($\emptyset_{\boldsymbol{C}}$, degrees)	30
Dilation angle ($\emptyset_{\boldsymbol{d}}$, degrees)	2-12

The mesh sensitivity analysis has been performed using the single seeding bias technique consisting of a number of elements (8). The bias ratio (0.5) has been selected to achieve

convergence behaviour. It further considers a flip bias from a near field to a far-field with increasing mesh size. The computational program considers a peak value of the angle of internal friction, $\emptyset_p$ $(\emptyset_p = \emptyset_c + \emptyset_d)$, which is a function of constant volume friction angle, $\emptyset_c$ and angle of dilation, $\emptyset_d$. The input parameters for the geomaterial medium have been defined in (Table 5.1).

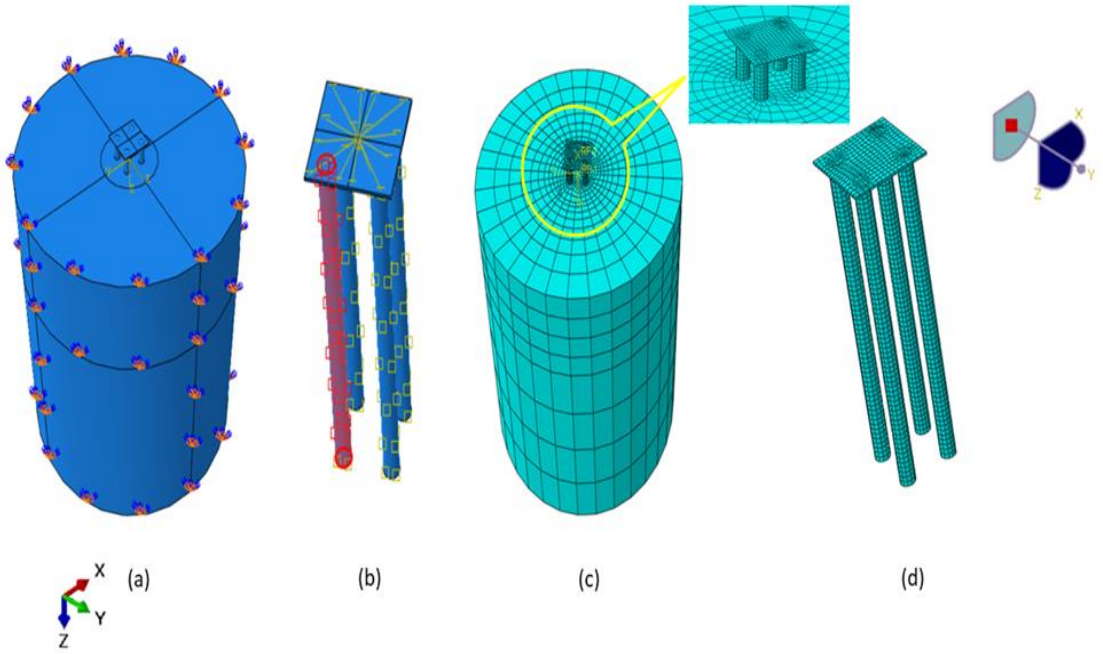

Figure 5.4(a) 3D pile group (2,2) model with the continuum of geomaterial and boundary conditions, (b) the surface-surface contact between the master (pile) and slave surface (geomaterial), (c) 3D pile group (2,2) model with C3D8R, an eight-node linear brick hexahedral element with reduced integration (d) isometric view of pile group (2,2)

5.8 Results, Discussion and Validation

The response of footings and structures supported by pile groups depends upon the cyclic stiffness and damping generated by geomaterial-pile group interaction. The variation of twist measured at the pile cap with the number of cycles of torsional loading evaluated for the (2,2) pile group at 40 N-m in the lab experimental setup has been shown in Figure 5.5. The experiments were performed at varying frequencies in the range of 0.1-10 Hz. The solid lines (Figure 5.5) as extrapolated from numerical and experimental data.

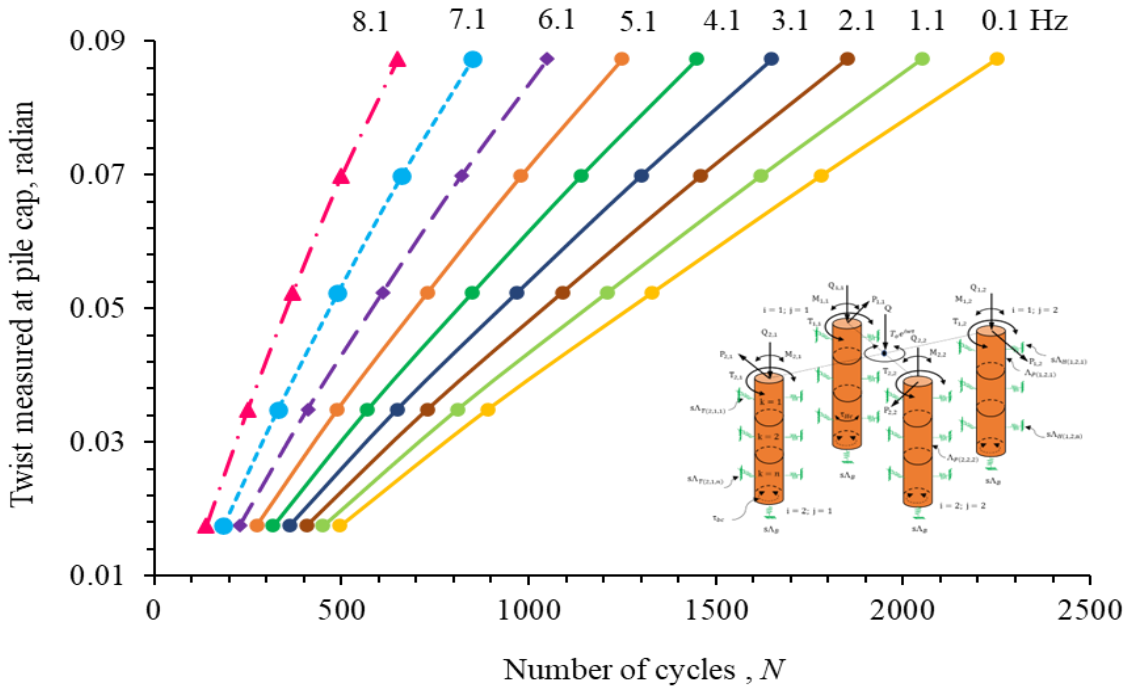

Figure 5.5 Variation of twist measured at pile cap with the number of cycles of torsional loading evaluated for (2,2) pile group at 40 N-m in the lab experimental setup (5-10 Hz), the solid lines as extrapolated from numerical and experimental data

The cyclic degradation parameters evaluated experimentally in a frequency range (5-10 Hz) and 40 N-m of cyclic torsional loading have been shown in Table 5.2.

Table 5.2 Experimental cyclic degradation parameter in a frequency range (5-10 Hz) and 40 N-m of cyclic torsional loading

Frequency (Hz)	a_{tep}	b_{tep}
0.1	0.0454	-0.2687
1.1	0.0453	-0.2644
2.1	0.0453	-0.2596
3.1	0.0453	-0.2543
4.1	0.0453	-0.2482
5.1	0.0453	-0.2412
6.1	0.0452	-0.2329
7.1	0.0452	-0.2228
8.1	0.0451	-0.2098

The three-dimensional view of the geomaterial-pile group (2,2) for $2^0, 6^0$ to 12^0 dilation, respectively is shown in Figure 5.6 (a, b, c). Figure 5.6 (d, e, f) shows the geomaterial-pile group (2,2) sectional view for plastic strain values for $2^0, 6^0$ to 12^0 dilation, respectively.

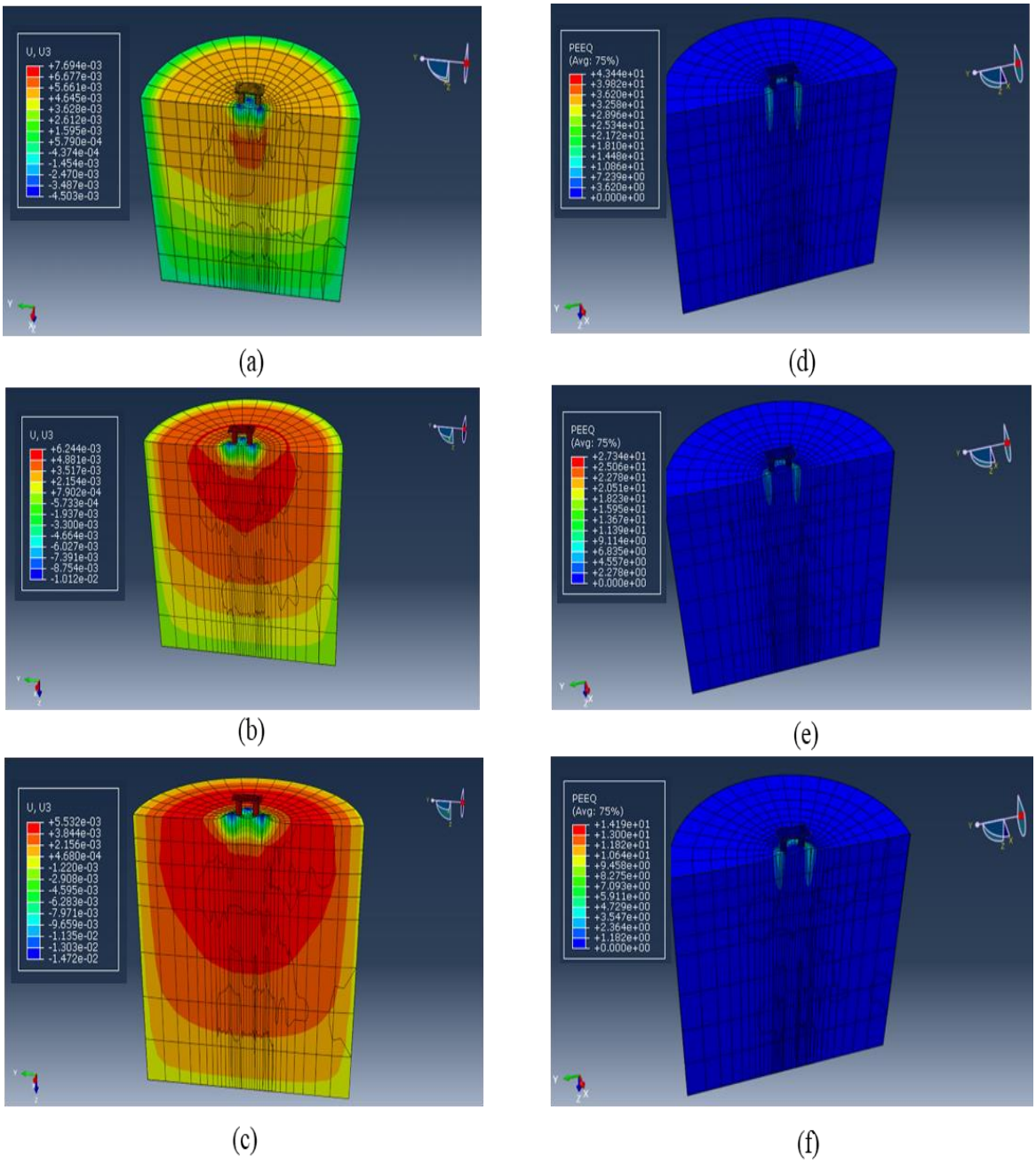

Figure 5.6(a, b, c) In the geomaterial-pile group (2,2) sectional view, the colour scheme is selected to represent the magnitude of displacement, where red and blue colour schemes are for maximum ($7.694x10^{-03}$) and minimum ($5.532x10^{-03}$) displacement respectively, (d, e, f). The geomaterial-pile group (2,2) sectional view showing plastic strain (43.44-14.19) % for 2^0 to 12^0 dilation

The colour scheme is selected to represent the intensity of plastic strain, where the green colour scheme is for maximum and minimum plastic strain for 2^0 and 12^0 dilation, respectively. The peak plastic strain of the geomaterial has been computed as 43.44; 27.34 and 14.19% for $2^0, 6^0$ to 12^0 dilation, respectively (Table 5.3).

Table 5.3 Peak values of plastic strain (%) of the geomaterial

Cycle	$\emptyset_D = 12^0$	$\emptyset_D = 6^0$	$\emptyset_D = 2^0$
1	0.92	1.34	1.67
10	7.08	12.74	18.49
20	11.02	20.76	32.35
30	14.19	27.34	43.44

Figure 5.7 shows the variation of twist angle measured at the pile cap with the number of cycles of normalized cyclic torque for pile group (2,2) evaluated for $2^0, 6^0$ to 12^0 dilation.

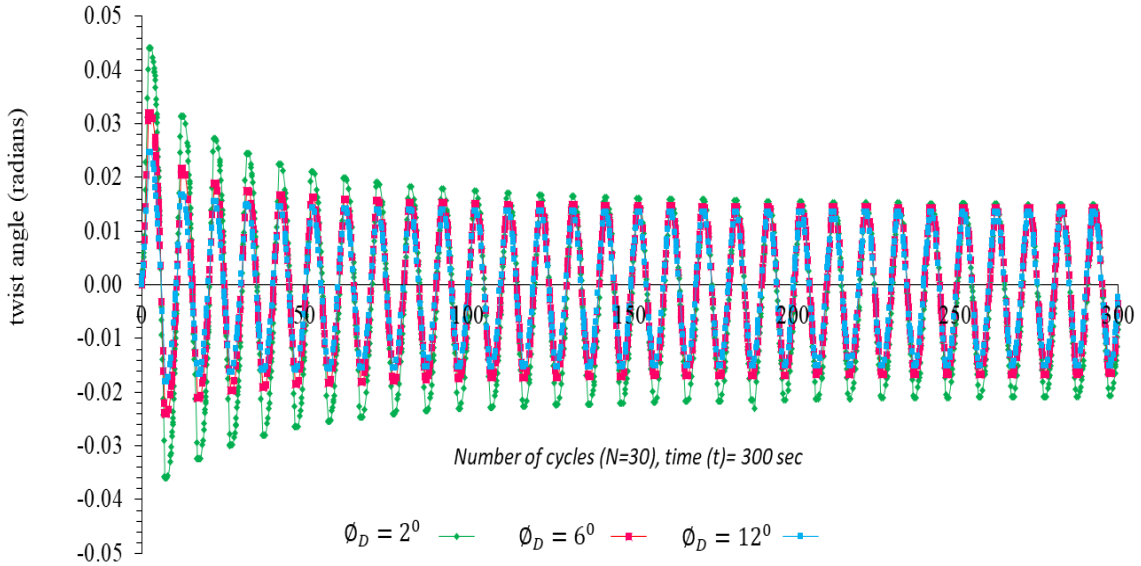

Figure 5.7 Variation of twist angle with number of cycles for pile group (2,2) evaluated for 2^0, 6^0 and 12^0 dilation, respectively at 1000 N-m in the numerical analysis at 0.1 Hz

The Variation of peak twist with the number of cycles for pile group (2,2) evaluated 2^0, 6^0 and 12^0 dilation, respectively has been presented in Figure 5.8. The peak twist angle decreases with an increase in dilation. The peak twist logarithmically decreases with an increase in the number of cycles and dilation and then becomes asymptotic after 30 cycles of loading in a flow-controlled geomaterial.

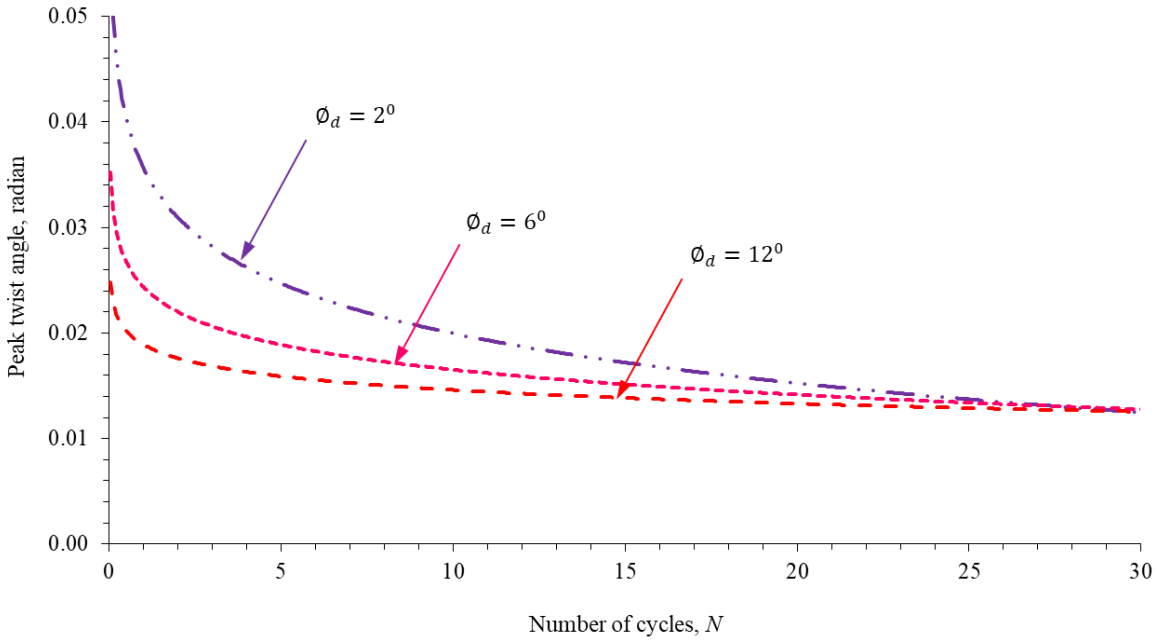

Figure 5.8 Variation of peak twist with number of cycles for pile group (2,2) evaluated 2^0, 6^0 *and* 12^0 *dilation, respectively*

The relationship between the peak twist angle and the number of cycles, *N* is expressed in matrix form as follows:

$$[\theta_t] = [\log_e N \quad 1] \begin{bmatrix} a_t \\ b_t \end{bmatrix} \tag{5.31}$$

$$\theta_t = a_t \log_e N + b_t \tag{5.32}$$

$$N = e^{\frac{\theta_t - b_t}{a_t}};\ N = 1;\ \theta_t = b_t \tag{5.33}$$

where, a_t and b_t are the logarithmic degradation parameters for the twist (Table 5.4) which depend upon the number of cycles, dilation angle and plastic strain. The logarithmic parameter b_t, is a measure of the residual angle of twist (θ_0) required in excess to mobilise the torque in the pile group over and above the maximum dilation at the end of the first cycle (*N=1*). There are two parameters namely, damping and plastic strain influencing the magnitude of the twist. Normally, increasing plastic strain increases twist at higher frequencies (Figure 5.5), however at lower frequencies the effect of damping offsets plastic strain and tends to reduce twist as shown in Figure 5.7. The anticipated concept of such a reduction at lower frequencies is shown by a dotted line in Figure 5.8.

Table 5.4 Flow-controlled cyclic degradation parameters at a frequency of 0.1 Hz and 1000 N-m of cyclic torsional loading

$\emptyset_D$	$D_f^{"}$	D_f'	D_f	a_t	b_t	a_s	b_s	ε_p	D
2°	−0.019	2.006	0.1445	−0.007	0.0357	−1.079	8.289	43.44	0.054
6°	−0.0156	1.3342	0.6356	−0.003	0.0244	−1.298	8.246	27.34	0.060
12°	−0.009	0.7087	0.6871	−0.002	0.0189	−1.364	8.118	14.19	0.061

Figure 5.9 shows the variation of plastic strain (%) with the number of cycles for pile group (2,2) evaluated for $2^0, 6^0$ and 12^0 dilation with enlarged views magnifying the convexities of plastic strain. The plastic strain increases with an increase in the number of cycles. The variation of the peak shear stress with the number of cycles for pile group (2,2) evaluated for $2^0, 6^0$ and 12^0 dilation, respectively has been shown in Figure 5.10. The relationship between the peak values of plastic strain and the number of cycles has been expressed in matrix form as follows:

$$[\varepsilon_p] = [N^2 \quad N \quad 1] \begin{bmatrix} D_f'' \\ D_f' \\ D_f \end{bmatrix} \tag{5.34}$$

Where $D_f^{"}$ is the power law cyclic degradation parameter which reduces the magnitude of plastic strain at a decrement rate for increasing dilation angle, D_f' represents the linear cyclic degradation parameter which decreases with the increasing dilation angle and D_f represents the constant cyclic degradation parameter for a cyclic strain which increases with the dilation angle (Figure 5.11(a) and Table 3).

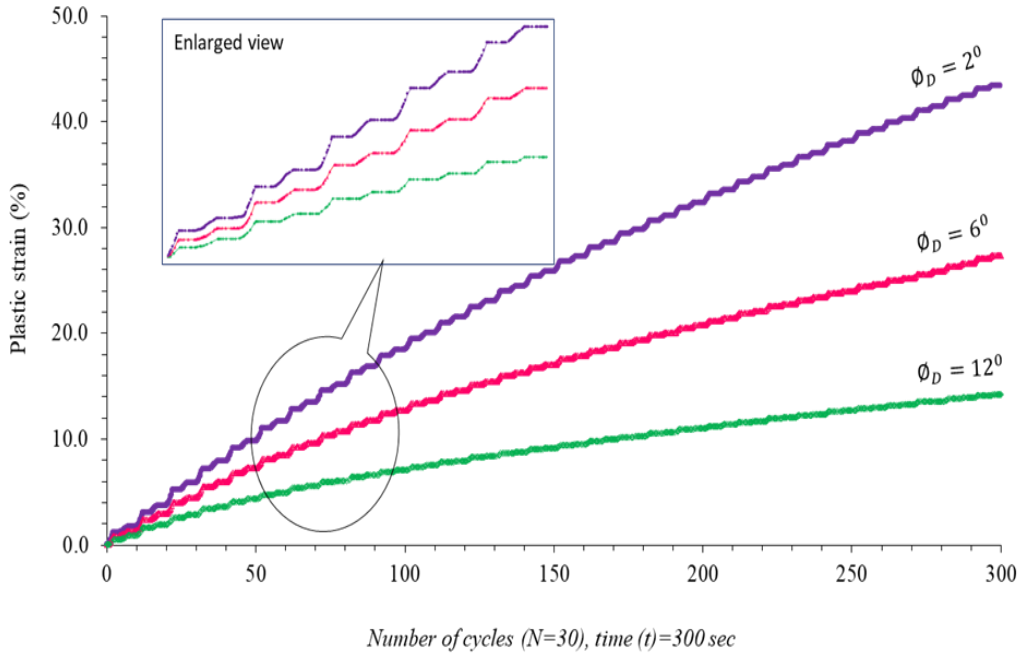

Figure 5.9 Variation of plastic strain with number of cycles for pile group (2,2) evaluated for 2^0, 6^0 and 12^0 dilation with enlarged views magnifying the convexities of plastic strain

The peak shear stress for pile group (2,2) and a single pile for normalized cyclic torque is found in the range (5-8.2) kPa at the dilation of 2^0 to 12^0, respectively in the present analysis. The peak shear stress for the pile group (2,2) logarithmically decreases and then asymptotically converges after 60 cycles of loading in a flow-controlled geomaterial which

in turn is a function of the number of cycles and dilation (Figure 5.10). The relationship between the peak shear stress and the number of cycles, *N* is expressed in matrix form as follows:

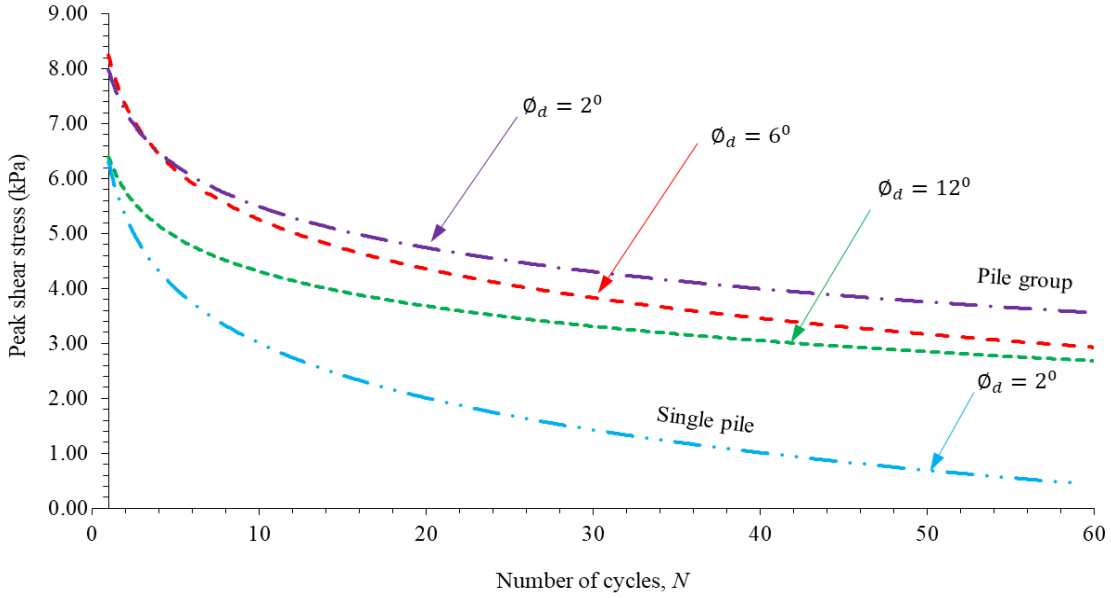

Figure 5.10 Variation of peak shear stress with the number of cycles in a flow-controlled geomaterial. The peak shear stress for pile group (2,2) and a single pile for normalized cyclic torsional load is captured at the dilation of 2^0, 6^0 *and* 12^0, *respectively in the present analysis*

$$[\tau_p] = [\log_e N \quad 1] \begin{bmatrix} a_s \\ b_s \end{bmatrix} \tag{5.35}$$

$$\tau_p = a_s \log_e N + b_s \tag{5.36}$$

$$N = e^{\frac{\tau_p - b_s}{a_s}};\ N = 1;\ \tau_p = b_s \tag{5.37}$$

where, a_s and b_s are the logarithmic degradation parameters for shear stress. The experimental data of Cudmani and Gudehas (2001) has the value of $a_s = -0.782$ and $b_s = 2.9964$ and the same for the present analysis for a single pile are -1.438 and 6.3183,

respectively. Figure 5.11(b) shows the variation of a set of logarithmic degradation parameters with the angle of dilation (Table 3).

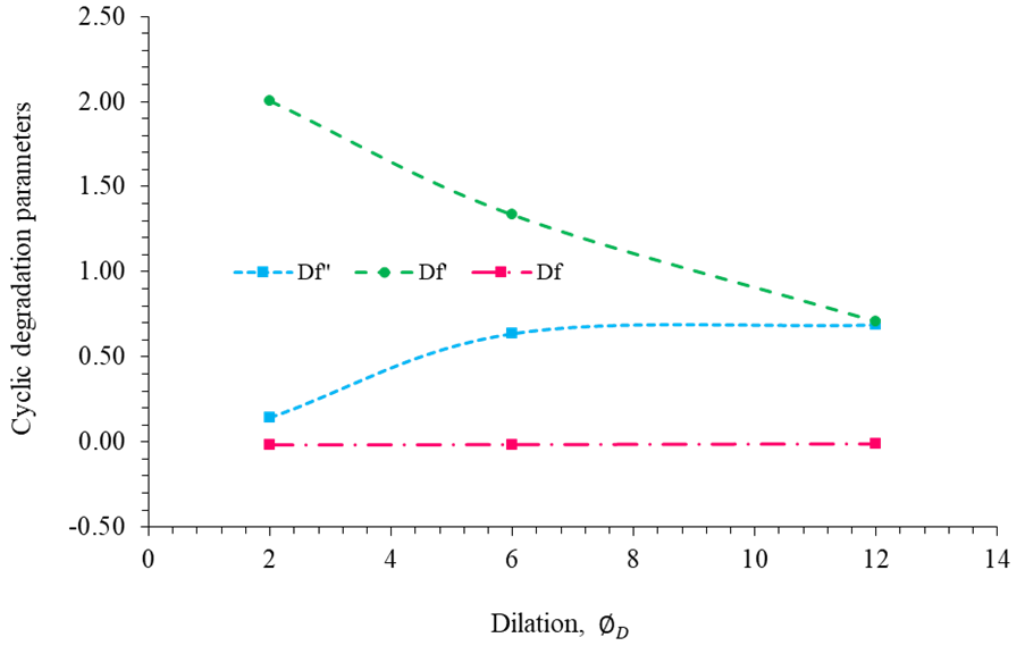

(a)

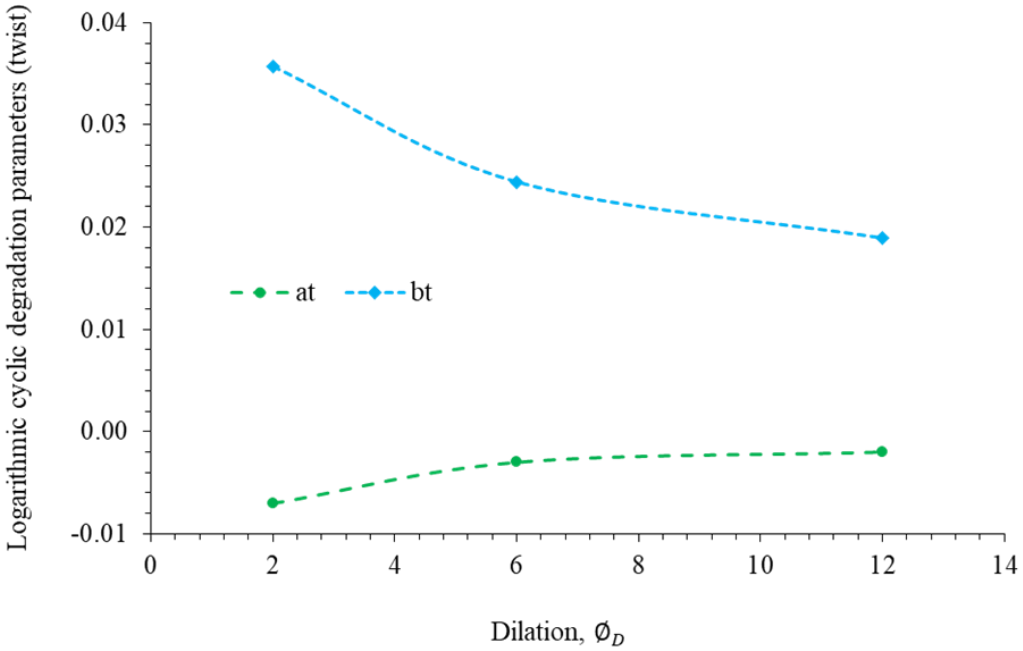

(b)

Figure 5.11(a) Variation of cyclic degradation parameter for pile group (2,2) evaluated for 2^0, 6^0 and 12^0 dilation (b) Variation of logarithmic cyclic degradation parameter for pile group (2,2) evaluated for 2^0, 6^0 and 12^0 dilation

5.9 Conclusions

This study considers the degradation of the geomaterial medium associated with the plastic flow reflecting the actual response of the interaction of pile groups and the geomaterial which is normally ignored by the classical design of pile foundations.

- Due to the application of the cyclic torsional loading, there is a progressive deterioration of the strength and stiffness of the surrounding geomaterial, creating a substantial degradation of the pile group capacity. The main conclusions of the study are as follows:
- A cyclic degradation parameter for plastic strain and a logarithmic degradation parameter for twist and shear has been identified as a function of frictional characteristics of flow-controlled geomaterial which in turn depend upon the number of cycles, plastic strain and dilation. The flow-controlled cyclic degradation parameters for plastic strain ($D_f^{"}, D_f', D_f$) and logarithmic degradation parameters for the twist (a_t, b_t) and shear (a_s, b_s) have been classified and recommended for designing pile groups.
- The plastic strain increases with an increase in the number of cycles for the pile group (2,2). The peak plastic stain has been obtained as 43.44, 27.34 and 14.19% for 2, 6 and 12^0 dilation, respectively.
- The 3D numerical model on the pile group (2,2) and the single pile have been compared with the result of the experimental data of the single pile. The peak shear stress for pile group (2,2) and a single pile for normalized cyclic torque is found in the range (5-8.2) kPa at the dilation of 2^0 to 12^0, respectively in the present analysis.

- The peak shear stress for the pile group (2,2) logarithmically decreases and then asymptotically converges after 60 cycles of loading in a flow-controlled geomaterial which in turn is a function of the number of cycles and dilation

References

Anagnostopoulos, C., & Georgiadis, M. (1993). “Interaction of axial and lateral pile responses.” *J. Geotech. Eng.,* 119(4), 793-798.

Bolton, M. D. (1986). “The strength and dilatancy of sands.” *Geotechnique*, 36(1), 65-78.

Basack, S., & Nimbalkar, S. (2017). “Numerical solution of single pile subjected to torsional cyclic load.” International Journal of Geomechanics, 17(8), 04017016.

Chow, Y. K. (1985). “Torsional response of piles in nonhomogeneous soil.” Journal of Geotechnical Engineering, 111(7), 942-947.

Cudmani, R., & Gudehus, G. (2001). “Settlements of sand due to cyclic twisting of a tube. In IUTAM Symposium on Theoretical and Numerical Methods in Continuum Mechanics of Porous Materials.” Proceedings of the IUTAM Symposium held at the University of Stuttgart, Germany, September 5–10, 1999 (pp. 387-396). Dordrecht: Springer Netherlands.

Chen, S. L., Kong, L. G., & Zhang, L. M. (2016). “Analysis of pile groups subjected to torsional loading.” *Computers and Geotechnics, 71, 115-123.*

Chen, S. L., Kong, L. G., & Zhang, L. M. (2016). “Analysis of pile groups subjected to torsional loading.” *Computers and Geotechnics, 71, 115-123.*

Fahey, M., & Carter, J. P. (1993). “A finite element study of the pressure meter test in sand using a nonlinear elastic plastic model.” *Canadian Geotech. J.*, 30(2), 348-362.

Georgiadis, M. (1987). “Interaction between torsional and axial pile responses.” *Int. J. numerical and analytical methods in Geomech*., 11(6), 645-650.

Guo, W. D., & Randolph, M. F. (1996). “Torsional piles in non-homogeneous media.” *Computers and Geotechnics*, 19(4), 265-287.

Hutton, D. V. (2004). *Fundamentals of finite element analysis*. McGraw-Hill.

Kong, L.G. (2006). “Behavior of pile groups subjected to torsion.” *PhD Thesis, Hong Kong University of Science and Technology, Hong Kong,* 339p.

Kong, L.G. and Zhang, L.M. (2008). “Experimental study of interaction and coupling effects in pile groups subjected to torsion,” *Canadian Geotechnical Journal*, 45, 1001-1017.

Kong, L. G., & Zhang, L. M. (2009). “Nonlinear analysis of torsionally loaded pile groups.” *Soils and foundations*, 49(2), 275-286.

Kong, L. G., Zhang, Z. C., & Chen, Y. M. (2020). “Nonlinear analysis of pile groups subjected to combined lateral and torsional loading”. *J. Zhejiang University-SCIENCE A,* 21(3), 179-192.

Long, J. H., & Vanneste, G. (1994). “Effects of cyclic lateral loads on piles in sand.” *J. Geotech. Engg.,* 120(1), 225-244.

Ladhane, K. B., & Sawant, V. A. (2016). “Effect of pile group configurations on nonlinear dynamic response.” *Int. J. Geomech.,* 16(1), 04015013.

Mehra, S. and Trivedi, A. (2018). “Experimental studies on model single pile and pile groups subjected to torque.” *Proceedings of China-Europe Conference, Geotech. Engg.,* 10.1007/978-3-319-97115-5_24, pp 997-1000.

Mehra, S. & Trivedi, A. (2018). “Analysis and simulation of cyclic torque application on pile groups.” *Proceeding of 12th International Super Pile World, Nanjing, Jiangsu, China,* 277-282.

Mehra, S & Trivedi, A. (2019). “Deep foundations subjected to combined axial and torsional loads.” *Int. Symposium on Testing and Technology for Bearing Capacity of Deep Foundation, Delhi,* ISBN:978-93-5391-519-3, 19-20.

Mehra, S., & Trivedi, A. (2021). “Pile Groups Subjected to Axial and Torsional Loads in Flow-Controlled Geomaterial.” *Int. J. Geomech.,* 21(3), 04021002.

Novak, M. (1974). “Dynamic stiffness and damping of piles.” *Canadian Geotech. J.,* 11(4), 574-598.

Novak, M., & Howell, J. F. (1977). “Torsional vibration of pile foundations.” *J. Geotech. Eng. Div.,* 103(4), 271-285.

Novak, M., & El Sharnouby, B. (1983). “Stiffness constants of single piles.” *Journal of Geotechnical Engineering,* 109(7), 961-974.

Novak, M., & Sharnouby, B. E. (1984). “Evaluation of dynamic experiments on pile group.” *J. Geotech. Eng.,* 110(6), 738-756.

Poulos, H. G. (1971). “Behaviour of laterally loaded piles: II-pile groups.” *J. Soil Mech. and Foundation Div.,* 97(5), 733-751.

Poulos, H. G. (1975). “Torsional response of piles.” *J. Geotech. Geoenviron. Eng.,* 101(10), 1019-1035.

Poulos, H. G. (1982). “Single pile response to cyclic lateral load.” *J. Geotech. Engg. Div.,* 108(3), 355-375.

Randolph, M. F. (1981a). “The response of flexible piles to lateral loading.” *Geotechnique,* 31(2), 247-259.

Randolph, M. F. (1981b). “Piles subjected to torsion.” *J. Geotech. Eng.,* 107(8), 1095-1111.

Timoshenko, S. , & Goodier, J. N. (1970). “Theory of Elasticity.” *McGraw-Hill. New York, NY, 65.*

Zhu, C. Q., & Huang, Y. (2016). “Safety assessment of anti liquefaction performance of a constructed reservoir embankment II: Numerical assessment.” *Journal of Performance of Constructed Facilities,* 31(2), 04016102.

6.0 SURFACE DISPLACEMENT OF THE GEOMATERIAL DUE TO CYCLIC TORSIONAL LOADING

This chapter is based on the papers proposed to be submitted to a reputed journal for publication. The details presented here may change wrt to the published paper to maintain consistency in the presentation throughout the thesis. To ensure consistency in the presentation throughout the thesis, some aspects may differ from those in the published paper.

6.1 Introduction

Dynamic analysis of pile groups is a problem of great importance in geotechnical ocean engineering. It involves evaluating the response of a group of piles under dynamic loading conditions, namely earthquake-induced vibrations or machine foundations for heavy structures. The dynamics of pile groups is a complex problem due to the interaction between the piles and the surrounding geomaterial. While dynamic analysis of single piles is relatively well-established, the behaviour of pile groups involves additional complexities and uncertainties. The interaction between the piles and the geomaterial affects the stiffness and deformation characteristics of the pile group system. Neglecting this interaction may result in overestimating the stiffness, leading to unrealistic predictions of the pile group system behaviour (Noval and Sharnouby 1984). Investigations on the piles undergoing lateral and torsional loading (Poulos 1975; Randolph 1981a; Randolph 1981b; Chow 1985; Georgiadis 1987; Anagnostopoulos and Georgiadis 1993; Guo and Randolph 1996; Kong 2006; Guo et al 2007; Kong and Zhang 2008, 2009; Basile 2010; Chen et. al. 2016; Kong et. al. 20201, Novak and Howell 1977; Noval and Sharnouby 1983, 1984; Basack & Nimbalkar 2017; Li 2019) are amplified to the analysis of pile groups in the present research. Experimental studies involving torsional loads have been performed on the pile groups (Mehra and Trivedi 2018a, 2018b, 2021, 2023a, 2023b). The interconnection

between the axial and torsional response and the torsional energy around the pile groups has been researched (Mehra and Trivedi 2023a, 2023b). The dynamic analysis (Novak and Howell 1977; Noval and Sharnouby 1983, 1984; Basack & Nimbalkar 2017; Li 2019) concentrated on the comprehensive behaviour of pile groups subjected to torsion without considering the cyclic torsional loading. The cyclic degradation parameters of the flow-controlled geomaterial for pile groups subjected to torsional loads were identified by Mehra and Trivedi (2023b). When torsional cyclic loads are applied to a pile group surrounding geomaterial, it leads to a phenomenon called surface displacement namely heave. The term heave typically refers to the uplift and lateral flow of the geomaterial. The heave occurring in sands undergoing cyclic torsional loading causes the sand particles to rearrange leading to a reduction in the shear strength and change in volume. The volume change experienced by sand depends on several factors, including the initial density of the sand, the stress level, and the confining pressure. The patterns of surface displacements around the foundation have been studied by several investigators (Borst and Vermeer, 1984; Zienciewicz et. al. 1975). The large surface displacements were observed with a larger dilation angle (Borst and Vermeer, 1984). The ground movements around the tunnel for various stages of tunnel construction were investigated by Zienciewicz et al. (1975). The dilatant soil was observed to exhibit larger movements. The heave due to cyclic loads is often observed in areas such as coastal regions where there are wave actions or in areas with high seismic activity. It is seen in geotechnical engineering applications involving dynamic loads, such as machine foundations, vibratory compactors, or pile driving. Appropriate foundation designs considering this phenomenon are to be implemented to interpret heave displacement due to cyclic torsional load.

Overall, the present investigation aims to contribute to the understanding and estimation of the surface displacement of the geomaterial surrounding a pile group under cyclic torsional

loading through the development and application of a numerical modelling framework which is observed in the results of this paper. Based on a numerical campaign, a 3D-FEM analysis was performed to investigate the surface displacement of the adjoining geomaterial around the pile group subjected to cyclic torsional loads. The findings from numerical analysis of a pile group subjected to front-reverse cyclic loading align well with the published experimental results. Therefore, to understand the mechanism of the surface displacements of the flow-controlled geomaterial (FCG), the following investigations have been performed, namely, (a) the uplift behaviour of heave of the FCG due to the front and reverse cycles of torsional loading applied on the head of the pile group; (b) the lateral flow due to heave of the FCG; (c) angle of the heave ($\emptyset_h$) which in turn depends upon the number of cycles and the peak angle of friction.

6.2 Surface displacements due to cyclic torsional loading on the pile group

When the cyclic loads are applied in the form of torsional forces (Figure 6.1a-b), it leads to surface displacement, heave, and uplift of the geomaterial around the pile group. It results in changes in the ground surface elevation. Moreover, it induces a lateral flow in the geomaterial surrounding the pile group. These displacements might occur in the form of lateral spreading, lateral shifting, and lateral tilting of the geomaterial mass. The differential equilibrium equation modified for the pile-geomaterial system subjected to cyclic torsional loads (Figure 6.1) extended from (Mehra and Trivedi 2023b) is described as:

$$m\frac{\partial^2\delta(\mathrm{z,t})}{\partial \mathrm{t}^2} + c_h\frac{\partial\delta(\mathrm{z,t})}{\partial \mathrm{t}} + c_\theta\frac{\partial\delta(\theta,\mathrm{t})}{\partial \mathrm{t}} + k_{hN}\,\delta(\mathrm{z,t}) + k_{\theta N}\,\theta(z,\mathrm{t}) + E_P I_P\frac{\partial^4\delta(\mathrm{z,t})}{\partial \mathrm{z}^4} + G_P J_P\frac{\partial^2\theta\,(\mathrm{z,t})}{\partial \mathrm{z}^2} = T_c \tag{6.1}$$

The magnitude of uplift and lateral flow depends upon the stiffness of the geomaterial, the pile arrangement, and the interaction between the piles and the geomaterial.

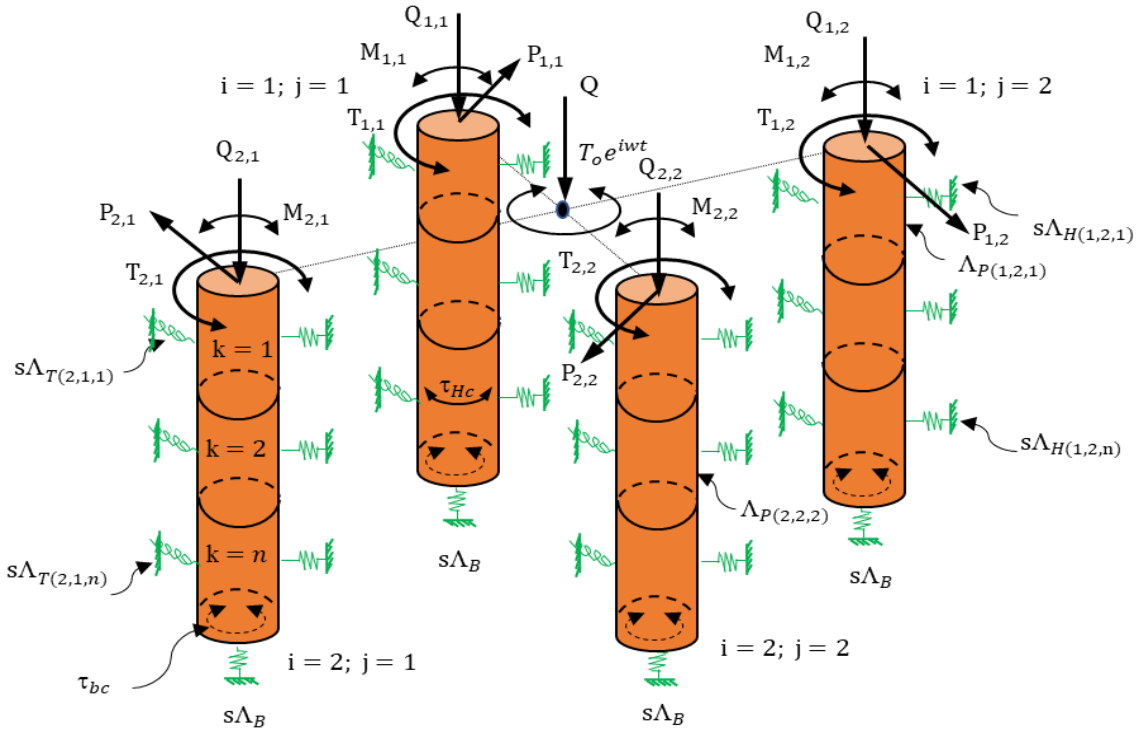

(a)

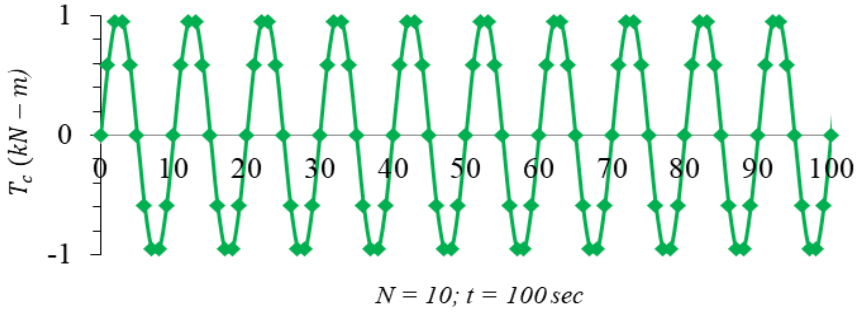

(b)

Figure 6.1(a) Diagrammatic representation of the pile group (2,2) embedded in the geomaterial due to the application of cyclic torsional loading on the centre, (b) Variation of cyclic torsional loading with time applied on the pile group in the numerical analysis

The surface displacements of the geomaterial are investigated under cyclic torsional load application at the centre of the pile group using the numerical campaign. A numerical model has been demonstrated using a simplified representation of the physical pile group system A numerical model has been demonstrated using a simplified representation of the physical

pile group system (Figure 6.1). The stiffness matrix in bending of the pile element (Figure 6.1) extended from (Mehra and Trivedi 2023b) is described as:

$$[\Lambda_{PP}]_c = \rho A \int_0^L \left(N_m \frac{\partial^2 \delta}{\partial t^2} + N_n \frac{\partial^2 \delta}{\partial t^2} \right) dz + c \int_0^L \left(N_m \frac{\partial \delta}{\partial t} + N_n \frac{\partial \delta}{\partial t} \right) dz + EI \int_0^L \frac{d^2 N_m}{dz^2} \frac{d^2 N_n}{dz^2} dz \tag{6.2}$$

The stiffness matrix in torsion of the pile element extended from (Mehra and Trivedi 2023b) is described as:

$$[\Lambda_{PT}]_c = \rho A \int_0^L \left(N_m \frac{\partial^2 \delta}{\partial t^2} + N_n \frac{\partial^2 \delta}{\partial t^2} \right) dz + c \int_0^L \left(N_m \frac{\partial \delta}{\partial t} + N_n \frac{\partial \delta}{\partial t} \right) dz + G_P J \int_0^L \frac{dN_m}{dz} \frac{dN_n}{dz} dz \tag{6.3}$$

6.3 Geomaterial reaction to cyclic torsional loads

The reaction of geomaterial to cyclic torsional loading, particularly in the context of pile groups, involves a complex set of forces. The geomaterial surrounding the pile group resists the applied cyclic torsional force due to the friction among the particles, as well as the interaction among the piles and the geomaterial. When cyclic torsional loading is applied to the pile group, the geomaterial undergoes shear deformation. As the torsional load is applied and reversed, the geomaterial experiences hysteresis and the stress-strain plot is not fully reversed. This can result in the accumulation of resilient and permanent deformation. Resilient deformation occurs during loading and unloading cycles, while permanent deformation can accumulate over time due to factors namely particle sliding or rearrangement. Assumptions for the flow-controlled geomaterial to cyclic loading application are described as follows:

a) In the front loading cycle, the yield surface is isotropic and has an inception of nonlinearity at $\varepsilon_{ij}^{p} > 0$. It conforms to a mixed hardening model in the reverse loading cycle following the hardening rule of the yield surface expansion and translation.

b) In the front and reverse cycles, the yield function is described as follows:

$$f_f = f\left(\varepsilon_{ij}^{f} - \alpha_{ij}^{f}\right) - r_0 \tag{6.4}$$

$$f_r = f\left(\varepsilon_{ij}^{r} - \alpha_{ij}^{r}\right) - r_0 \tag{6.5}$$

where, f_f and f_r are the yield functions of the strain ε_{ij}^{f} and ε_{ij}^{r}, in the front and reverse cycle respectively; α_{ij}^{f} and $\alpha_{ij}^{r}$are the centre of the yield surface in the front and reverse cycle respectively; r_0 is the constant describing the size of the original yield surface.

c) The centre of the yield surface α_{ij}^{f} changes due to plastic flow, the yield function rigidly transforms to a new location without changing its shape and size. Combining Eq. (6.4-6.5) is described as follows:

$$f_f - f_r = f\left(\varepsilon_{ij}^{f} - \alpha_{ij}^{f}\right) - \left(\varepsilon_{ij}^{r} - \alpha_{ij}^{r}\right) \tag{6.6}$$

d) The magnitude of $f_f - f_r$ is always a positive quantity which is consistent with the hysteresis effect applied to observed cyclic twist on the number of cycles.

e) The transition of the yield surface of the flow controlled geomaterial due to cyclic loading at the varied magnitudes of dilation is described as follows:

$$\frac{df}{dt} = f\left(\frac{d\varepsilon_{ij}}{dt} - \frac{d\alpha_{ij}}{dt}\right) \tag{6.7}$$

The element of the pile (dz) experiences complex lateral displacement $\delta(z,t)$, it will encounter a lateral geomaterial reaction and is described as follows:

$$V_h = G_s(S_{h1} + iS_{h2}\,)[\delta(z,t)]dz \tag{6.8}$$

where $i = \sqrt{-1}$ and the parameters S_{h1} and S_{h2} are the functions of the dimensionless frequency (a_0) depending upon the Poison's ratio of the geomaterial are described as follows:

$$S_h(a_0, \mu) = G_s[S_{h1}(a_0, \mu) + iS_{h2}(a_0, \mu)] \tag{6.9}$$

$$= 2\pi G_s a_0 * \frac{\frac{1}{\sqrt{q}} H_2^{(2)}(a_0)H_1^{(2)}(a_0) + H_1^{(2)}(x_0)H_1^{(2)}(a_0)}{H_0^{(2)}(a_0)H_1^{(2)}(x_0) + H_0^{(2)}(x_0)H_2^{(2)}(a_0)} \tag{6.10}$$

Where a_0 is the dimensionless frequency $= wR\sqrt{\frac{\rho}{G}}$; $q = (1 - 2\mu)/2(1 - \mu)$; $x_0 = a_0\sqrt{2}$; $H_n^{(2)}$ is the Hankel functions of the second kind of order n. The parameters S_{h1} and S_{h2} depends upon Poisson's ratio of the geomaterial as proposed by Beredugo and Novak (1972). The stiffness of the lateral spring (Figure 6.1) at a lumped mass (node) has been associated with the inner yield surface criterion assuming, $\delta(z,t)$, is described as follows:

$$[s\Lambda_{He}]_c = \rho A \int_0^L \left(N_m \frac{\partial^2 \delta}{\partial t^2} + N_n \frac{\partial^2 \delta}{\partial t^2} \right) dz + G_s(S_{h1} + iS_{h2}\,)[\delta(z,t)]dz \tag{6.10}$$

where $(s\Lambda_{He})$ is the stiffness as long as $f \to 0$. Similarly, the stiffness of the lateral spring (Figure 6.1) at a lumped mass (node) has been associated with the yield flow criterion assuming, $\delta(z,t)$, is described as follows:

$$\left[\mathrm{s}\Lambda_{Hf}\right]_c = f\left(\mathrm{s}\Lambda_{\mathrm{He}}, \mathrm{s}\Lambda_{\mathrm{Hp}}\right) = \tag{6.11}$$

$$(G_s(S_{h1} + iS_{h2}\,)[\delta(z,t)]dz\; f(G_{se}))\int_0^L \frac{dN_m}{dz}\frac{dN_n}{dz}dz$$

where $(s\Lambda_{H_p})$ is the flow-controlled stiffness (Mehra and Trivedi 2023b) and G_{se} is the equivalent shear modulus of the geomaterial (Mehra and Trivedi 2021). The pile undergoing complex harmonic rotation (Novak and Howell 1977; Novak and EI Sharnouby 1983) around the vertical axis is described as follows:

$$\theta(z,t\,) = \theta(z)e^{iwt} \tag{6.12}$$

where $\theta(z,t) =$ complex amplitude of pile twist at depth z. The motion of the pile element subjected to cyclic torsional loads is resisted by the torsional geomaterial reaction. The geomaterial reaction on a pile element (dz) is described as follows:

$$\theta_h = G_s R^2\,(S_{\theta 1} + iS_{\theta 2}\,)[\theta(z,t)]dz \tag{6.13}$$

$$S_{\theta 1}(a_0) = 2\pi\left(2 - a_0\frac{J_0J_1 + Y_0Y_1}{J_1^2 + Y_1^2}\right) \tag{6.14}$$

$$S_{\theta 2}(a_0) = \frac{4}{J_1^2 + Y_1^2} \tag{6.15}$$

where a_0 (dimensionless frequency) $= wR\sqrt{\frac{\rho_s}{G_s}}$; $J_0(a_0), J_1(a_0)$ are the bessel functions of the first kind of order 0 and 1, respectively; $Y_0(a_0), Y_1(a_0)$ are the bessel functions of the second kind of order 0 and 1, respectively. The stiffness of the torsional spring (Figure 6.1)

at a lumped mass (node) has been associated with the inner yield surface criterion assuming, $\delta(z,t)$, is described as follows:

$$[s\Lambda_{\theta e}]_c = \rho A \int_0^L \left(N_m \frac{\partial^2 \delta}{\partial t^2} + N_n \frac{\partial^2 \delta}{\partial t^2} \right) dz + G_s R^2 \, (S_{\theta 1} + iS_{\theta 2}\,)[\theta(z,t)]dz \tag{6.16}$$

Where, the parameters $S_{\theta 1}$ and $S_{\theta 2}$ depend upon the material damping of the geomaterial (Novak and Howell 1977; Novak and EI Sharnouby 1983). Similarly, the stiffness of the torsional spring (Figure 6.1) at a lumped mass (node) has been associated with the yield flow criterion assuming, $\delta(z,t)$, is described as follows:

$$\left[s\Lambda_{\theta f}\right]_c = f\left(\mathrm{s}\Lambda_{\mathrm{Te}}, \mathrm{s}\Lambda_{\mathrm{Tp}}\right) = \tag{6.17}$$

$$(G_s R^2 \, (S_{\theta 1} + iS_{\theta 2}\,)[\theta(z,t)]dz f(G_{se})) \int_0^L \frac{dN_m}{dz}\frac{dN_n}{dz}dz$$

6.4 Equations for balancing forces in the state of static equilibrium

The pile-geomaterial equilibrium equation considering Eq. (6.1-6.17) is described as follows:

$$\Big[EI \int_0^L \frac{d^2N_m}{dz^2}\frac{d^2N_n}{dz^2}dz + GJ \int_0^L \frac{dN_m}{dz}\frac{dN_n}{dz}dz + +\big(G_s R^2 (S_{\theta 1} + iS_{\theta 2}\,)[\theta\,(z,t)] + \tag{6.18}$$

$$G_s R^2 (S_{\theta 1} + iS_{\theta 2}\,)[\theta\,(z,t)]\, f(G_{se})\big) \int_0^L \frac{dN_m}{dz}\frac{dN_n}{dz}dz + \big(G_s (S_{h1} + iS_{h2}\,)[h\,(z,t)] +$$

$$G_s (S_{h1} + iS_{h2}\,)[h\,(z,t)] f(G_{se})\big) \int_0^L \frac{dN_m}{dz}\frac{dN_n}{dz}dz + k_{HT} + k_{HT}\Big] = 0$$

where $\{\delta, \psi, \theta\} = \{\delta_1 \delta_2 \delta_3 \delta_4 \psi_5 \psi_6 \psi_7 \psi_8 \theta_9 \theta_{10}\}\{t\}$

$$\{F(t)\} = \{\; P_{mx} P_{my}\; P_{nx}\; P_{ny}\; M_{mx}\; M_{my}\; M_{nx}\; M_{ny}\; T_m\;\; T_n\}\{t\}$$

The global stiffness matrix has been presented to solve the displacements at the nodes of the pile-geomaterial system undergoing cyclic torsional loading is described as follows:

$$[\Lambda_P]\{d_p(t)\} + [s\Lambda]\{\mathrm{d_s}(t)\} = \{T(t)\} \tag{6.19}$$

Where $[\Lambda_p]$ and $[s\Lambda]$ represent the stiffness matrices of elements of the piles and geomaterial, respectively; $\{d_s(t)\}$ and $\{d_p(t)\}$ represents the deformations vectors at the nodes of geomaterial and piles, respectively; $\{T(t)\}$ is the cyclic torsional load. These displacements, in turn, allow us to calculate the internal forces and stresses within each element of the geomaterial. The idealizations mentioned have been used to perform 3D-FEM analysis while capturing the essential behaviour of the geomaterial and the pile group.

6.5 Interaction of the geomaterial-pile group under cyclic torsional loading

Due to the complexities involved, analytical models for dynamic analysis of pile groups often rely on simplifying assumptions and making approximations. These simplified models may not capture the full range of behaviours and interactions that occur in practice. Therefore, in the present investigation, the three-dimensional finite element (3D-FE) analysis is used to simulate the behaviour of the geomaterial-pile group system subjected to cyclic torsional loads (Figure 6.1b). This campaign is implemented in the numerical program using Abaqus/CAE (2016) and numerous trial models have been executed. The analysis has been performed using the numerical campaign presented in Eq. (6.1-6.19). The input variables for the pile group for uplift and lateral flow associated with heave are taken into consideration as presented in Table 1 (Mehra and Trivedi 2019, 2021, 2022). The pile group is embedded in the geomaterial which is considered a continuous medium (Figure 6.2 a-c). The geomaterial is divided into small subdomains to discretize the problem for computational analysis (Figure 6.2 c).

Table 6.1 Variables for pile group and geomaterial

Variables	Description
Young modulus of the pile material (E_p, GPa)	210
Poisson's ratio (μ_p)	0.3
Unit weight (γ_p, kN/m^3)	78
Diameter (D_p, mm)	40
Length (L_p, mm)	600
Pile-to-pile spacing (S_p)	$3D_p$
Equivalent perimeter (mm)	50.3
Initial elastic modulus of the geomaterial (MPa)	20
Effective unit weight (γ_s, kN/m^3)	16
Initial Poisson's ratio (μ_s)	0.3
Constant volume friction angle ($\emptyset_{\boldsymbol{C}}$, degrees)	30
Peak friction angle ($\emptyset_{\boldsymbol{p}}$, degrees)	32-42

A general-purpose element (C3D8R) with eight nodes, six faces and four integration points per face has been selected for modelling in the present numerical analysis (Figure 6.2c). A relatively fine mesh has been used to discretize the geometry of the pile group to capture detailed behaviour accurately. In contrast, the surrounding geomaterial has been described by a coarser mesh to reduce computational costs while obtaining reasonable results with due precision. The single seeding bias technique has been used to control the mesh density with a selected (eight) number of elements. A flip bias ratio of 0.5 has been selected such that the size of each element doubles from one element to the next in the sequence to achieve a gradual increase in element size, ensuring a gradual spread transition, and avoiding abrupt changes in mesh density.

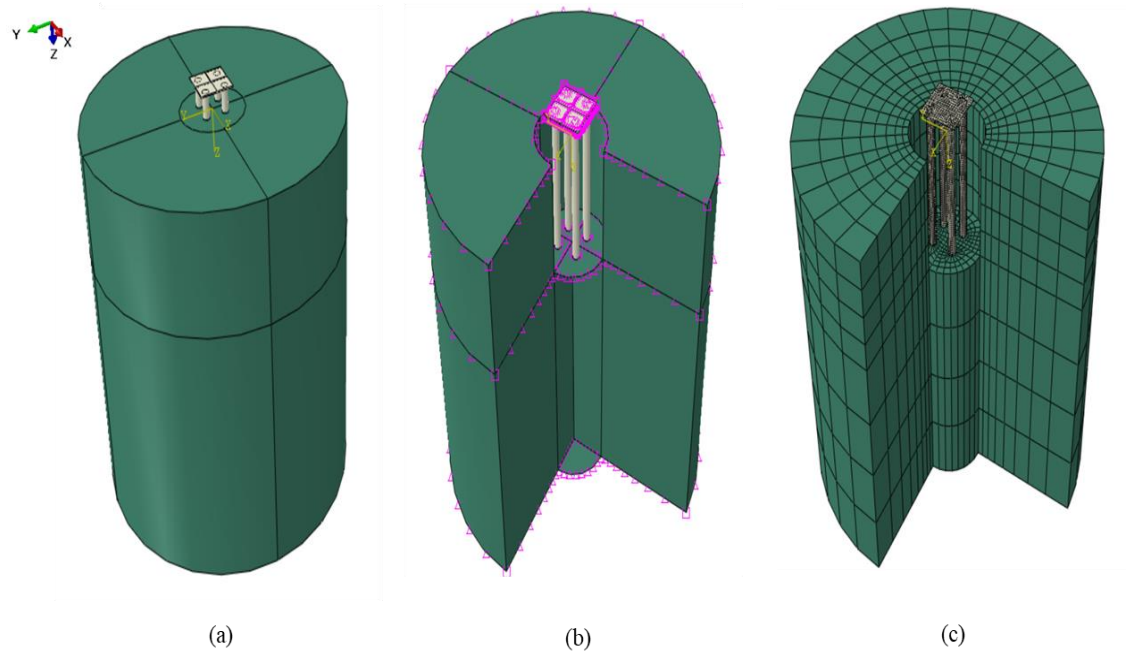

Figure 6.2(a) Geomaterial-pile group (2,2) 3D model, (b) Single seeding bias technique consisting of eight elements, (c) Part pile group (2,2) 3D-model with eight-node linear brick hexahedral element (C3D8R)

The flip bias technique has been used for reversing the mesh seeding direction as it moves away from the region of interest (near field) to regions farther away (far field) to ensure an appropriate mesh density gradient, with finer elements near the pile group and coarser elements away from it (Figure 6.2b). The master surface represents the exterior surface of the pile that imposes contact conditions on the geomaterial interior surface which has been described as the slave surface in the present numerical analysis. The master and slave surfaces interact through frictional forces using a penalty friction formulation. The ratio of tangential force to normal force at the interface of the pile and the geomaterial has been defined using a friction coefficient (0.36). When the slave surface slips relative to the master surface, frictional resistance is introduced according to the specified friction coefficient. The amount of relative displacement slip allowed between the pile and the geomaterial before frictional resistance comes into play is specified as a fragment of the distinctive surface dimension (0.005). A constitutive model has been used to define the

behaviour of the geomaterial in the present analysis as defined by Mehra and Trivedi (2019, 2021, 2023a, 2023b). A mesh sensitivity analysis has been conducted for the numerical simulation of the pile group and the surrounding geomaterial to get an appropriate mesh density that yields consistent and convergent results. The numerical program takes into (Mehra and Trivedi 2019, 2021, 2023a, 2023b) consideration a peak value of the angle of internal friction, $\emptyset_p$ $\left(\emptyset_p = \emptyset_c + \emptyset_d\right)$. The input variables for the geomaterial have been defined in (Table 1).

6.6 Outcomes, Discussions and Reliability of the Numerical Campaign

The consequences of surface displacements namely heave formulation of geomaterial consist of uplift and lateral flow that can be detrimental to the satisfactory performance of structures, such as buildings and roads, as the upward movement of the geomaterial can lead to cracking, tilting, or shifting of foundations. To mitigate heave, it is essential to consider geomaterial conditions during construction and implement appropriate engineering measures for foundation design. Dilation leads to the volume change of the granular material. As particles dilate, they tend to move apart horizontally and uplift which increases in volume of the geomaterial. This lateral expansion can contribute to surface movements, such as heaving. When soil particles dilate, the effective stress between the particles decreases, resulting in a decrease in shear strength. This reduction in shear strength leads to increased surface movement of soil particles under applied torsional loads. Similarly, confining pressure on the geomaterial affects the dilation behaviour. Higher confining pressures tend to restrict the dilation of soil particles, resulting in less surface movement. Conversely, lower confining pressures can facilitate dilation and increase the potential for surface movement. The 3D-FEM deformed shape with colour contours plotted for the pile group embedded in a geomaterial subjected to a front and reverse cyclic torsional loading (Figure 6.1b) at the centre at $N = 60$ has been shown in Figure 6.3.

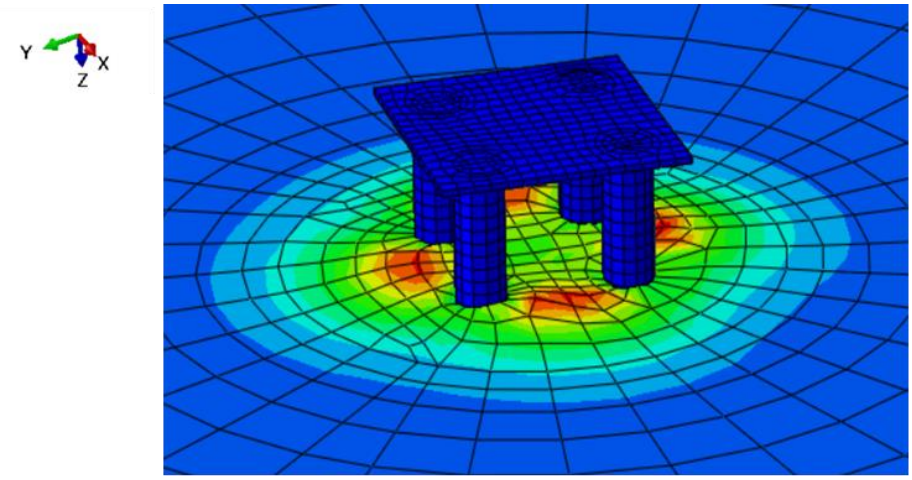

(a) $\emptyset_p = 32^0$

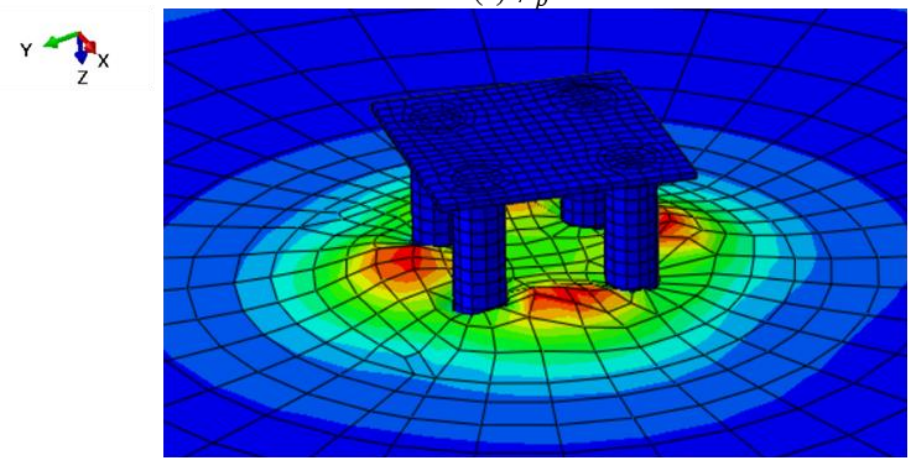

(b) $\emptyset_p = 36^0$

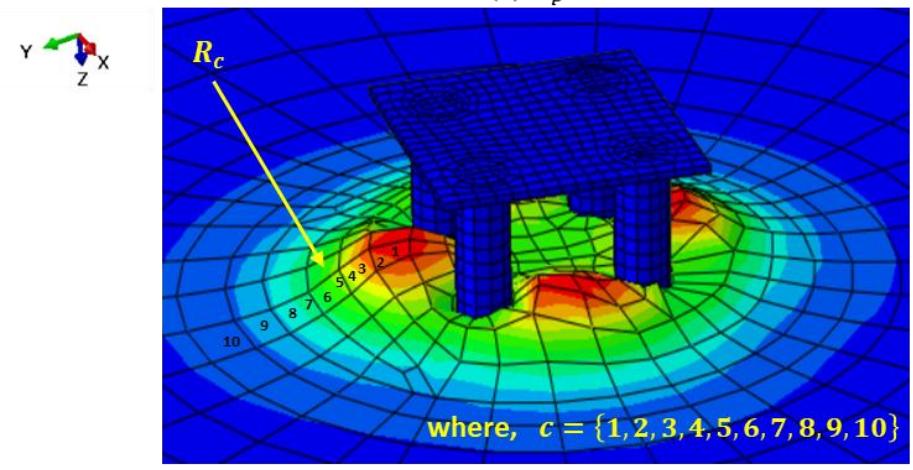

(c) $\emptyset_p = 42^0$

Figure 6.3 Three-dimensional view of the geomaterial-pile group (2,2), the heave displacement is shown to increase with the peak friction angle ($\emptyset_p = 32^0 - 42^0$) in the range (12.6-24.7 mm). The maximum and minimum heave displacement is shown by red and blue colour contours (12.58-0.75; 18.81-1.98; 24.70-1.93) mm assessed by R_c, where c =1 to 10. R_c are the surface heave contours

The uplift due to heave is shown to increase with varying peak friction angles. The maximum and minimum uplift is shown by red and blue colour contours (12.58-0.75; 18.81-1.98; 24.70-1.93 mm) described by R_c, where R_c are the surface heave contours, c =1 to 10. The variation of the uplift due to heave with the number of cycles for pile group (2,2) for varying peak angles of friction has been shown (Figure 6.4-6.6). The uplift due to heave increases with an increase in the number of cycles and peak angle of friction (Figure 6.4-6.6). The effective densification is anticipated more towards the peak at R_1. It has a sharper slope of the heave at a number of cycles N-60 compared to a lower number say N-5 to 10. The angle of the heave ($\emptyset_h^{R_c}$) is the ratio of the surface displacement in uplift and lateral flow due to heave at surface heave contour, $R_{c\rightarrow(1-10)}$ and is described as follows:

$$\left[\emptyset_h^{R_c} = \tan^{-1}\left(\frac{U_h^{R_c}}{L_h^{R_c}}\right)\right]_{R_{c=1}}^{R_{c=10}} \tag{6.20}$$

Where, $U_h^{R_c}$ and $L_h^{R_c}$ are the uplift and lateral flow due to heave at the surface heave contour, $R_{c\rightarrow(1-10)}$ for the number of cycles, *N*. The relationship in matrix form between the uplift due to heave, $U_h^{R_c}$ at $R_{c\rightarrow(1-10)}$ and the number of cycles, *N* (Fig. 6.4-6.6) is described as follows:

$$\left[U_h^{R_c} = L_h^{R_c}\tan\emptyset_h^{R_c}\begin{bmatrix}N^2 & N & 1\end{bmatrix}\begin{bmatrix}u_h'' \\ u_h' \\ u_h\end{bmatrix}\right]_{R_{c=1}}^{R_{c=10}} \tag{6.21}$$

$$U_h = \sum_{N=1}^{60} U_h^{R_c} \tag{6.22}$$

Where, $u_h^{"}$ is the surface parameter for the uplift due to heave which increases the magnitude of heave for increasing the peak angle of friction, u_h' represents the linear surface parameter for the uplift due to heave which decreases with the decreasing peak angle of friction and u_h represents the constant surface parameter for the uplift due to heave

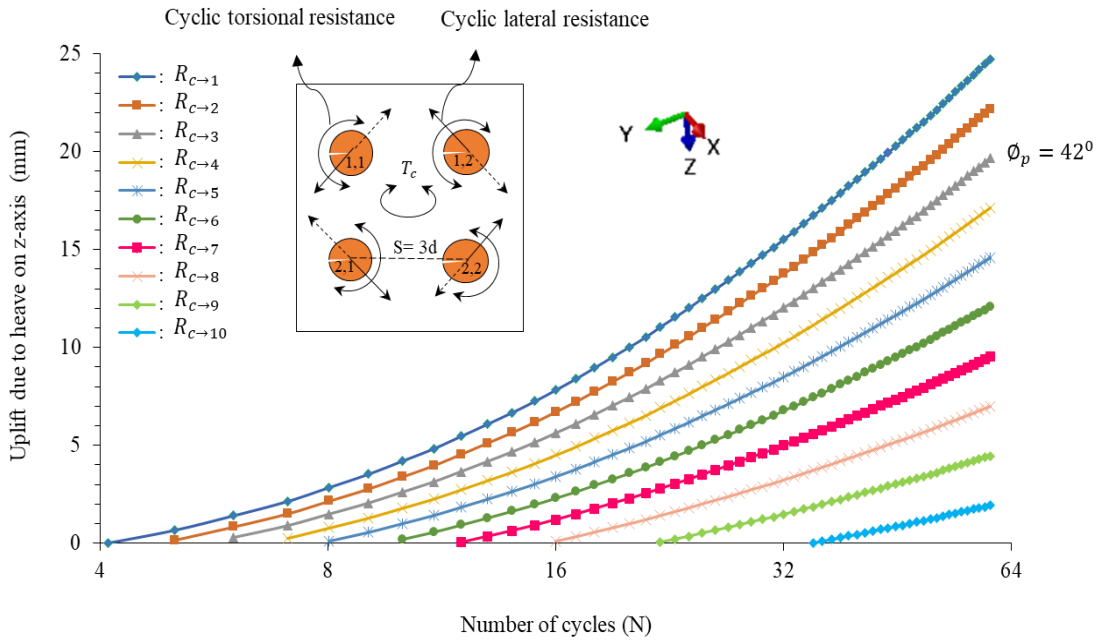

Figure 6.4 Variation of uplift due to heave with the number of cycles in the flow-controlled geomaterial captured for cyclic torsional loading on pile group (2,2) assessed for peak friction angle, 42^0

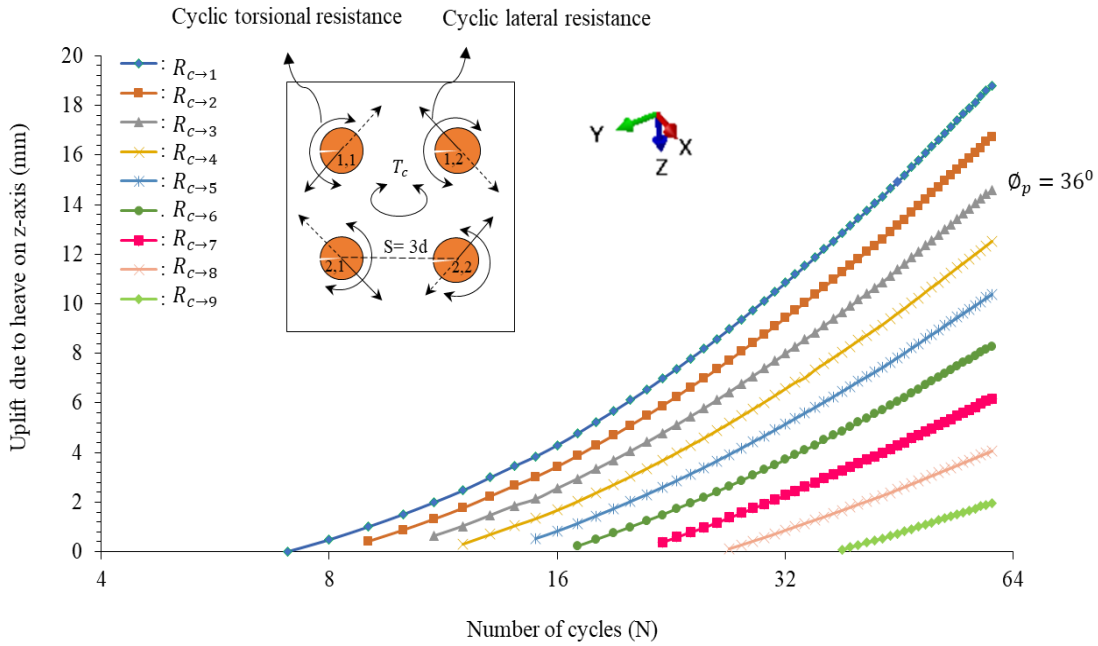

Figure 6.5 Variation of uplift due to heave with the number of cycles in the flow-controlled geomaterial captured for cyclic torsional loading on pile group (2,2) assessed for peak friction angle, 36^0

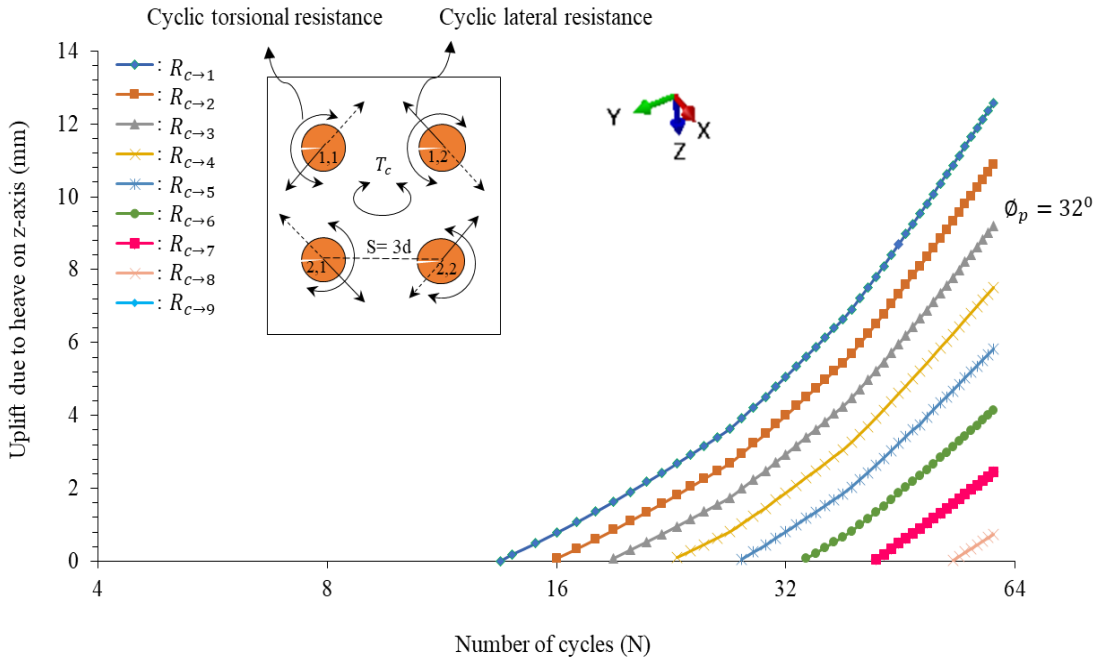

Figure 6.6 Variation of uplift due to heave with the number of cycles in the flow-controlled geomaterial captured for cyclic torsional loading on pile group (2,2) assessed for peak friction angle, 32^0

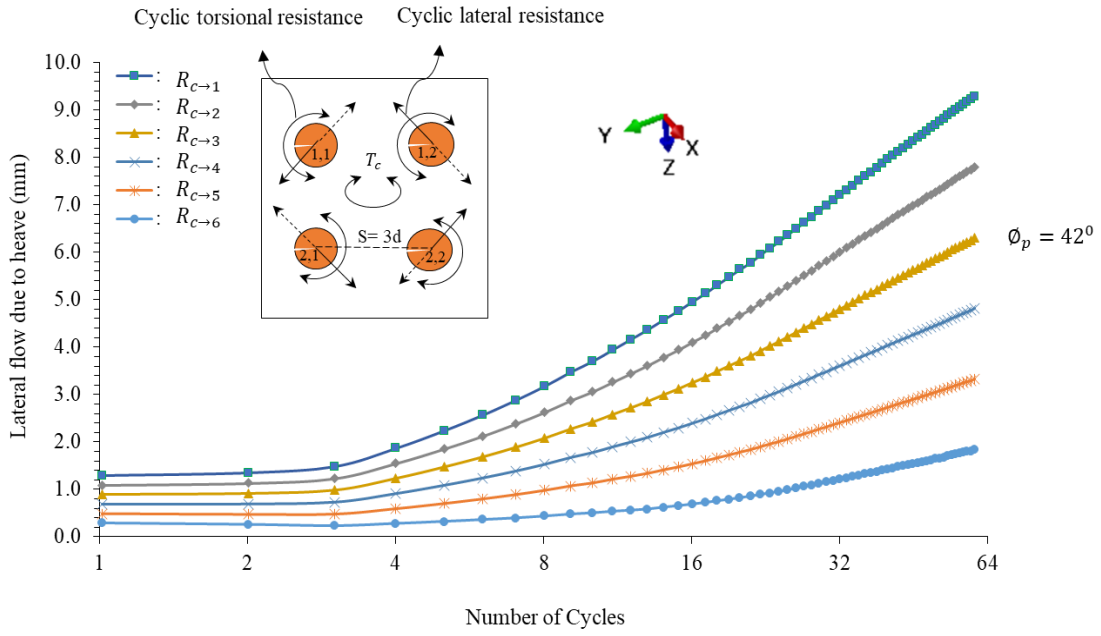

Figure 6.7 Variation of lateral flow due to heave with the number of cycles in the flow-controlled geomaterial captured for cyclic torsional loading on pile group (2,2) assessed for peak friction angle, 42^0

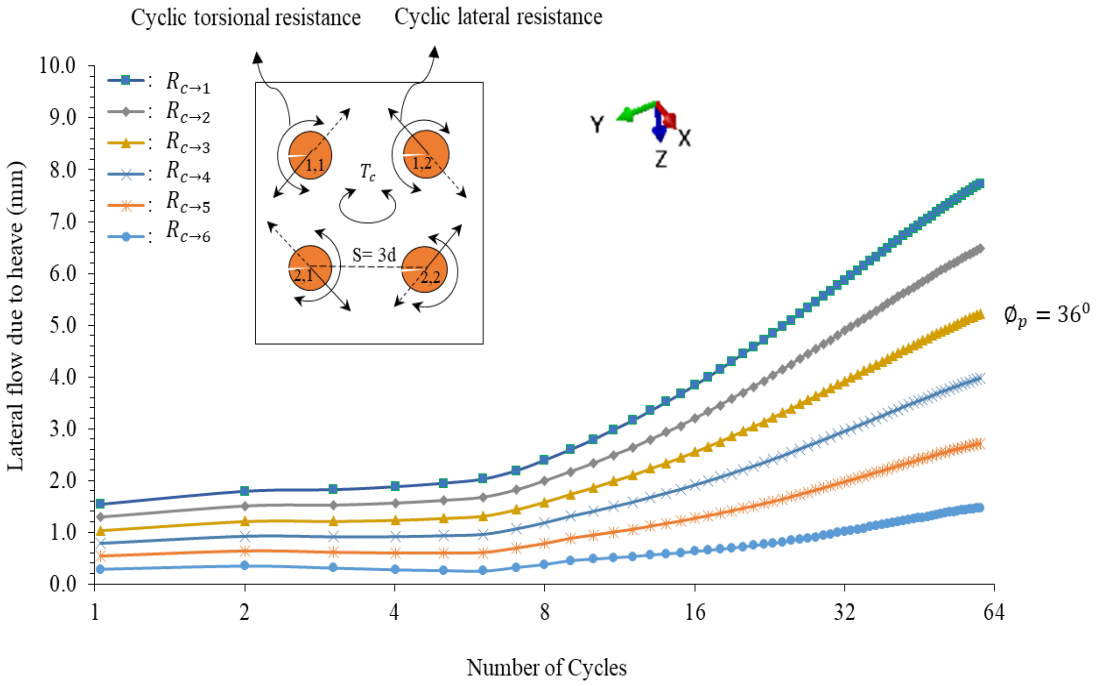

Figure 6.8 Variation of lateral flow due to heave with the number of cycles in the flow-controlled geomaterial captured for cyclic torsional loading on pile group (2,2) assessed for peak friction angle, 36^0

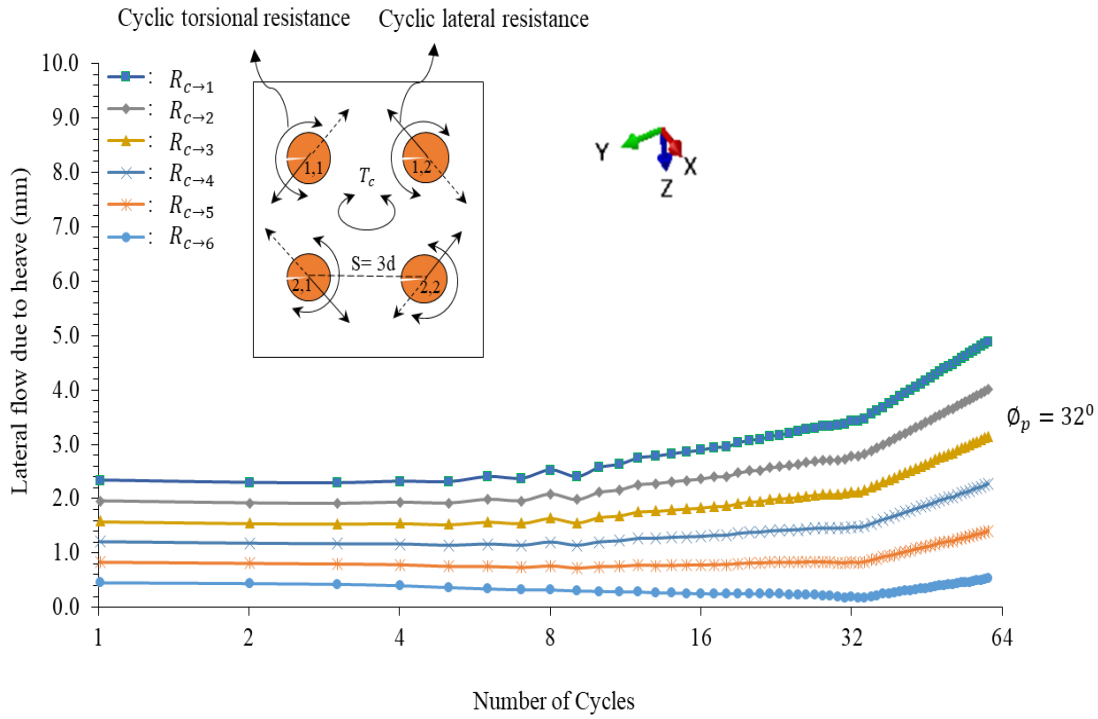

Figure 6.9 Variation of lateral flow due to heave with the number of cycles in the flow-controlled geomaterial captured for cyclic torsional loading on pile group (2,2) assessed for peak friction angle, 32^0

which decreases with an increase in the peak angle of friction (Table 6.2). The variation of the lateral flow due to heave with the number of cycles for pile group (2,2) for varying peak angles of friction evaluated for R_c, where c =1 to 10 have been shown (Fig. 6.4-6.6). The lateral flow due to heave increases with an increase in the number of cycles and peak angle of friction (Fig. 6.7-6.9). The relationship in matrix form between the lateral flow due to heave, $L_h^{R_c}$ at $R_{c\rightarrow(1-10)}$ and the number of cycles, *N* (Fig. 6.7-6.9) is described as follows:

$$\left[L_h^{R_c} = U_h^{R_c} \tan \emptyset_h^{R_c} \begin{bmatrix} N^2 & N & 1 \end{bmatrix} \begin{bmatrix} l_h'' \\ l_h' \\ l_h \end{bmatrix}\right]_{R_{c=1}}^{R_{c=10}} \tag{6.23}$$

$$L_h = \sum_{N=1}^{60} L_h^{R_c} \tag{6.24}$$

Where, $l_h^{"}$ is the surface parameter for the lateral flow due to heave which increases the magnitude of lateral flow for increasing the peak angle of friction, l_h' represents the linear surface parameter for the lateral flow due to heave which decreases with the decreasing peak angle of friction and l_h represents the constant surface parameter for the lateral flow due to heave which decreases with an increase in the peak angle of friction (Table 6.3). The numerical analysis results on the pile group and the single pile have been compared with the experimental observations of Cudmani and Gudehus (2001) for the single pile with outer diameter and length of 100 mm and 1120 mm respectively, installed in a cylindrical chamber with loose fine uniform quartz sand with $C_u = 2.3$, $G = 2.65$, and $\emptyset_p = 33^0$.

Table 6.2 Surface displacement parameters for heave in uplift

$\emptyset_p$	42^0			36^0			32^0		
	u_h''	u_h'	u_h	u_h''	u_h'	u_h	u_h''	u_h'	u_h
$R_{c\to1}$	0.0041	0.6909	2.3646	0.0028	0.5375	3.5669	0.00005	0.2681	3.546
$R_{c\to2}$	0.0037	0.6275	2.5252	0.0025	0.4896	3.7293	0.00009	0.2481	3.8203
$R_{c\to3}$	0.0033	0.5642	2.6877	0.0023	0.4426	3.9080	0.00008	0.2220	4.2143
$R_{c\to4}$	0.0029	0.5023	2.8710	0.0020	0.3654	4.0817	0.00006	0.2123	4.8248
$R_{c\to5}$	0.0025	0.4415	3.0692	0.0018	0.3485	4.2529	0.0003	0.2051	5.5104
$R_{c\to6}$	0.0021	0.3783	3.2261	0.0015	0.3001	4.3999	-0.0005	0.2098	6.5085
$R_{c\to7}$	0.0017	0.3168	3.4106	0.0012	0.2472	4.446	-0.0001	0.2304	7.9489
$R_{c\to8}$	0.0013	0.2530	3.5417	0.0009	0.1950	4.4956	-0.0012	0.2418	9.3179
$R_{c\to9}$	0.0009	0.1182	3.6359	0.0006	0.1426	4.5253	-	-	-
$R_{c\to10}$	0.0004	0.1143	3.4852	-	-	-	-	-	-

Table 6.3 Surface displacement parameters for heave in lateral flow

$\emptyset_p$	42^0			36^0			32^0		
	l_h''	l_h'	l_h	l_h''	l_h'	l_h	l_h''	l_h'	l_h
$R_{c\to1}$	-0.0021	0.2589	1.1605	-0.0014	0.1905	1.1252	0.0002	0.0346	2.225
$R_{c\to2}$	-0.0017	0.2148	0.9555	-0.0011	0.1584	0.9354	0.0002	0.0242	1.870
$R_{c\to3}$	-0.0013	0.1707	0.7507	-0.0009	0.1264	0.7452	0.0002	0.0138	1.5149
$R_{c\to4}$	-0.001	0.1266	0.5457	-0.0006	0.0944	0.5552	0.0003	0.0034	1.1603
$R_{c\to5}$	-0.0006	0.0825	0.3408	-0.0004	0.0623	0.3655	0.0003	-0.007	0.805
$R_{c\to6}$	-0.0002	0.0384	0.1361	-0.0001	0.0303	0.1756	0.0003	-.0174	0.4502

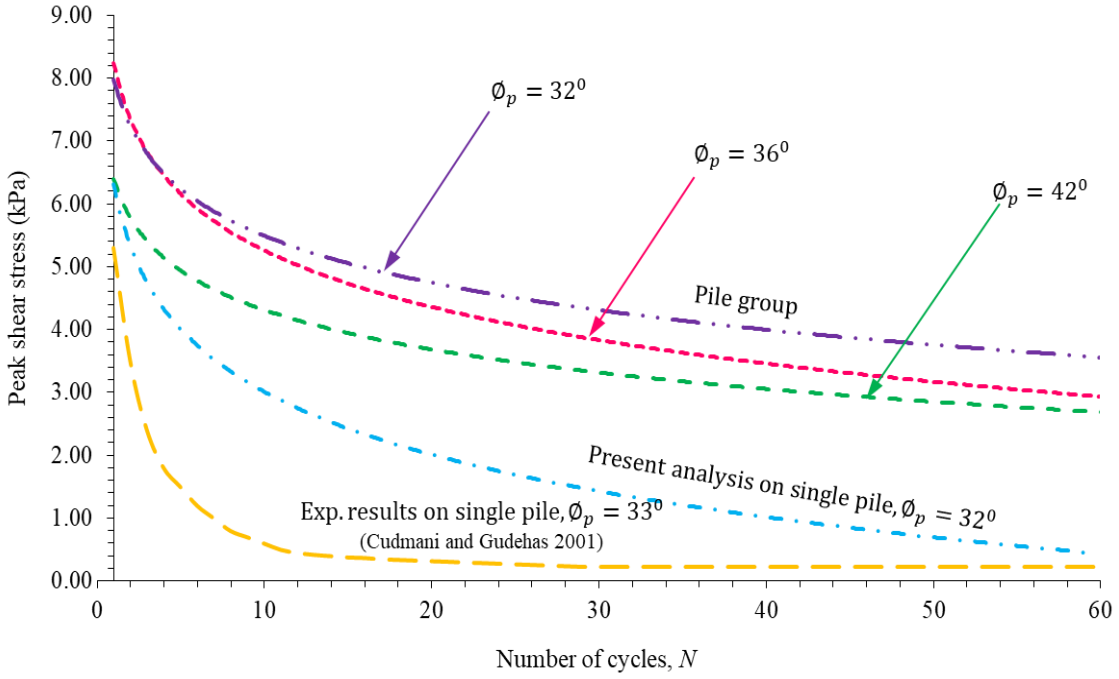

Figure 6.10 Variation of peak shear stress with a number of cycles at varying peak angle of friction for single pile (Cudmani and Gudehas 2001 and present work) and pile group (2,2) captured for cyclic torsional loading

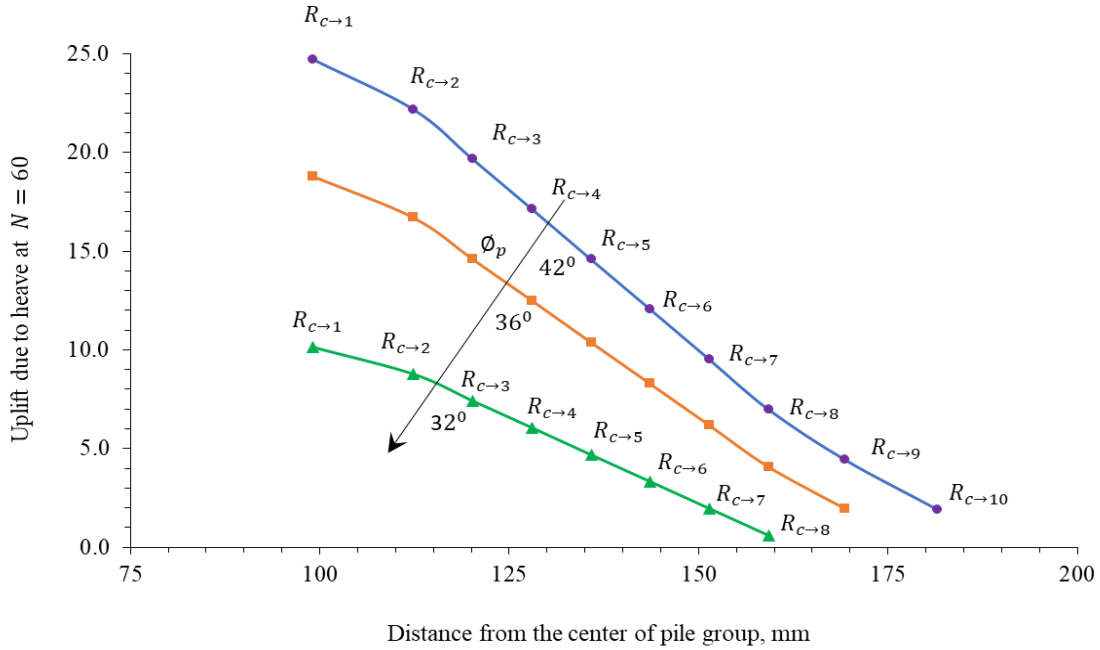

Figure 6.11 Variation of heave with distance from the centre of the pile group at $N = 60$ and peak friction angle in the range ($\emptyset_p = 32^0 - 42^0$)

The peak shear stress for the pile group (2,2) and a single pile for normalized cyclic torque are plotted with the varying peak angles of friction in the present analysis (Figure 6.10). The results obtained show good agreement with the observed experimental results. The variation of heave due to cyclic torsional loading with the distance from the centre of the pile group has been plotted as shown in Figure 6.11. There is a cyclic build-up of heave that occurs first near the centre of the heave and then mounts up to the peak at R_1. Therefore the latest cyclic effect spreads outward and away from the peak of the mounting heaves.

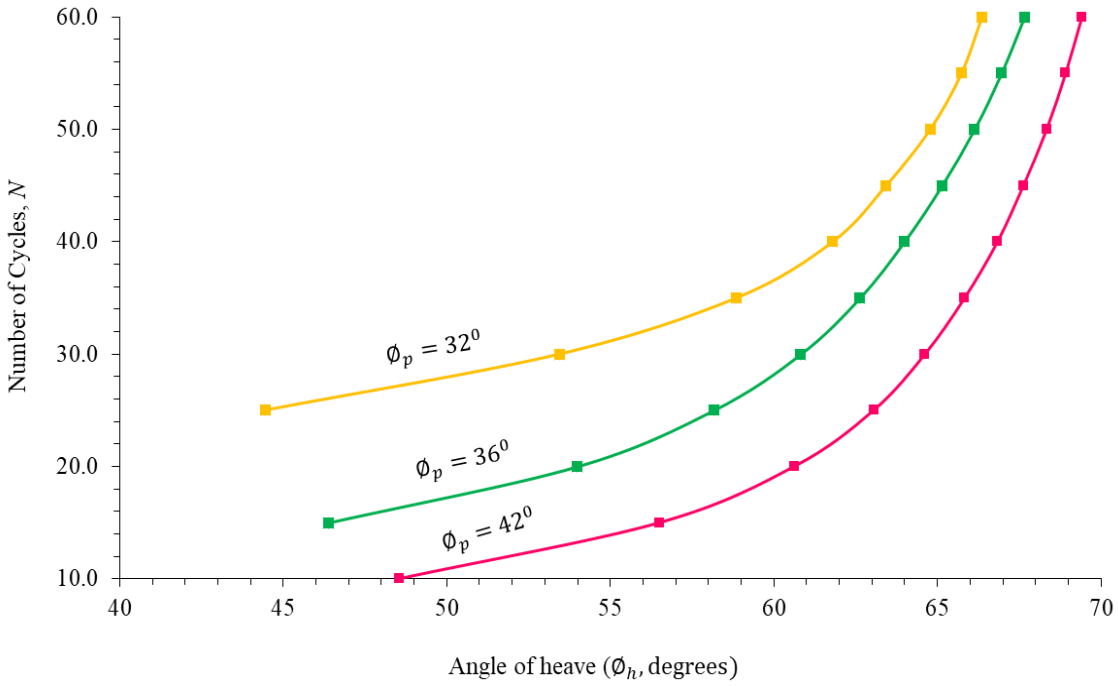

Figure 6.12 Variation of the number of cycles with the angle of heave assessed for varying peak angle of friction

The magnitude of the displacement increases with the peak angle of friction of the geomaterial. The variation of a number of cycles with the angle of heave for pile group (2,2) has been evaluated for varying peak angles of friction (Figure 6.12). The angle of heave is the ratio of the surface displacement in uplift and lateral flow due to heave. The angle of heave increases with an increase in the number of cycles and peak angle of friction.

After sixty cycles of torsional loading in the geomaterial, the angle of the heave starts to level off.

6.7 Conclusions

The paper investigates the surface displacements of the geomaterial considering the plastic flow potential of the yield surface. The flow potential considered for the yield surface represents the actual geomaterial-pile group interaction which tends to provide a more robust and safe design by assuming the worst-case scenario. The main conclusions of the investigation are as follows:

- When the cyclic loads are applied in the form of torsional forces, there is a formation of heave. The uplift and lateral flow due to heave is a concern for structures and foundations, as it can be uneven settlement, damage, or even structural failure. It is important to consider the potential for heave to design appropriate foundation systems and demonstrate the effects.
- After a number of torsional loading cycles, the surface heave was observed consisting of uplift and lateral flow ranges between 12.6-24.7 mm and 4.89-9.29 mm, respectively for varying peak angles of friction. Significant surface displacements have been observed for higher peak angles of friction.
- A set of surface displacement parameters have been identified which vary based on the number of cycles and peak angle of friction.
- The results of the present numerical analysis have been compared with the experimental observations of Cudmani and Gudehus. The results obtained show good agreement with the observed experimental results.

- The angle of heave increases with an increase in the number of cycles and peak angle of friction. After sixty cycles of loading in the geomaterial, the angle of the heave starts to level off.

-

References

Anagnostopoulos, C., & Georgiadis, M. (1993). “Interaction of axial and lateral pile responses.” Journal of Geotechnical Engineering, 119(4), 793-798.

De Borst, R., & Vermeer, P. A. (1984). “Possibilities and limitations of finite elements for limit analysis.” Geotechnique, 34(2), 199-210.

Beredugo, Y. O., & Novak, M. (1972). “Coupled horizontal and rocking vibration of embedded footings.” Canadian Geotechnical Journal, 9(4), 477-497.

Chow, Y. K. (1985). “Torsional response of piles in nonhomogeneous soil.” Journal of Geotechnical Engineering, 111(7), 942-947.

Cudmani, R., & Gudehus, G. (2001). “Settlements of sand due to cyclic twisting of a tube. In IUTAM Symposium on Theoretical and Numerical Methods in Continuum Mechanics of Porous Materials.” Proceedings of the IUTAM Symposium held at the University of Stuttgart, Germany, September 5–10, 1999 (pp. 387-396). Dordrecht: Springer Netherlands.

Chen, S. L., Kong, L. G., & Zhang, L. M. (2016). “Analysis of pile groups subjected to torsional loading.” Computers and Geotechnics, 71, 115-123.

Georgiadis, M. (1987). “Interaction between torsional and axial pile responses.” International Journal numerical and analytical methods in Geomechanics, 11(6), 645-650.

Guo, W. D., & Randolph, M. F. (1996). “Torsional piles in non-homogeneous media.” Computers and Geotechnics, 19(4), 265-287.

Guo, W.D. Chow, Y.K., and Randolph, M.F. (2007). “Torsional pile in two-layered non-homogenous soil.” International Journal of Geomechanics, 10.1061/ (ASCE) 1532-3641(2007)7:6(410), 410-422.

Hache, R.A.G., and Valsangkar, A.J. (1988). “Torsional resistance of single pile in layered soil.” Journal of Geotechnical Engineering, 10.1061/ (ASCE) 0733-9410(1988)114:2(216), 216-220.

Kong, L.G. (2006). “Behavior of pile groups subjected to torsion.” PhD Thesis, Hong Kong University of Science and Technology, Hong Kong, 339p.

Kong, L. G., & Zhang, L. M. (2009). “Nonlinear analysis of torsionally loaded pile groups.” Soils and foundations, 49(2), 275-286.

Kong, L. G., Zhang, Z. C., & Chen, Y. M. (2020). “Nonlinear analysis of pile groups subjected to combined lateral and torsional loading”. Journal Zhejiang University-SCIENCE A, 21(3), 179-192.

Long, J. H., & Vanneste, G. (1994). “Effects of cyclic lateral loads on piles in sand.” Journal of Geotechnical Engineering, 120(1), 225-244.

Ladhane, K. B., & Sawant, V. A. (2016). “Effect of pile group configurations on nonlinear dynamic response.” International Journal of Geomechanics, 16(1), 04015013.

Mehra, S. and Trivedi, A. (2018). “Experimental studies on model single pile and pile groups subjected to torque.” Proceedings of China-Europe Conference, Geotech. Engg., 10.1007/978-3-319-97115-5_24, pp 997-1000.

Mehra, S. & Trivedi, A. (2018). “Analysis and simulation of cyclic torque application on pile groups.” Proceeding of 12th International Super Pile World, Nanjing, Jiangsu, China, 277-282.

Mehra, S. & Trivedi, A. (2019). “Deep foundations subjected to combined axial and torsional loads.” Int. Symposium on Testing and Technology for Bearing Capacity of Deep Foundation, Delhi, ISBN:978-93-5391-519-3, 19-20.

Mehra, S., & Trivedi, A. (2021). “Pile Groups Subjected to Axial and Torsional Loads in Flow-Controlled Geomaterial.” International Journal of Geomechanics, 21(3), 04021002.

Mehra, S., & Trivedi, A. (2023a). “Progressive twist, displacement and torsional energy around pile groups.” International Journal of Geotechnical Engineering, 1-14.

Mehra, S., and Trivedi, A. (2023b). "Cyclic Degradation Parameters of Flow-Controlled Geomaterial for Pile Group Subjected to Torsional Loads" Applied Sciences 13, no. 19: 10895. https://doi.org/10.3390/app131910895.

Novak, M., & Howell, J. F. (1977). “Torsional vibration of pile foundations.” Journal of Geotechnical Engineering Division, 103(4), 271-285.

Novak, M., & El Sharnouby, B. (1983). “Stiffness constants of single piles.” Journal of Geotechnical Engineering, 109(7), 961-974.

Novak, M., & Sharnouby, B. E. (1984). “Evaluation of dynamic experiments on a pile group.” Journal of Geotechnical Engineering, 110(6), 738-756.

Poulos, H. G. (1971). “Behaviour of laterally loaded piles: II-pile groups.” Journal of Soil Mechanics and Foundation Division, 97(5), 733-751.

Poulos, H. G. (1975). “Torsional response of piles.” Journal of Geotechnical and Geoenvironmental Engineering, 101(10), 1019-1035.

Poulos, H. G. (1982). “Single pile response to cyclic lateral load.” Journal of Geotechnical Engineering Division, 108(3), 355-375.

Randolph, M. F. (1981a). “The response of flexible piles to lateral loading.” Geotechnique, 31(2), 247-259.

Randolph, M. F. (1981b). “Piles subjected to torsion.” Journal of Geotechnical Engineering, 107(8), 1095-1111.

Rajapakse, R.K.N.D. (1988). “A torsion load transfer problem for a class of non-homogenous elastic solids.” International Journal of Solids and Structures, 24(2), 139-151.

Rajashree, S. S., & Sundaravadivelu, R. (1996). “Degradation model for one-way cyclic lateral load on piles in soft clay.” Computers and Geotechnics, 19(4), 289-300.

Timoshenko, S., and Goodier, J. N. (1970). “Theory of Elasticity.” McGraw-Hill. New York, NY, 65.

Zienkiewicz, O. C., Humpheson, C., & Lewis, R. W. (1975). “Associated and non-associated visco-plasticity and plasticity in soil mechanics.” Geotechnique, 25(4), 671-689.

Li, Z. (2019). “Torsional vibration of a large-diameter pipe pile embedded in inhomogeneous soil.” Ocean Engineering, 172, 737-758.

7 DESIGN RECOMMENDATIONS

This chapter presents the recommendations for the design based on the response of the pile groups subjected to cyclic torsional loads. A solved problem has been presented at the end of this chapter.

7.1 Design Recommendations

The existing Indian Standard (IS) Codes (Bureau of Indian Standard 1997, 2002, 2010) do not have scope for consideration of the points namely, cyclic torsional loads, coupling effect between axial and torsional loads, and the torsional energy concept. The Indian Standard (IS) Code of Practice for Design and Construction of Pile Foundations uses the subgrade modulus approach for evaluating the axial and lateral pile capacity of individual piles. However, the coupling effect of axial load on torsional pile response conversely has been studied with a nonlinear three-dimensional finite-element analysis, while the conventional subgrade reaction method of pile analysis cannot consider this interaction. Additionally, the component of energy resulting from torsional force and moments for progressive twist and progressive displacement respectively have not been taken into account while designing pile groups subjected to torsional loads. Moreover, the IS codes do not take into consideration the effect of cyclic torsional loads on the pile groups.

The design considerations for the pile groups subjected to cyclic torsional loads to ensure the stability and performance of the foundation system shall be based on the following steps.

7.1.1 Define the flow potential for the flow controlled geomaterial for pile groups subjected to cyclic torsional loading as per Chapter 4. The input parameters for the execution of this step are $\boldsymbol{E_s}$, $\boldsymbol{G_s}$, $\boldsymbol{\rho_s}$, $\boldsymbol{D_s}$, $\boldsymbol{t_s}$, μ_s $\boldsymbol{\emptyset_p}$, $\boldsymbol{\emptyset_D}$, $\in$, $\boldsymbol{I_1}$,$\boldsymbol{J_2}$,$\boldsymbol{J_3}$, $\boldsymbol{\sigma_3}$, $\boldsymbol{\sigma_1}$, *e, c, p,* and the output parameter is *g* (Mehra and Trivedi 2021). The resulting equations (4.32-4.34) are

expressed as follows:

$$g = \sqrt{(\in \mathrm{c} \tan \emptyset_d)^2 + (R_{mw} q)^2} - p \tan \emptyset_d$$

Where, $R_{mw}(\Theta, \mathrm{e}) = \frac{4(1-e^2)cos^2\Theta+(2\mathrm{e}-1)^2}{2(1-e^2)\cos\Theta+(2e-1)\sqrt{4(1-e^2)cos^2\Theta+5e^2-4e}} R_{mc}\left(\frac{\pi}{3}, \emptyset\right)$

$$R_{mc}\left(\frac{\pi}{3}, \emptyset\right) = \frac{3 - \sin \emptyset}{6 \cos \emptyset}$$

7.1.2 The progressive twist, displacement and torsional energy around the pile groups have been computed as per Chapter 3. The input parameters for the execution of this step are $\boldsymbol{E_s}$, $\boldsymbol{E_p}$, $\boldsymbol{G_s}$, $\boldsymbol{G_p}$, $\boldsymbol{\rho_s}$, $\boldsymbol{\rho_p}$, $\boldsymbol{D_p}$, μ_s $\boldsymbol{t_s}$, $\boldsymbol{S_s}$, μ_s, μ_p, $\emptyset_p$, $\emptyset_D$,$\in$ and the output parameters are τ, τ_u, δ, $\boldsymbol{\theta}$, $\varepsilon_\mathbf{p}$, $\frac{U_z{}^c}{D_P}$, $\frac{U_z{}^h}{D_P}$,τ, τ_u, ξ_p, ζ_p, ξ_n , ζ_n, ξ_{min}, ζ_{min}, ξ_{max}, ζ_{max}, $\boldsymbol{E_T^\theta}$, $\boldsymbol{E_T^d}$, η_θ, $\mathbf{1} - \eta_\theta$ (Mehra and Trivedi 2023a) The resulting equation (3.34) is expressed as follows:

$$[E_T] = \eta_\theta . [E_T^\theta] + (1 - \eta_\theta) . [E_T^d]$$

7.1.3 The pile groups subjected to axial and torsional loads in the flow controlled geomaterial have been designed as per Chapter 4. The input parameters for the execution of this step are $\boldsymbol{E_s}$, $\boldsymbol{E_p}$, $\boldsymbol{G_s}$, $\boldsymbol{G_p}$, $\boldsymbol{\rho_s}$, $\boldsymbol{\rho_p}$, $\boldsymbol{D_p}$, $\boldsymbol{t_s}$, $\boldsymbol{t_s}$, $\boldsymbol{S_p}$, $\boldsymbol{L_p}$, μ_s, μ_p, $\emptyset_p$, $\emptyset_D$, $\in$, $\boldsymbol{Q}$, $\boldsymbol{Q_{max}}$, $\boldsymbol{T}$, $\boldsymbol{T_{max}}$ and the output parameters are τ, τ_u, δ, $\delta_{\mathbf{max}}$, $\boldsymbol{\theta}$, $\boldsymbol{\theta}_{\mathbf{max}}$, $\varepsilon_\mathbf{p}$, $\boldsymbol{C_T^{''}}$, $\boldsymbol{C_T'}$, $\boldsymbol{C_T}$, $\boldsymbol{C_Q^{''}}$, $\boldsymbol{C_Q'}$, $\boldsymbol{C_Q}$ (Mehra and Trivedi 2021). The resulting equations (4.42-4.43) are expressed as follows:

$$[\delta/\delta_{max}] = [(Q/Q_{max})^2 \quad Q/Q_{max} \quad 1] \begin{bmatrix} C_T'' \\ C_T' \\ C_T \end{bmatrix}$$

$$[\theta/\theta_{max}] = [(T/T_{max})^2 \quad T/T_{max} \quad 1] \begin{bmatrix} C_Q'' \\ C_Q' \\ C_Q \end{bmatrix}$$

7.1.4 The cyclic degradation parameters of the flow controlled geomaterial for the pile groups subjected to torsional loads have been designed as per Chapter 5. The input parameters for the execution of this step are $\boldsymbol{E_s}$, $\boldsymbol{E_p}$, $\boldsymbol{G_s}$, $\boldsymbol{G_p}$, $\boldsymbol{\rho_s}$, $\boldsymbol{\rho_p}$, $\boldsymbol{D_p}$, $\boldsymbol{t_p}$, $\boldsymbol{t_s}$, $\boldsymbol{S_p}$, $\boldsymbol{L_p}$, μ_s, μ_p, $\emptyset_p$, $\emptyset_D$, $\in$, $\boldsymbol{T_0}$ and the output parameters are τ (t), δ (t), $\psi(\mathbf{t})$, $\boldsymbol{\theta}$ (t), $\varepsilon_{\mathbf{p}}$(t), $\mathbf{k_{hN}}$, $\mathbf{k}_{\theta\mathbf{N}}$, $\boldsymbol{D_f''}, \boldsymbol{D_f'}, \boldsymbol{D_f}$, $\boldsymbol{a_t}$, $\boldsymbol{b_t}$, $\boldsymbol{a_s}$, $\boldsymbol{b_s}$ (Mehra and Trivedi 2023b, 2023c). The resulting equations (5.31-5.33; 5.35-5.37) are expressed as follows:

$$[\theta_t] = [\log_e N \quad 1] \begin{bmatrix} a_t \\ b_t \end{bmatrix}$$

$$\theta_t = a_t \log_e N + b_t$$

$$N = e^{\frac{\theta_t - b_t}{a_t}};\ N = 1;\ \theta_t = b_t$$

$$[\tau_p] = [\log_e N \quad 1] \begin{bmatrix} a_s \\ b_s \end{bmatrix}$$

$$\tau_p = a_s \log_e N + b_s$$

$$N = e^{\frac{\tau_p - b_s}{a_s}};\ N = 1;\ \tau_p = b_s$$

7.1.5 The surface displacement of the geomaterial subjected to cyclic torsional loads has been designed as per Chapter 5. The input parameters for the execution of this step are $\boldsymbol{E_s}$, $\boldsymbol{E_p}$, $\boldsymbol{G_s}$, $\boldsymbol{G_p}$, $\boldsymbol{\rho_s}$, $\boldsymbol{\rho_p}$, $\boldsymbol{D_p}$, $\boldsymbol{t_p}$, $\boldsymbol{t_s}$, $\boldsymbol{S_p}$, $\boldsymbol{L_p}$, μ_s, μ_p, $\emptyset_p$, $\emptyset_D$, $\in$, $\boldsymbol{T_0}$ and the output parameters are τ (t), δ (t), $\psi(\mathbf{t})$, $\boldsymbol{\theta}$ (t), $\varepsilon_{\mathbf{p}}$(t), $\mathbf{k_{hN}}$, $\mathbf{k}_{\theta\mathbf{N}}$, $\emptyset_{\boldsymbol{h}}^{\boldsymbol{R_c}}$, $\boldsymbol{u_h''}$, $\boldsymbol{u_h'}$, $\boldsymbol{u_h}$, $\boldsymbol{l_h''}$, $\boldsymbol{l_h'}$, $\boldsymbol{l_h}$ (Mehra and Trivedi

2024). The resulting equations (6.20-6.24) are expressed as follows:

$$\left[\emptyset_h^{R_c} = \tan^{-1}\left(\frac{U_h^{R_c}}{L_h^{R_c}}\right)\right]_{R_{c=1}}^{R_{c=10}}$$

$$\left[U_h^{R_c} = L_h^{R_c}\tan\emptyset_h^{R_c}\,[N^2 \quad N \quad 1]\begin{bmatrix}u_h''\\ u_h'\\ u_h\end{bmatrix}\right]_{R_{c=1}}^{R_{c=10}}$$

$$U_h = \sum_{N=1}^{60} U_h^{R_c}$$

$$\left[L_h^{R_c} = U_h^{R_c}\tan\emptyset_h^{R_c}\,[N^2 \quad N \quad 1]\begin{bmatrix}l_h''\\ l_h'\\ l_h\end{bmatrix}\right]_{R_{c=1}}^{R_{c=10}}$$

$$L_h = \sum_{N=1}^{60} L_h^{R_c}$$

7.1.5.1 Problem Statement for Designing Pile Groups for Axial and Torsional Loading

A (2,2) pile group has been subjected to an axial load of 6000 kN and a torque of 8000 kN-m. The open-ended pipe pile has an outer diameter of 400 mm with a wall thickness of 40 mm and an embedded length of 50 m. The pile cap in a pile group is assumed to be rigid and the pile-cap connection is assumed fixed. The initial Young's modulus of the flow controlled geomaterial has been assumed to be uniform and is taken as 25000 kN/m^2. The initial shear modulus of the flow-controlled geomaterial has been 9.6 MN/m^2. The allowable deflection has been 16 mm and twists 0.5 degrees.

7.1.5.2 Solution Based on Proposed Design Recommendations

Step 1: For T $= 8000$ kN, -and Q $= 6000$ kN, the normalized applied torque and normalized axial load have been expressed as 0.8 and 0.5.

Step2: From Figure (4.11-4.12), the twist and displacement parameters have been expressed as follows:

$C_T^{"} = 1.96, C_T' = 0.15, C_T = -0.001, C_Q^{"} = 1.06, C_Q' = 0.04, C_Q = -0.005$

Step 3: The normalized axial load and normalized displacement, using Eq. (4.42-4.43) have been expressed as follows:

$$\delta/_{\delta_{max}} = 0.565, \qquad \theta/_{\theta_{max}} = 0.7054$$

Step 4: Using step 2, the displacement and twist at the pile head have been expressed as follows:

$$\delta = 28 \text{ mm}, \theta = 0.65^0$$

Therefore, displacement and twist at pile head for a combined axial load of 6000 kN and a torque of 8000 kN-m exceeds the allowable limit.

Step 5: Now consider, T $= 2400$ kN-m, Q $= 6000$ kN, Repeat steps 1-4.

Step 6: The displacement and twist at the pile head have been expressed as follows:

$$\delta/_{\delta_{max}} = 0.30, \qquad \theta/_{\theta_{max}} = 0.0572$$

Step 7: Using step 6, the displacement and twist at the pile head have been expressed as follows:

$$\delta = 15 \text{ mm}, \theta = 0.05^0$$

Therefore, displacement and twist at the pile head for a combined axial and torsional load of 6000 kN and 2000 kN-m respectively are within the allowable limit. In summary, cyclic torsional loads can have a significant impact on the performance and longevity of structures, leading to fatigue failure, stress concentration and vibration. Engineers must consider these factors carefully during the design and analysis process to ensure the reliability and safety of the final solution.

References

Bureau of Indian Standards. (1997). “Indian Standard Code of Practice for Design and Construction of Pile Foundations.” IS: 2911 (Part I/Sec 1)-1979 (Reaffirmed 1997) First Revision, November 1997.

Bureau of Indian Standards. (1997). “Indian Standard Code of Practice for Design and Construction of Pile Foundations.” IS: 2911 (Part I/Sec 2)-1979 (Reaffirmed 1997) First Revision, December 1998..

Bureau of Indian Standards. (2002). “Indian Standard Code of Practice for Design and Construction of Pile Foundations.” IS: 2911 (Part I/Sec 1)-1979 (Reaffirmed 2002) Edition 2.3 (1987-09).

Bureau of Indian Standards. (2010). “Indian Standard Code of Practice for Design and Construction of Pile Foundations.” IS: 2911 (Part I/Sec 1)-1979 Second Revision, May 2011.

Cudmani, R., & Gudehus, G. (2001). “Settlements of sand due to cyclic twisting of a tube. In IUTAM Symposium on Theoretical and Numerical Methods in Continuum Mechanics of Porous Materials.” Proceedings of the IUTAM Symposium held at the University of Stuttgart, Germany, September 5–10, 1999 (pp. 387-396). Dordrecht: Springer Netherlands.

Georgiadis, M. (1987). “Interaction between torsional and axial pile responses.” International Journal numerical and analytical methods in Geomechanics, 11(6), 645-650.

Guoliang, D., Weiming, G., Lin, J., & Qinzhong, Y. (2002). “Static loading test of a self-balanced approach to a pile in the Yangtze River.” *In Advances in Building Technology,* 695-701. Elsevier.

Guoliang, D., & Xiaojuan, L. (2019). “The Statistical Study on Bearing Capacity of the Self-Balanced Loading Test.” *Int. Symposium on Testing and Technology for Bearing Capacity of Deep Foundation, Delhi*, ISBN:978-93-5391-519-3, 19-20.

Kong, L. G., & Zhang, L. M. (2009). “Nonlinear analysis of torsionally loaded pile groups.” Soils and foundations, 49(2), 275-286.

Mehra, S., & Trivedi, A. (2021). “Pile Groups Subjected to Axial and Torsional Loads in Flow-Controlled Geomaterial.” International Journal of Geomechanics, 21(3), 04021002.

Mehra, S., & Trivedi, A. (2023a). “Progressive twist, displacement and torsional energy around pile groups.” International Journal of Geotechnical Engineering, 1-14.

Mehra, S., and Trivedi, A. (2023b). "Cyclic Degradation Parameters of Flow-Controlled Geomaterial for Pile Group Subjected to Torsional Loads" Applied Sciences 13, no. 19: 10895. https://doi.org/10.3390/app131910895.

Mehra, S., and Trivedi, A. (2023c). "Cyclic Torsional Loads on Pile Groups" Indian Geotechnical Conference, IIT Roorkee, India, 14-16 December 2023.

Mehra, S., and Trivedi, A. (2024). “Surface Displacement of the Geomaterial Due to Cyclic Torsional Loading on Pile Groups.” Under Review.

8 CONCLUSIONS AND SCOPE FOR FUTURE RESEARCH

This chapter presents the conclusions based on the response of the pile groups subjected to cyclic torsional loads. The detailed conclusions have been drawn at the end of each chapter, while the overall key findings and have been presented in this chapter. Finally, the scope of future research based on the experience of this present work has been proposed.

8.1 General Conclusions

This thesis is the result of the numerical analysis and laboratory experimentation to quantify the behaviour of pile groups subjected to cyclic torsional loads. Large structures such as offshore platforms, tall buildings, bridge bents, and electric transmission towers are subjected to cyclic lateral loads of considerable magnitude from wind and wave actions, ship impact and high-speed vehicles, significant cyclic torsional forces can be transferred to the foundation piles by the virtue of eccentric lateral loading. Therefore, torsional resistances of their foundations are very important for these structures. Devastating outcomes could arise from inadequate foundation design against these loads. This study focuses on the analysis and design of pile and pile groups to axial, lateral and torsional forces and moments.

In this study, an attempt has been made to find out the energy components due to progressive twist and displacement. Speculatively, the torsional resistance is elusively approximated among 20% or more while 80% or less of torsional energy depends upon the mobilisation of lateral resistance related to pile locations within the group and pile-soil interactions. However, in this study, the component of energy resulting from torsional force and moments for progressive twist and progressive displacement are obtained.

Additionally, the effects of torsional loading on axial pile displacements along with the influence of axial loads on the torsional pile response are investigated. The twist parameters $(C_T^{"}, C_T', C_T)$ and logarithmic degradation parameters (a, b), which depend upon the plastic strain and dilation angle have been classified and recommended for designing piles for displacement and twist. Further, to this study, the progressive deterioration of strength and stiffness of the surrounding geomaterial subjected to cyclic torsional loading creating a substantial degradation of the pile group capacity has been studied with the aid of the numerical scheme solved using the computational analysis. A cyclic degradation parameter for plastic strain and a logarithmic degradation parameter for twist and shear has been identified as a function of frictional characteristics of flow-controlled geomaterial which in turn depend upon the number of cycles, plastic strain and dilation.

Moreover, the surface displacement of the geomaterial surrounding a pile group under cyclic torsional loading through the development and application of a numerical modelling framework has been investigated. When the cyclic loads are applied in the form of torsional forces, there is a formation of heave. The uplift and lateral flow due to heave is a concern for structures and foundations, as it can be uneven settlement, damage, or even structural failure. It is important to consider the potential for heave to design appropriate foundation systems and demonstrate the effects. A set of surface displacement parameters have been identified which vary based on the number of cycles and peak angle of friction. To achieve the objectives of this study, several model experiments have been performed to establish the torque-twist plots and to find the cyclic torsional response of the pile groups in homogenous and using the in-house developed to set up in the laboratory at Delhi Technological University, Delhi, India. The frequency, number of cycles, dilation and plastic strain play an important role in analysing and designing the pile groups subjected to torsional loads.

8.2 Specific Conclusions

Based on the current investigation, the following broad conclusions are drawn from the literature analysis and each of the particular research facets.

- The torque-twist relationship for the pile group is a necessary design step; therefore, the study is required to capture the behaviour of the pile group relative to the single pile. The plot between the normalized applied torque and twist rigidity factor has been evaluated to predict the torque-twist relationship for the pile groups using the experimental output of the single pile.

- There is a remarkable difference among the torque-twist behaviour of the single pile and pile groups at the initial stages of the torque application while at ultimate values, the modulus ratio less than 0.7 has no effect on the twist rigidity factor for soils undergoing cavity and heave formation simultaneously. The torsional energy and twist rigidity parameters were evaluated for a range of initial shear modulus ratios of the soil. The twist rigidity decreases significantly with an increase in the normalised torsional loads.

- It has been observed that the torsional energy of the pile group (1,2) is significantly higher than pile groups (1,3; 2,2). The torsional energy is obtained in the range of 5~15, 6~16 and 49~100 percent for pile groups (2,2; 1,3; 1,2) respectively. The component of energy resulting from torsional force and moments for progressive twist ($\eta_{\boldsymbol{\theta}}$) and progressive displacement (1-$\eta_{\boldsymbol{\theta}}$) are obtained in the range 0.43~0.50 and 0.50~0.57, respectively. The soil element around the pile group behaves as linear elastic ($\xi_{\boldsymbol{p}} \sim \mathbf{0}, \zeta_{\boldsymbol{p}} \sim \mathbf{0}$), transitional ($\xi_{\boldsymbol{p}} > \mathbf{0}, \zeta_{\boldsymbol{p}} > \mathbf{0}$), and fully plastic ($\xi_{\boldsymbol{p}} \sim \mathbf{1}, \zeta_{\boldsymbol{p}} \sim \mathbf{1}$).

- In designing pile groups to resist combined axial and torsional loads, the criterion for design is not the ultimate capacity but the displacement and twist of piles. The resultant

displacement and twist should be considered while designing pile groups subjected to combined loads. The coupling effect of axial load on torsional pile response conversely can be studied with a nonlinear three-dimensional finite-element analysis, while the conventional subgrade reaction method of pile analysis cannot consider this interaction.

- The resultant displacement increases on the application of the torsional load for the LDP and pile groups (1,2; 2,2). The resultant displacement increases in a range of 19-235%; 20-140%; and 20-245% for the LDP and pile group (1,2; 2,2), respectively, the normalized applied torque and normalized axial load applied in the range 0.6 to 1 and 0.33 to 0.67, respectively. The twist increases with an increase in axial load. The twist increases in a range of 18-530%; 30-475%; and 22-650%, respectively, and the normalized axial load and normalized applied torque are in the range of 0.5 to 1 and 0.2 to 0.8, respectively. Due to the increase in the torsional loads from 8000 to 10000 kN, the pile head displacement increases from 13 to 27 mm for an axial load of 4440 kN. Similarly, pile head displacement increases from 18 to 27 mm with an increase of torsional loads from 6000 to 8000 kN for an axial load of 6000 kN. The twist parameters ($\boldsymbol{C_T^{''}, C_T', C_T}$) and displacement parameters ($\boldsymbol{C_Q^{''}, C_Q', C_Q}$), which depends upon the plastic strain and dilation angle have been classified and recommended for designing piles for displacement and twist.

- A cyclic degradation parameter for plastic strain and a logarithmic degradation parameter for twist and shear have been identified as a function of frictional characteristics of flow-controlled geomaterial which in turn depend upon the number of cycles, plastic strain and dilation. The flow-controlled cyclic degradation parameters for plastic strain ($\boldsymbol{D_f^{''}, D_f', D_f}$) and logarithmic degradation parameters for the twist ($\boldsymbol{a_t}$, $\boldsymbol{b_t}$) and shear ($\boldsymbol{a_s}$, $\boldsymbol{b_s}$) have been classified and recommended for designing pile

groups.

- The twist decreases with an increase in the number of cycles and dilation captured for the pile group (2,2). The peak twist logarithmically decreases and then becomes asymptotic after 30 cycles of loading in a flow-controlled geomaterial. The plastic strain increases with an increase in the number of cycles for the pile group (2,2). The peak plastic stain has been obtained as 44, 28 and 15% for 2^0, 6^0 and 12^0 dilation, respectively.

- The peak shear stress for pile group (2,2) and a single pile for normalized cyclic torque is found in the range of 5-8.2 kPa at the dilation of $\mathbf{2^0}$ to $\mathbf{12^0}$, respectively in the present analysis. The peak shear stress for the pile group (2,2) logarithmically decreases and then asymptotically converges after 60 cycles of loading in a flow-controlled geomaterial which in turn is a function of the number of cycles and dilation.

- When the cyclic loads are applied in the form of torsional forces, there is a formation of heave. The uplift and lateral flow due to heave is a concern for structures and foundations, as it can be uneven settlement, damage, or even structural failure. It is important to consider the potential for heave to design appropriate foundation systems and demonstrate the effects. After a number of torsional loading cycles, the surface heave was observed consisting of uplift and lateral flow ranges between 12-25 mm and 5-10 mm, respectively for varying peak angles of friction. Significant surface displacements have been observed for higher peak angles of friction.

- A set of surface displacement parameters namely, uplift ($\boldsymbol{u_h^{''}}$, $\boldsymbol{u_h'}$, $\boldsymbol{u_h}$) and lateral flow ($\boldsymbol{l_h^{''}}$, $\boldsymbol{l_h'}$, $\boldsymbol{l_h}$) due to heave have been identified which vary based on the number of cycles and peak angle of friction. The angle of heave increases with an increase in the number of cycles and peak angle of friction. After sixty cycles of loading in the geomaterial,

the angle of the heave starts to level off.

8.3 Scope for Future Research

The following is a summary of potential research topics for subsequent studies:

- The progressive twist, displacement and torsional energy around the pile groups have been evaluated considering flow controlled geomaterial. The study may be conducted considering the geomaterial with distinct functions of stresses in the meridional and deviatoric stress planes.
- In the present study, the pile groups subjected to axial and torsional loads have been evaluated. Further, the study may be conducted taking into account axial, torsional and lateral loads on the pile groups.
- The present research focused on finding the behaviour of the pile groups subjected to cyclic torsional loads considering cohesionless geomaterial medium. Further study may be conducted on rock socketed pile groups considering the interfacial behaviour between the pile groups and the rock.
- The surface displacement of the geomaterial has been evaluated for the (2,2) pile group, subjected to cyclic torsional loads. Further, the addition of the axial load to the pile groups on the surface displacement of the geomaterial may be considered.